GEORGIA INSTITUTE OF TECHNOLOGY — OFFICE OF CONTRACT ADMINISTRATION

PROJECT ADMINISTRATION DATA SHEET

[x] ORIGINAL
[ ] REVISION NO. ____

Project No. E-16-629 (Subproject is G-33-606)/Brouner/Ch * DATE: 8/26/81

Project Director: Ben T. Zinn School/Lab AE

Sponsor: Office of Naval Research; Arlington, VA

Type Agreement: Contract No. N00014-80-C-0432, Mod. 2

Award Period: From 7/1/81 To ~~1/31/82~~ 8/30/84 (Performance) ~~3/31/82~~ 8/30/82 (Reports)

Sponsor Amount: $50,000 (includes $1,705 in G-33-606) Contracted through:

Cost Sharing: $11,155 (E-16-361) GTRI/~~GIT~~

Title: The Reduction of the Smoke Hazards Resulting from the Burning of Shipboard Materials Utilized by the Navy

ADMINISTRATIVE DATA OCA CONTACT Leamon R. Scott

1) Sponsor Technical Contact: Scientific Officer; Director, Chemistry Division; Naval Research Laboratory; 4555 Overlook Ave., S.W.; Washington, D.C. 20375

2) Sponsor Admin./Contractual Contact: Tom Bryant, Office of Naval Research; Research Representative; 206 O'Keefe Bldg.; Georgia Tech; Atlanta, GA 30332

Reports: See Deliverable Schedule Security Classification: N/A

Defense Priority Rating: DO-C9 under DMS Reg. 1.

RESTRICTIONS

See Attached Government Supplemental Information Sheet for Additional Requirem

Travel: Foreign travel must have prior approval - Contact OCA in each case. Domestic travel requires sponsor approval where total will exceed greater of $500 or 125% of approved proposal budget category.

Equipment: Title vests with Government; unless otherwise determined by contracting officer (see contract section H-4); except that items costing less than $1K vest with GIT upon acquisition if prior approval to purchase is obtained from contracting officer.

COMMENTS: * Continuation of E-16-669/G-33-675.

COPIES TO:

Administrative Coordinator
Research Property Management
Accounting Office
Research Security Services
Reports Coordinator (OCA)
Legal Services (OCA)
EES Research Public Relati
Project File (OCA)
Other: P. Oliver

EORGIA INSTITUTE OF TECHNOLOGY OFFICE OF CONTRACT ADMINISTRATION

SPONSORED PROJECT TERMINATION/CLOSEOUT SHEET

AK-668

Date 9/17/86

oject No. E16-629 School/~~XXX~~ AE

cludes Subproject No.(s) G-33-606, G33-685

oject Director(s) B. T. Zinn GTRC / ~~GTT~~

ponsor Office of Naval Research

tle The Reduction of the Smoke Hazards Resulting from the Burning of Shipboard Materials Utilized by the U.S.

ffective Completion Date: 9/30/84 (Performance) 11/30/84 (Reports)

rant/Contract Closeout Actions Remaining:

- [ ] None
- [X] Final Invoice or Final Fiscal Report
- [X] Closing Documents
- [ ] Final Report of Inventions - already submitted.
- [X] Govt. Property Inventory & Related Certificate
- [ ] Classified Material Certificate
- [ ] Other

ntinues Project No. E16-669 Continued by Project No.

OPIES TO:

oject Director
esearch Administrative Network
esearch Property Management
ccounting
ocurement/GTRI Supply Services
esearch Security Services
eports Coordinator (OCA)
gal Services

Library
GTRC
Research Communications (2)
Project File
Other I. Newton
A. Jones
R. Embry

ORM OCA 69.285

PROGRESS TO DATE

This section is divided into three parts. In the first part the efforts under Task A that have been concerned with the investigation of the amounts and physical properties of the smoke particulates generated by the tested samples are discussed; in the second part the status of the chemical analysis work conducted under Task A is reviewed; and in the third part the status of the Task B investigation of the mechanisms of soot formation is discussed. In addition to the above, results of the investigation of the effect of various additives upon soot formation in polyethylene diffusion flames is described. Finally, a listing of papers that resulted from these research efforts is provided and these papers are enclosed in Appendix A of the proposal.

Summary of Task A Progress

A-I. Investigation of the Physical Properties of Smoke Particulates.

Efforts conducted under this project can be divided into the following five subtasks: (1) modifications to the optical system, (2) refurbishing of the combustion products test chamber (CPTC), (3) modification of the data acquisition/data reduction system, (4) testing of polyphosphazene hull insulation material, and (5) testing of paints. The first three subtasks were completed prior to the last project amendment and are described in the last proposal (April 1981). Testing of the polyphosphazene hull insulation material has now been completed and the principal results will be described below. Testing of the chlorid alkyd paint has begun and the room

temperature tests have been completed. Testing of the paints was interrupted by failure of the argon-ion laser plasma tube. This required shipment of the laser to the manufacturer for warranty replacement of the plasma tube, which resulted in a twelve week delay in the testing program. After reinstallation of the laser and alignment and calibration of the optical system, the remaining tests of the chlorid alkyd paint and the tests of the intumescent paint will be completed under the previous project amendment. A report will be prepared shortly describing the results of the polyphosphazene tests, while the results of the tests of the paints will be presented in a separate report to be prepared later.

Polyphosphazene Tests. The physical properties of the smoke particulates produced during combustion of the polyphosphazene hull insulation material were determined for the conditions given in Table 1. The results of these tests are summarized in Tables 2 and 3.

Mean particle diameters and smoke optical densities were determined for all test conditions except for nonflaming combustion in the 300°C atmosphere. For this condition no measurable light scattering by particulates was detected, and the optical density was probably due to absorption by gaseous species. The determination of particulate size distributions using cascade impactor sampling was attempted for all room temperature tests. For both flaming and nonflaming tests with a radiant flux of 5 W/cm^2, the amounts of sample collected on the cascade impactor plates was insufficient for determination of the size distribution. For this reason an

Table 1. Polyphosphazene Test Matrix.

Test	Radiant Flux (W/cm^2)	Ventilation Gas Temperature (^oC)	Type of Combustion	Ventilation Gas Composition
1	5	25	Nonflaming	Air
2	5	100	"	"
3	5	300	"	"
4	7.5	25	"	"
5	5	25	Flaming	"
6	5	100	"	"
7	5	300	"	"

additional nonflaming test at 7.5 W/cm^2 was conducted for which sufficient particulates were collected for measurement of the size distribution. For all room temperature tests the fraction of the sample weight loss converted to particulates (Γ) was also determined. Sample weight loss histories using the force transducer could not be obtained during the flaming tests, because the sample expanded and bulged up to contact the pilot burner tube which interfered with the weight loss measurement. This problem was circumvented during the nonflaming tests by removing the pilot burner tube.

The polyphosphazene material (12 mm thick) was cut for testing into 50 mm squares weighing about 4.5 g each. After testing the char residue was weighed. The peak mass loss rate was determined from the force transducer data for the nonflaming tests. This data is summarized in Table 2. During combustion, the sample expands to about 2.5 times its original volume, forming a black porous char. The char weight ranged from 52% to 67% of the initial sample weight, with char weight decreasing as the radiant flux or ventilation gas temperature is increased. Under identical test conditions, the amount of char residue produced under flaming combustion is somewhat less than that produced under nonflaming combustion. For the nonflaming tests the greatest mass loss rate (about 0.5 $mg/s\text{-}cm^2$) was observed at the higher radiant flux or the highest ventilation gas temperature.

The smoke physical properties data for burning polyphosphazene insulation material is summarized in Table 3. The mean particle size D_{32} and optical density vary with time during a test, thus the peak optical density and the corresponding mean particle size are given in Table 3. For the nonflaming tests, the mean particle size ranged between 0.4 and 0.5

Table 2. Sample Weight Loss Data for Polyphosphazene Foam Insulation Material.

Mode	Ventilation Air Temperature (°C)	Radiant Flux (W/cm^2)	Peak Mass Loss Rate (mg/cm^2-s)	Char Residue (% of Initial Weight)
NF	25	5 W/cm^2	0.16	66.9
NF	25	7.5 W/cm^2	0.52	53.8
NF	100	5 W/cm^2	0.22	63.1
NF	300	5 W/cm^2	0.52	55.6
F	25	5 W/cm^2	-	63.7
F	100	5 W/cm^2	-	58.7
F	300	5 W/cm^2	-	51.9

Table 3. Smoke Properties Data for Polyphosphazene Wall Insulation Material.

Mode	T (^{o}C)	Radiant Flux (W/cm^2)	D_{MMD} (μm)		OD_{max} (m^{-1})		D_{32}* (μm)	Time to Peak OD (min)
					Blue	Red		
NF	25	5	.019		0.21	0.10	0.39	3.3
NF	25	7.5	.046	0.51 1.44	1.23	0.79	0.47	0.9
NF	100	5			0.24	0.17	0.42	2.4
NF	300	5			0.56[a]	0.27[a]		1.1
F	25	5	.017		0.64	0.49	1.07	1.7
F	100	5			0.56	0.51	1.12	1.1
F	300	5			1.17[b]	0.90[b]	1.17	0.5

* Average of data points near OD_{max}.

a Attributed to gas phase absorption, no measurable scattered light.

b First and largest of two peaks.

micron, while much larger particles of about 1.1 micron were produced during flaming combustion. Ambient temperature had little effect upon mean particle size. For the nonflaming test at 7.5 W/cm^2, the mass median diameter (D_{MMD}) obtained from the cascade impactor sample is in excellent agreement with the D_{32} value obtained optically. For this case the particles consisted of a mixture of spherical yellowish liquid droplets and a dark brown material. For flaming combustion, the sampling and optical data indicated the smoke consisted mostly of irregularly shaped soot particles.

A comparison of D_{32} versus time for flaming and nonflaming tests in room temperature air is given in Figure 1. The corresponding optical density curves are given in Figure 2. Visual observations during the flaming tests revealed that the period of flaming combustion (where peaks in D_{32} and optical density occur) is very brief, lasting only 20 to 30 seconds. Referring to Table 3, the highest peak optical densities (.488 μ m wavelength) of about 1.2 m^{-1} were obtained for nonflaming combustion at 7.5 W/cm^2 in room temperature air and for flaming combustion in air at 300°C. The lowest peak optical densities of about 0.2 m^{-1} were obtained for nonflaming combustion in low temperature (25°C and 100°C) atmospheres.

The fraction of mass loss converted to particulates (Γ-values) for the room temperature tests are also given in Table 3. For both flaming and nonflaming combustion only about 2% of the total mass loss is converted to smoke particulates under 5 W/cm^2 radiant flux. Increasing the radiant flux to 7.5 W/cm^2 more than doubles the value of Γ for nonflaming combustion.

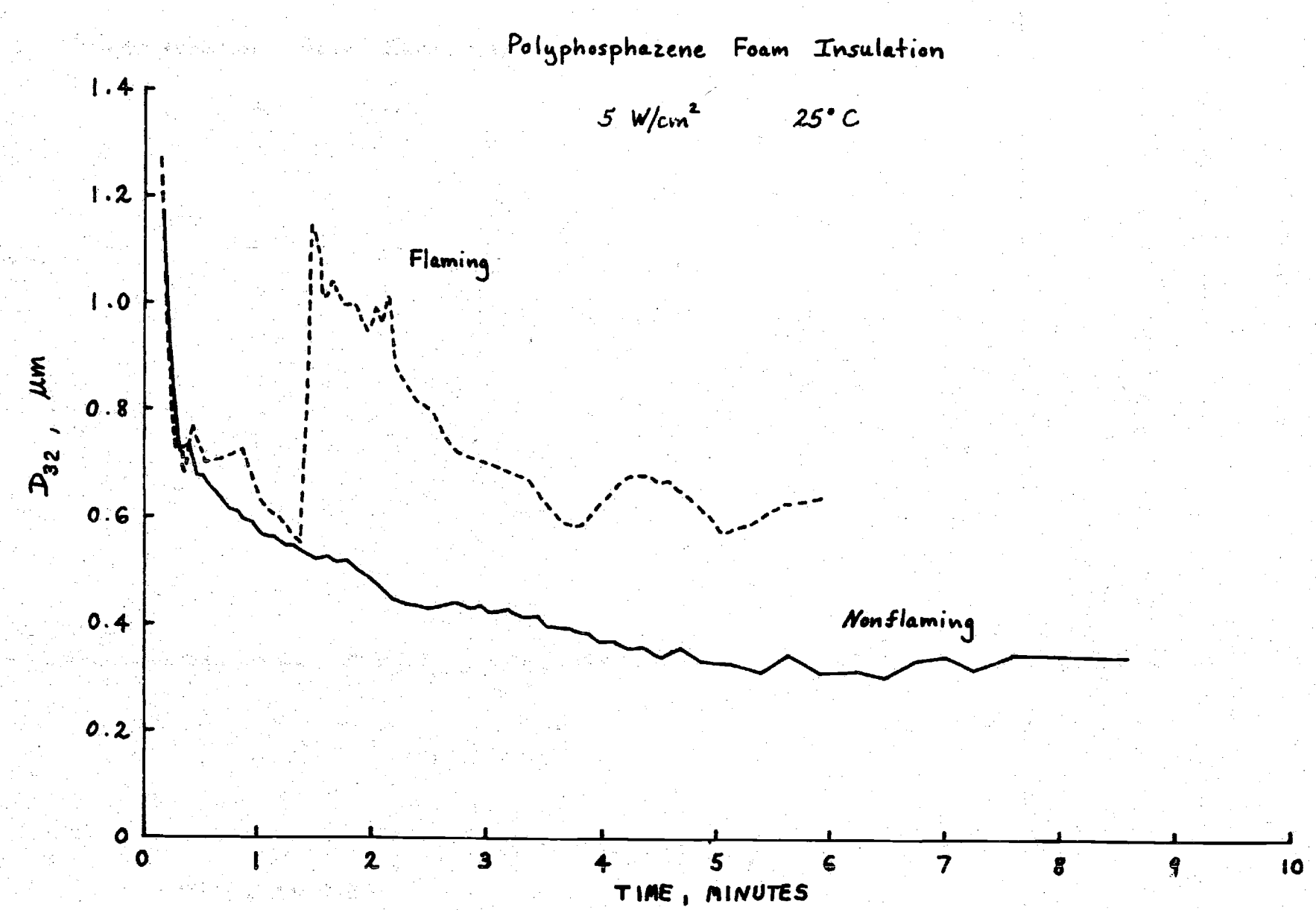

Figure 1. Smoke mean particle diameters for flaming and nonflaming combustion of polyphosphazene foam insulation exposed to a radiant flux of 5 W/cm^2 in room-temperature ventilation air (25°C).

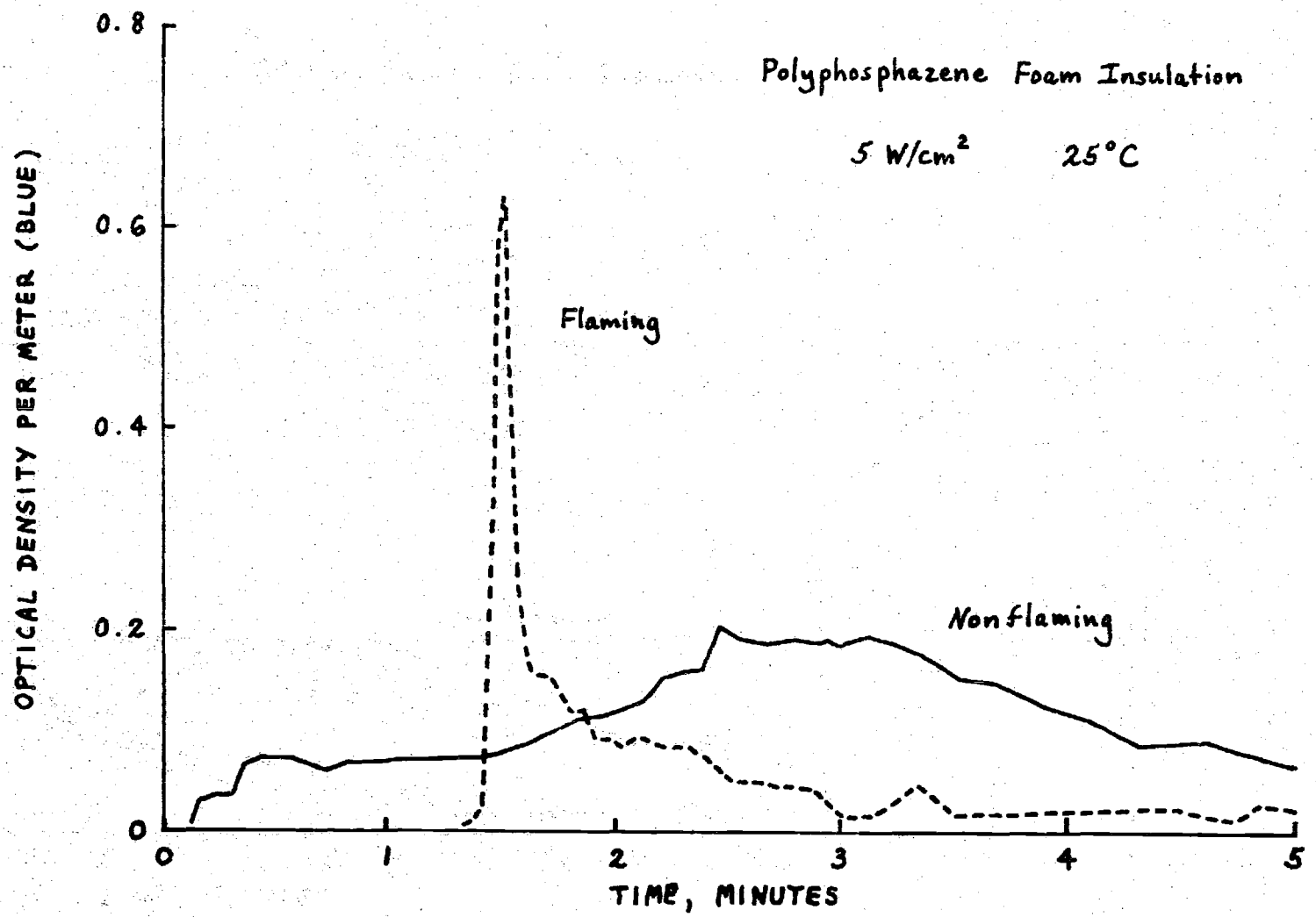

Figure 2. Smoke optical densities for flaming and nonflaming combustion of polyphosphazene foam insulation exposed to a radiant flux of 5 W/cm^2 in room-temperature ventilation air (25°C).

Tests of Chlorid Alkyd Paint. Both flaming and nonflaming tests of the chlorid alkyd paint have been conducted in room temperature atmospheres with a radiant flux of 5 W/cm^2. Samples consisted of ten coats of paint brushed onto 50 mm squares of 0.8 mm thick steel sheet stock (without primer), which gave about 10 g of paint per sample. After combustion the residue had a thin, brittle white surface skin with large cracks revealing black flaky char layers underneath. Some swelling occurred with a maximum thickness of about 6 mm. For both flaming and nonflaming conditions slightly more than 80% of the initial sample weight remained as char. Peak mass loss rates of about 0.4 $mg/s-cm^2$ were obtained from the force transducer data for both combustion modes.

Cascade impactor samples were obtained for both flaming and nonflaming tests. For nonflaming combustion the particulates consisted of pale yellow spherical liquid droplets with a mass median diameter (D_{MMD}) of about 0.9 micron. For this case slightly more than 10% of the total mass loss appeared as particulates. For flaming combustion black sooty particulates were collected with a D_{MMD} of about 0.6 micron, while only 3% of the total mass loss appeared as particulates.

The in situ optical system was used to obtain mean particle diameters (D_{32}) and optical densities produced by flaming and nonflaming combustion of the chlorid alkyd paint samples. A comparison of mean particle sizes for flaming and nonflaming combustion are given in Figure 3, while the corresponding optical densities are given in Figure 4.

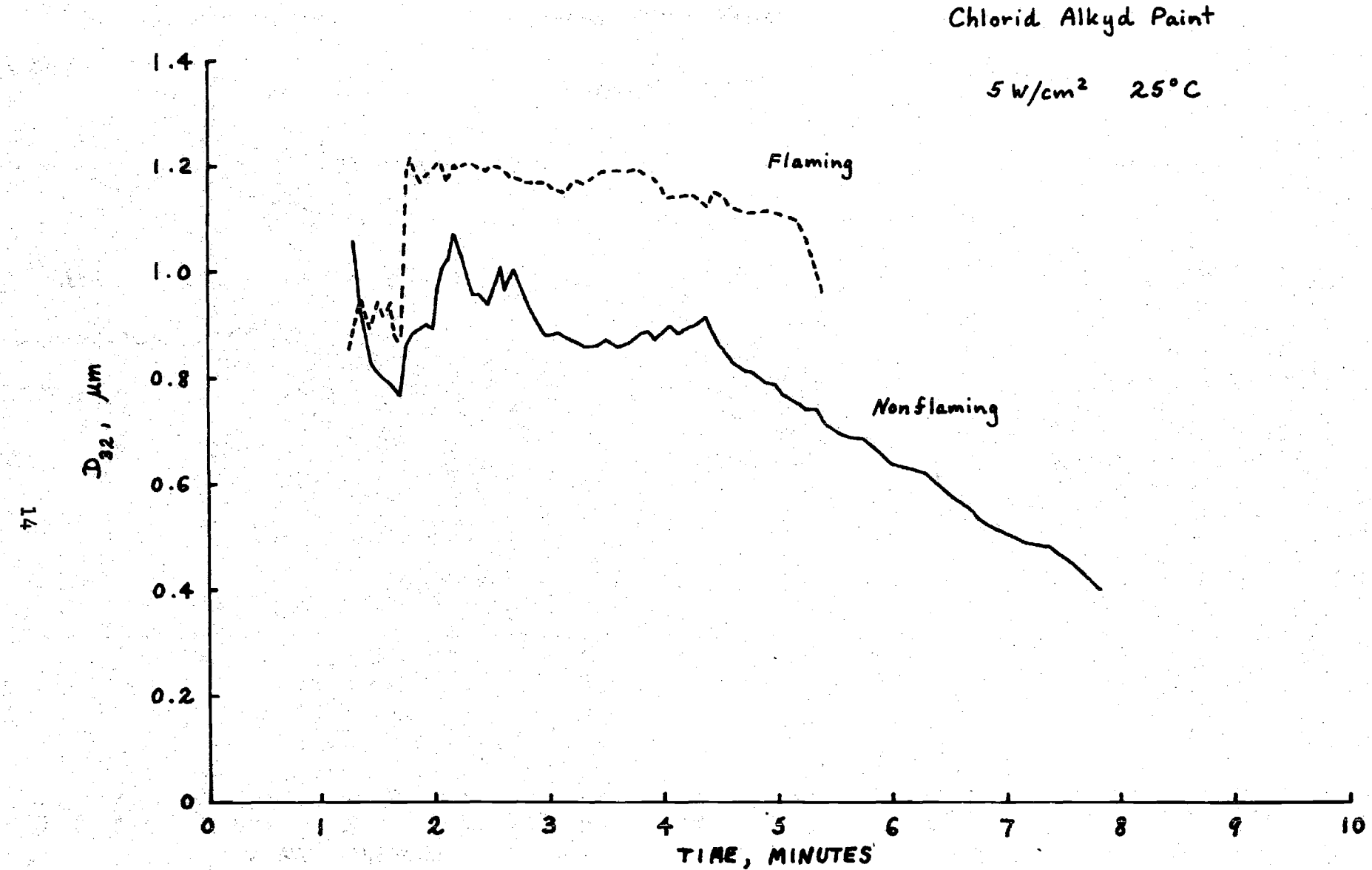

Figure 3. Smoke mean particle diameters for flaming and nonflaming combustion of chlorid alkyd paint exposed to a radiant flux of 5 W/cm^2 in room-temperature ventilation air (25°C).

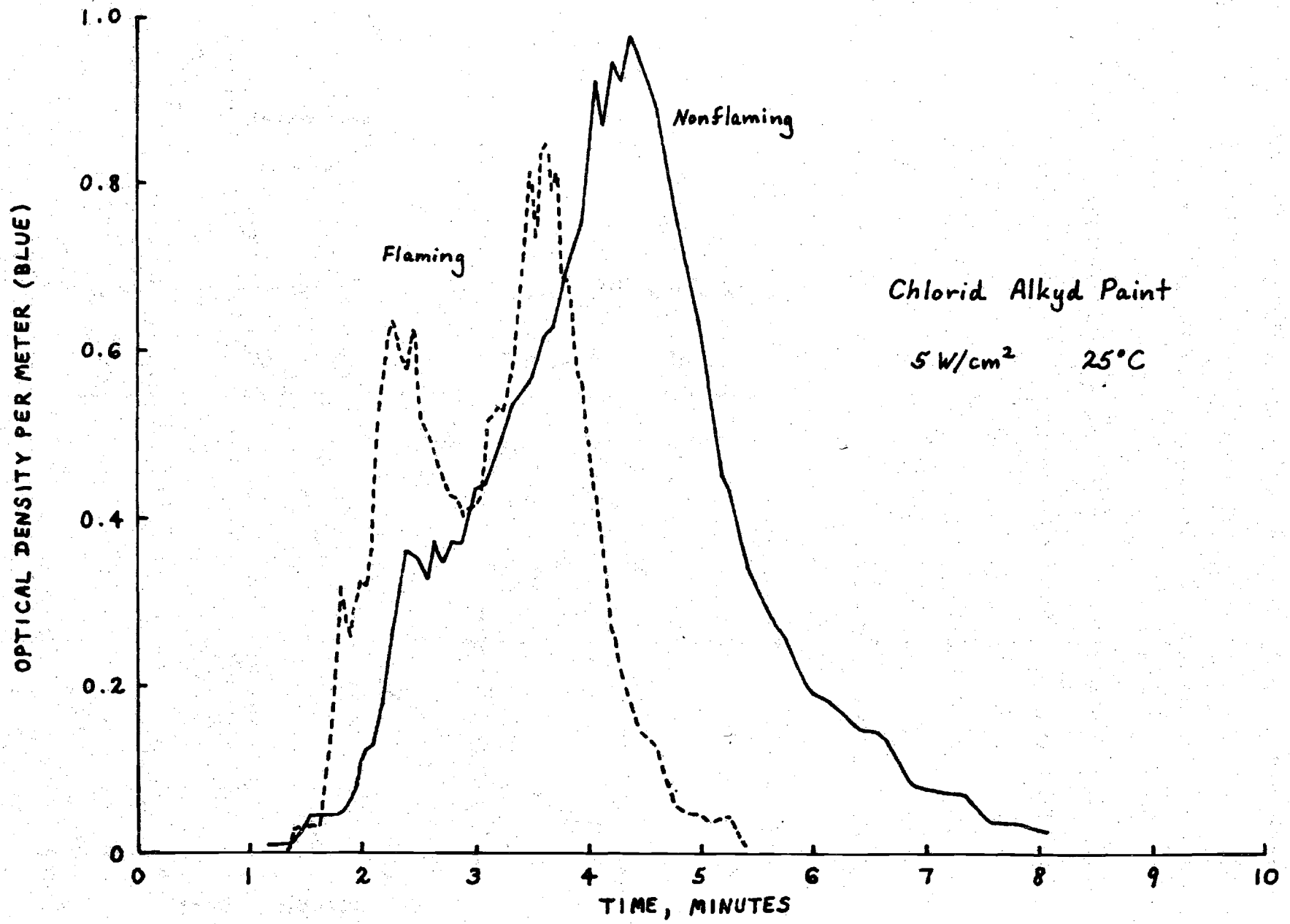

Figure 4. Smoke optical densities for flaming and nonflaming combustion of chlorid alkyd paint exposed to a radiant flux of 5 W/cm^2 in room-temperature ventilation air (25°C).

For nonflaming combustion, the mean particle diameters vary between 0.7 and 1.1 microns during the initial stages of pyrolysis and average about 0.85 micron during the time of maximum optical density. This latter value is in very good agreement with the mass median diameter obtained by cascade impactor sampling. The optical density at the blue-green argon line (.488 μ m) rises smoothly to a peak of about 1.0 m^{-1} about five minutes after initiation of exposure and then smoothly declines. The optical measurements obtained during the period of maximum light obscuration also yielded a particle refractive index of about 1.35 and a particle volume fraction of about 0.4 ppm.

For flaming combustion, the mean particle diameters are nearly constant throughout the test, ranging between 1.1 and 1.2 microns. The mean diameter obtained optically (D_{32}) is nearly twice that obtained by particle sampling (D_{MMD}) for flaming combustion. This discrepancy is probably due to the nonspherical shape of the soot particle agglomerates produced under flaming combustion. The curves of optical density versus time exhibit two pronounced peaks; the second of these occurring after about 3.5 minutes and reaching about 0.85 m^{-1} (blue-green).

A-II. Chemical Analysis of Smoke Particulates.

The effort during the current grant period has been directed towards two primary goals, namely investigation of the combustion products of polyphosphazene insulation material and an extension of mechanistic studies into processes leading to particulate smoke formation during combustion of

chlorinated polymers.

1) The precise composition of the polyphosphazene material supplied by the Office of Naval Research was unclear, in that the original supplier (Horizons, Co.) was no longer in production and personnel originally responsible for its manufacture were unable to provide detailed information on the polymer composition. The following description of the material is, nonetheless, believed to be reliable.

The backbone of the polymer is the 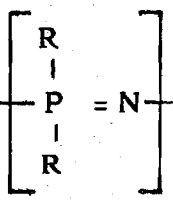 unit, in which R may be 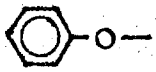 or 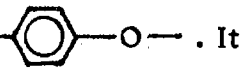 . It is not clear which functional group R was present in our samples, or whether this would make any significant difference to the test results. Additives in the formulation were alumina trihydrate ($Al_2O_3.3H_2O$), magnesium oxide (MgO), benzoyl peroxide $(C_6H_5.CO_2)_2$ and dialkyl phthalate $(C_6H_5(COOR)_2)$. The relative amounts of these substances present were not known.

2) The polyphosphazene samples were subjected to 5 W/cm^2 incident heat for nonflaming oxidative pyrolysis studies. A flaming combustion mode could not be sustained for a time adequate to collect smoke particulates reliably. All data reported herein refer, therefore, to nonflaming combustion studies.

3) Particulates were collected and separated into compound classes using well-established procedures developed in our laboratories and described previously[1]. Data on the extractable portion of the particulates indicated that 8.5 mg of smoke particulate was generated per gram of polymer combusted. Of this particulate matter, 2.3 mg was extractable organic material, representing approximately 27.1% of the total particulate smoke.

The major classes of extractable organic compounds identified in the particulate smoke were aliphatic hydrocarbons (63.7%), oxygenated aliphatic hydrocarbons (19.4%), cyano-aliphatic hydrocarbons (5.1%), polynuclear aromatic hydrocarbons (2.5%) and oxygenated aromatic hydrocarbons (9.3%). The figures in parentheses represent the mass percent found in each class. The lack of any phosphorus containing compounds in the particulate smoke is significant and indicates that probably any phosphorus compounds evolved, such as phosphine and organophosphorus compounds, are sufficiently volatile to remain in the vapor phase and are not trapped to any appreciable degree on smoke particulates. It is possible also that some phosphorus remains in the residue as inorganic phosphorus.

In addition to the studies with polyphosphazene polymeric material, chlorinated polymers of various formulations were tested to examine the influence of chlorinated species on the combustion process, in comparison with the corresponding unchlorinated species. Studies were run in tandem for flaming and nonflaming combustion modes with polyvinyl chloride polymer

and polypropylene. A complete description of this work, together with detailed compositional profiles of the tested materials, can be found in resulting publications which are enclosed in Appendix A. The results can be summarized briefly as follows.

1) In the nonflaming mode, the chemical composition profiles for both polyvinyl chloride (PVC) and polypropylene(PP) are very similar, with aliphatic compounds overwhelmingly predominating over the aromatic (typically 140:1 mass ratio). This indicates that the "fuel" molecules produced by the initial degradation step are similar.

2) By contrast, in the flaming mode of combustion, approximately twice the soot and about thirty times the relative amount of extractable organic compounds are cleared from PVC as compared to PP. It is postulated that this is a consequence of the presence of greater amounts of reactive substituted aromatic species resulting from the PVC combustion than from the PP combustion. As supporting evidence of this postulate, the compositions of the compounds extracted from the particulates show much similarity, and so it is unlikely that greatly different species are responsible for particulate formation from the two polymer types.

3) Chemical composition data show that a high percentage of aliphatic hydrocarbons are present in the nonflaming mode. This suggests that relatively small aliphatic hydrocarbons (C_2 to C_{12}) rather than large linear macromolecules go to form the building blocks of particulate smoke in flaming combustion.

4) The influence of typical additives used in PVC formulation shows as a relatively minor variation in the relative amounts of polynuclear aromatic species found in the particulate smoke. The variation in the overall net yields is considered to be primarily a consequence of physical changes in the combustion process induced by the additives, rather than resulting from any major changes in the chemical pathways leading to the soot formation.

Summary of Task B Progress

This section summarizes the accomplishments under Task B over the last twelve months. This task has been concerned with the investigation of the effect of additives upon soot formation in polymer diffusion flames and the development of an understanding of the mechanisms responsible for soot generation in these flames. Both of these activities are being pursued in an effort to develop effective means for the suppression of soot generation in polymer flames.

The activities under this task consisted of: (1) completion of the work on the effect of alkali and alkali earth metals upon soot formation in polyethylene diffusion flames; (2) preparation of publications describing the results of the additives research for Combustion and Flame and the European Combustion Symposium; (3) development of appropriate burners for the investigation of soot formation in opposed flow flat diffusion flames; (4) development of a theoretical model of soot formation in opposed flow diffusion flames; and (5) development of an optical system for the in situ

measurement of soot generation and growth in laboratory flames. In what follows, a brief description of these activities is provided and the resulting publications are enclosed in Appendix A.

B-I. Effect of Additives Upon Soot Formation in Polyethylene Diffusion Flames.

This study was motivated by the need to understand the mechanisms of soot formation on polymer flames whose use in all walks of life, including ships and submarines, has drastically increased in recent years. The main objective of the study was the determination of additives whose presence in polymer flames would destructively interfere with key steps in the soot formation process, leading to the suppression of soot formation.

In the present study a series of experiments was conducted in which 2 gm cylindrical discs of pure, filler free, unstabilized, low density polyethylene (LDPE) were burned in the Smoke Generation and Measurement Apparatus (SGMA)[2], shown in Fig. 5. Nebulized aqueous solutions of CsCl, NaCl, KCl and $BaCl_2$ additives were injected into the flames during the tests and their effects upon soot production were determined. In a test, the LDPE sample was placed in the pyrolysis cup shown in Fig. 6 and heat provided by the nichrome wire resulted in melting and thermal degradation of the sample. The generated mixture of gaseous fuels mixed with the surrounding stream of air and burned in a diffusion flame similar to the one shown in Fig. 7. When the smoke opacity measurement by the photomultiplier indicated that the flame reached a quasi-steady state, a

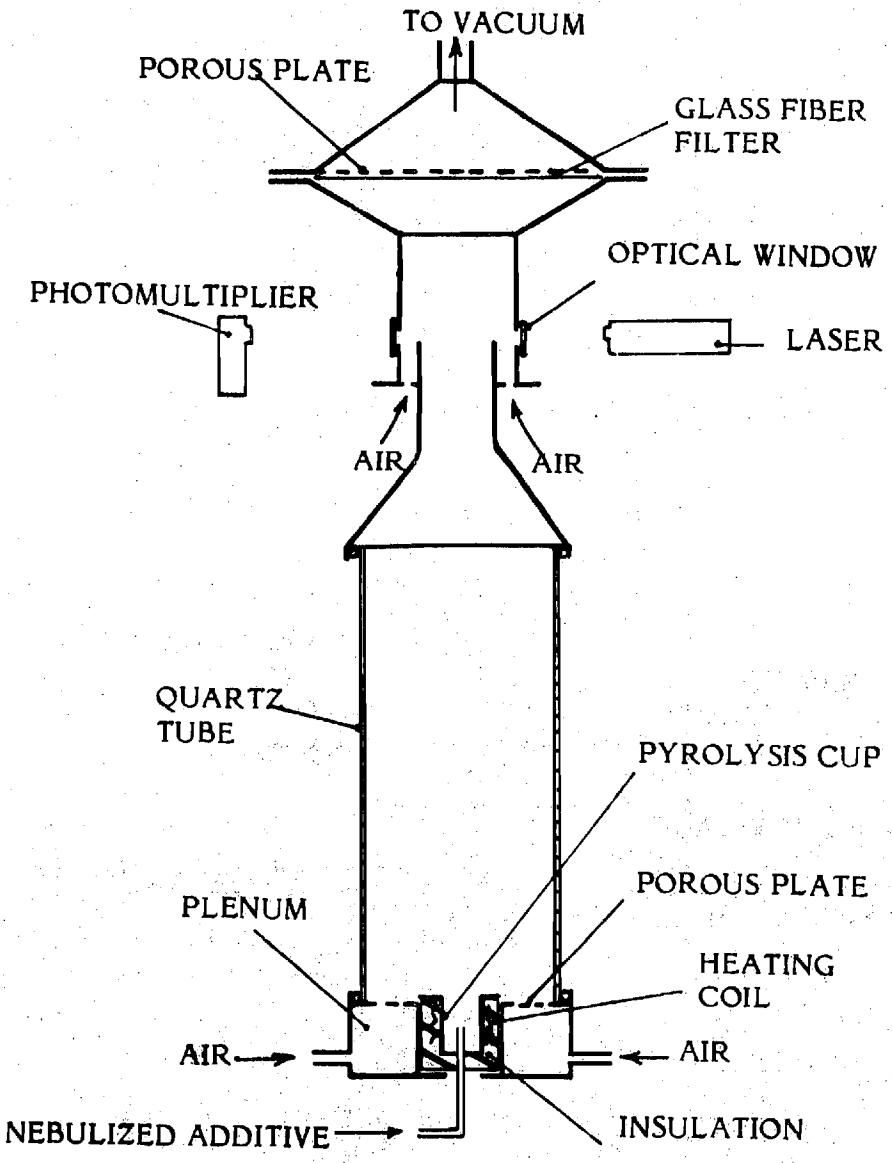

Figure 5. The smoke generation and measurement apparatus (SGMA).

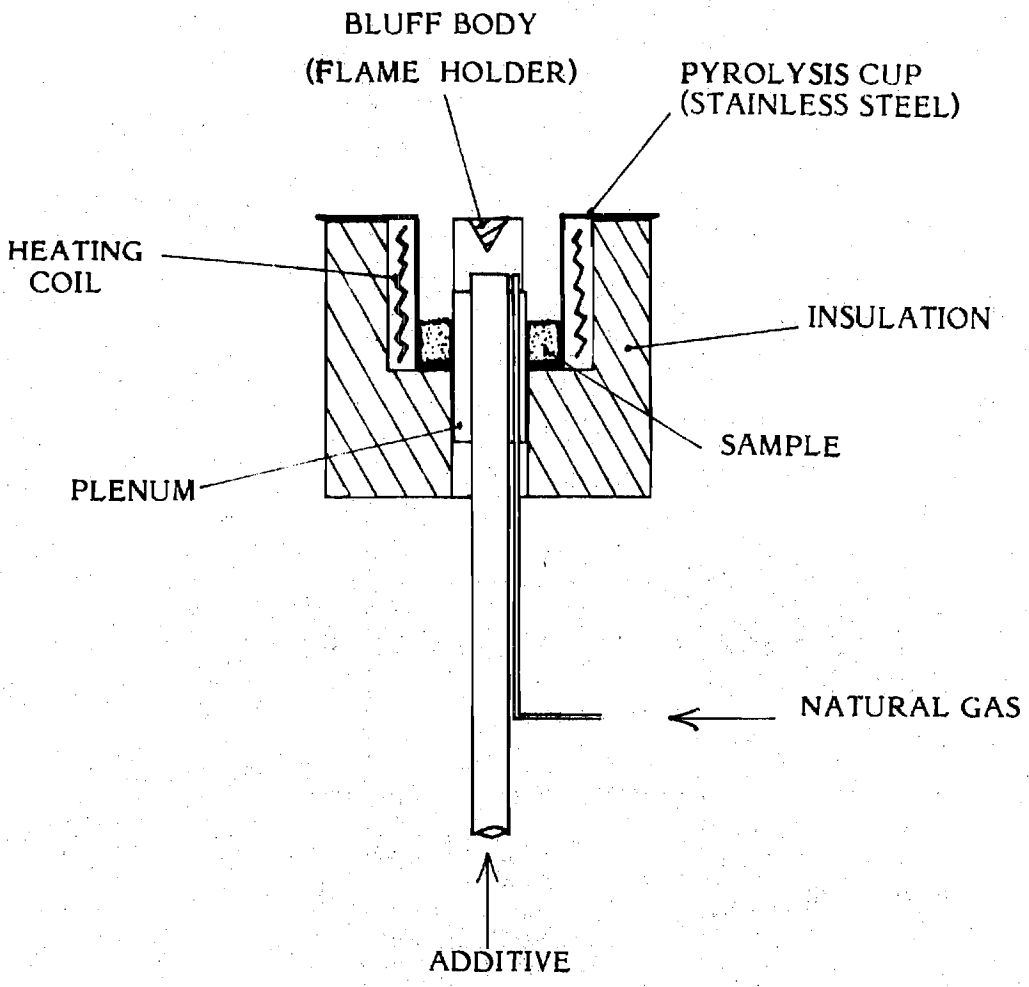

Figure 6. Heating arrangement for the stainless steel pyrolysis cup.

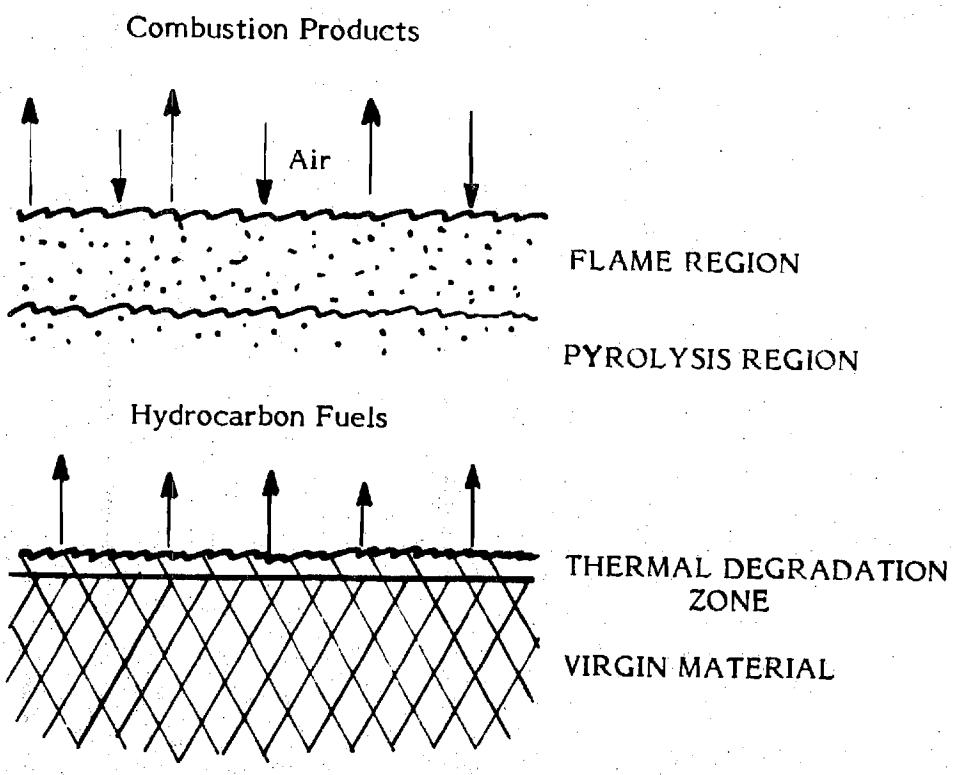

Figure 7. Schematic of a polymer diffusion flame.

stream of nebulized additive solution was injected into the pyrolysis region where it mixed with the fuel stream before and during combustion.

The generated particulates were filtered out of the flue gases by a glass-fiber filter paper of known initial weight. Differential weighing of the filter paper allowed for the determination of the total weight of particulates generated during the test, after accounting for the deposits on the apparatus walls. The light attenuation measurement provided a qualitative check on the gravimetric measurement. The tests were conducted using various concentrations of the additives and at two nichrome wire heating rates. Since the oxidizer flow rate was unchanged between tests, each nichrome wire heating rate resulted in a different fuel/air ratio in the flame.

At the end of every experiment, the tube carrying the additive from the nebulizer to the flame was repeatedly washed with deionized water and the resulting solution was run through an inductively coupled Plasma Emission Spectrophotometer to determine the amount of metal in the solution. Since the amount of metal in the solution before the experiment was known, the weight of metal that went into the flame could be determined.

Finally, to determine the effect of the various additives upon the physical characteristics of the generated smoke particulates, soot samples were extracted on copper electron microscope grids from the flame region and from the flue gases at a distance of 35 cm above the flame. Transmission electron micrographs (TEM) of the collected particulates were

taken (See Figs 8 and 9) to determine their sizes as well as their state of aggregation. For each test condition the diameters of over 800 individual soot particles were measured in a Zeiss image analyser and the mean of these diameters was determined.

Data collected in tests with Cs, K and Na are presented in graphical and tabular forms in Fig. 10 and Table 4, respectively. Figure 10 presents the mass fraction of the original sample that was converted into particulate matter plotted versus the amount of additive used up during the test, for experiments conducted at two effective fuel/air ratios. To better illustrate the behavior of the data, curves were drawn through the two sets of data obtained from Cs seeded flames. One should also note that many of the tests were repeated in order to check the reproducibility of the data.

The effect of the additives upon soot production are deduced by comparing the soot yield obtained in tests where additives were used with the yield obtained in a similar test where only deionized water (i.e., zero additive concentration) was added. This comparison reveals (see Fig. 10) that for the concentration levels used in this study the alkali metallic additives are effective soot suppressants and that their effectivenesses follows the order Cs > K > Na. Furthermore, Table 4 shows that the magnitude of the measured mean soot particle diameter depends upon the type of additive; being the smallest for Cs addition and increasing according to the indicated order. It should also be noted that the magnitudes of the first ionization potentials of these three metals follow the same order. Thus, the results of this investigation with LDPE diffusion flames support earlier claims[3,4,5,6]

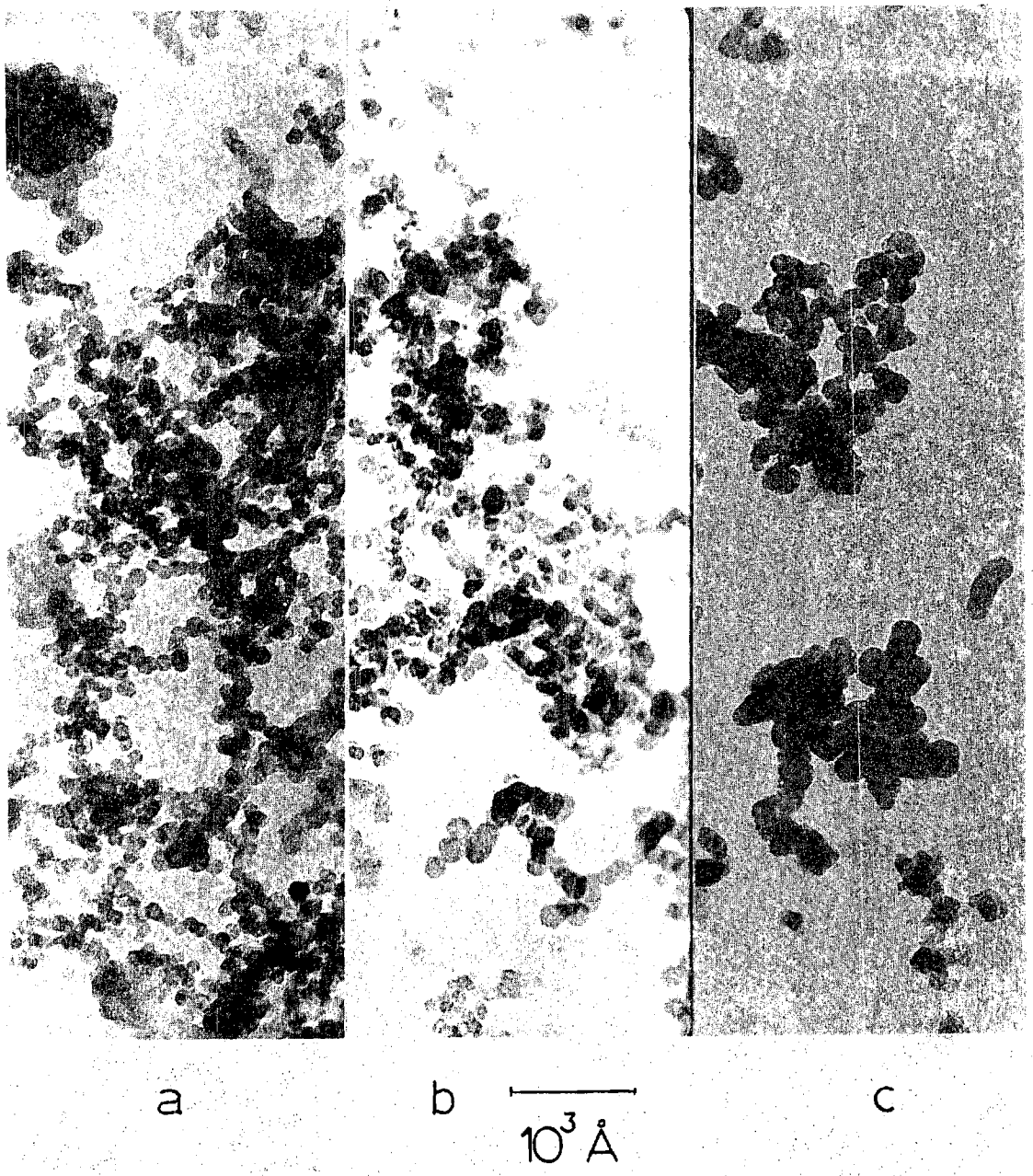

Figure 8. Electron transmission micrographs of smoke particulates extracted from polyethylene flame regions which were seeded with (a) no additive; (b) CsCl; and (c) $BaCl_2$.

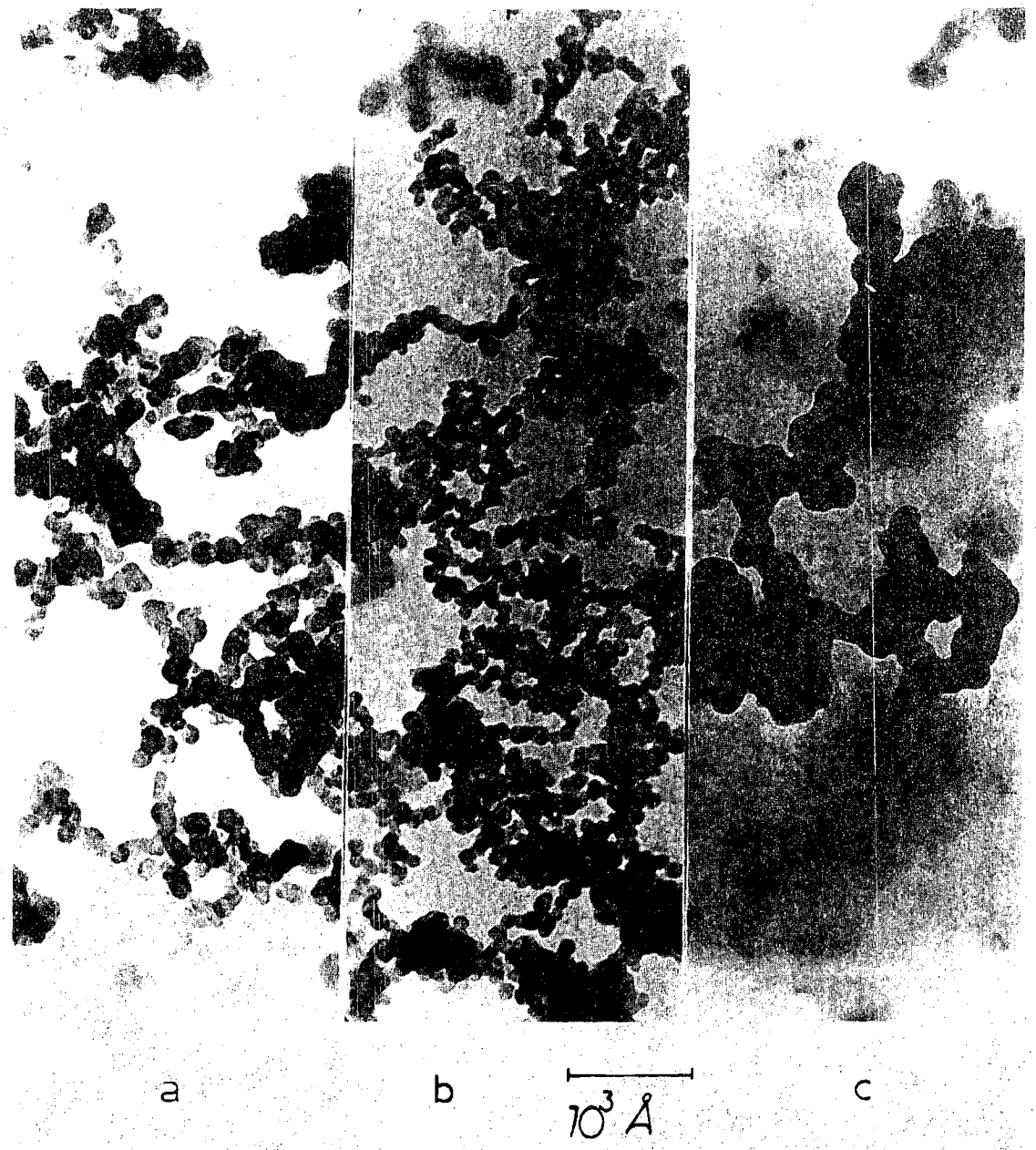

Figure 9. Electron transmission micrographs of smoke particulates extracted 35 cm above polyethylene flames which were seeded with (a) no additive, (b) CsCl; and (c) $BaCl_2$.

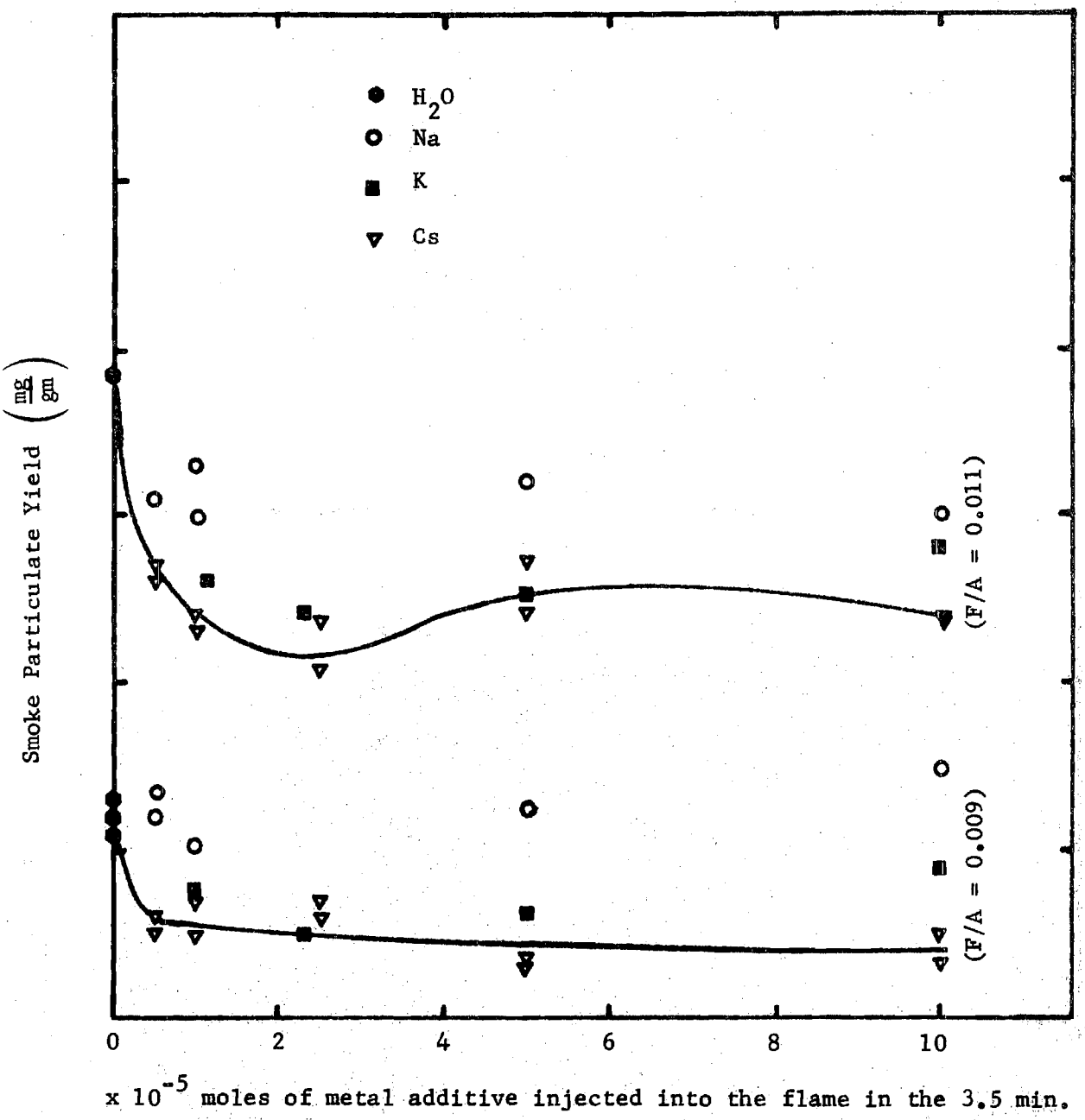

Figure 10. The effects of Na, K, and Cs upon soot formation in a LDPE flame.

Table 4. The Effects of Na, K, and Cs upon Soot Formation in a LDPE flame.

Additive	First Ionization Potential of the Metal eV	Mean Soot Particle Size in the Flame A	Percent Soot Suppression
H_2O	12.56	218	0 %
NaCl	5.12	211	20.9 %
KCL	4.32	174	27.4 %
CsCl (1.0M)	3.87	135	38.9 %
CsCl (.5M)		155	33.0 %
CsCl (.1M)		189	38.9 %

* The above results were obtained for fuel-rich flames and additive injection rates of 2.86×10^{-5} moles/min for alkali metals (1.0M). The statistically determined error range in the particle sizes is of the order of $\pm$ 4 A at 95 % confidence level.

that alkali metallic additives affect soot formation in flames via a mechanism that depends upon the magnitude of their ionization potentials.

Furthermore, comparisons of the measured soot yield (proportional to ND^3) and mean soot diameters (i.e., D) produced in flames with and without alkali additives indicate that the presence of the additive in the flame resulted in an increase in the density N of the soot particles. This observation is significant as it may help to resolve an existing controversy regarding the mechanisms through which these additives affect soot formation[7]. According to Haynes et al[4]; who investigated the effect of the same additives upon soot formation in premixed flames, these additives ionize in the flame and thus result in a higher concentration of ions in the flame region. This, in turn, leads to a more rapid and complete ionization of the young soot particles. The charged soot particles resist further coagulation by coulombic repulsion, which results in a larger number of smaller diameter particles. In contrast, Bulewicz et al[6], who investigated the effect of these additives in gaseous fuel diffusion flames, argued that alkali additives inhibit the nucleation process by ionizing in the flame and reducing the concentration of positively charged ion hydrocarbon precursors via charge transfer-reactions. Such a decrease in the concentration of hydrocarbon ions would then be expected to result in a decrease in the nucleation rate, the total amount of soot produced and the number density N of the soot particles. While Bulewicz et al observed both an increase and a reduction in the total amount of soot produced, depending upon the amount of additive, they did not measure the resulting particle number densities and size distributions.

The results of the present study are in agreement with the results of Haynes et al who also found that the alkali metal addition results in an increase in the number density of the soot particles and a decrease in the size of the soot particles. Consequently, the results of the present study lend further support to Haynes' hypothesis that argued that alkali metal additives exert a post nucleation effect by inhibiting the particle coagulation process. The observed soot reduction is attributed to the fact that a larger fraction of the smaller diameter particles burns as these particles move through the flame region.

While the present results support Haynes' hypothesis, a question remains regarding the particulate charging process. Haynes et al argued that the increased concentration of ionic species in the flames, due to the alkali metal addition, resulted in complete ionization of the young soot particles. Considering the low ionization potentials of the alkali metals, it is not clear how their presence can lead to the ionization of the soot particles; a question that was also raised in a recent review of this problem by Howard and Kausch[7]. An alternate explanation might be that the charging of the young soot particles occurs when they attach themselves to the alkali metal ions.

Another possible explanation of the trends observed in this study could be the "electronic mechanism" proposed by Bowser and Weinberg. According to this mechanism, the electrons released by the ionized metal neutralize some of the positively charged young soot particles. The resulting reduction in the concentration of charged soot particles may result, under certain conditions[5,7] in a decrease in the rate of particle coagulation,

leading to a larger number of smaller diameter particles, as observed in the current study.

The effect of barium upon soot formation is discussed separately as contrary to the previously discussed additives which are alkali metals, since barium is an alkaline earth metal. To examine the differences between these two classes of compounds, the effect of barium upon soot formation will be examined by comparing it with the effect of the previously discussed caesium addition. These two effects are examined in Fig. 11 that is similar to Fig. 10. Examination of Fig. 11 shows that barium exhibits anti-soot effects which increase with additive concentration. Furthermore, Figs. 8c and 9c show that the smoke particulates extracted from a Ba seeded flame are not as small, distinct or spherical as the particulates extracted from the Cs seeded flame. Actually, Table 5 shows that soot particulates from the Ba seeded flame have comparable diameters to those from the unseeded flame. One should also note that while the large particulates in Fig. 8c have the structure of soot particles (agglomerates) that appear in the other figures, the few small diameter particles in this figure do not have soot-like structure. It is possible that these small particles are actually barium salt crystals. Therefore, it seems that Ba and Cs affect soot formation in flames through different mechanisms.

Previous investigations[8] of related problems have explained the soot suppression action of Ba by the fact that Ba readily catalyses flame reactions that produce OH radicals[9]. These radicals then proceed to oxidize soot particles via the reaction:

$$C_{solid} + OH \rightleftharpoons CO + \frac{1}{2} H_2$$

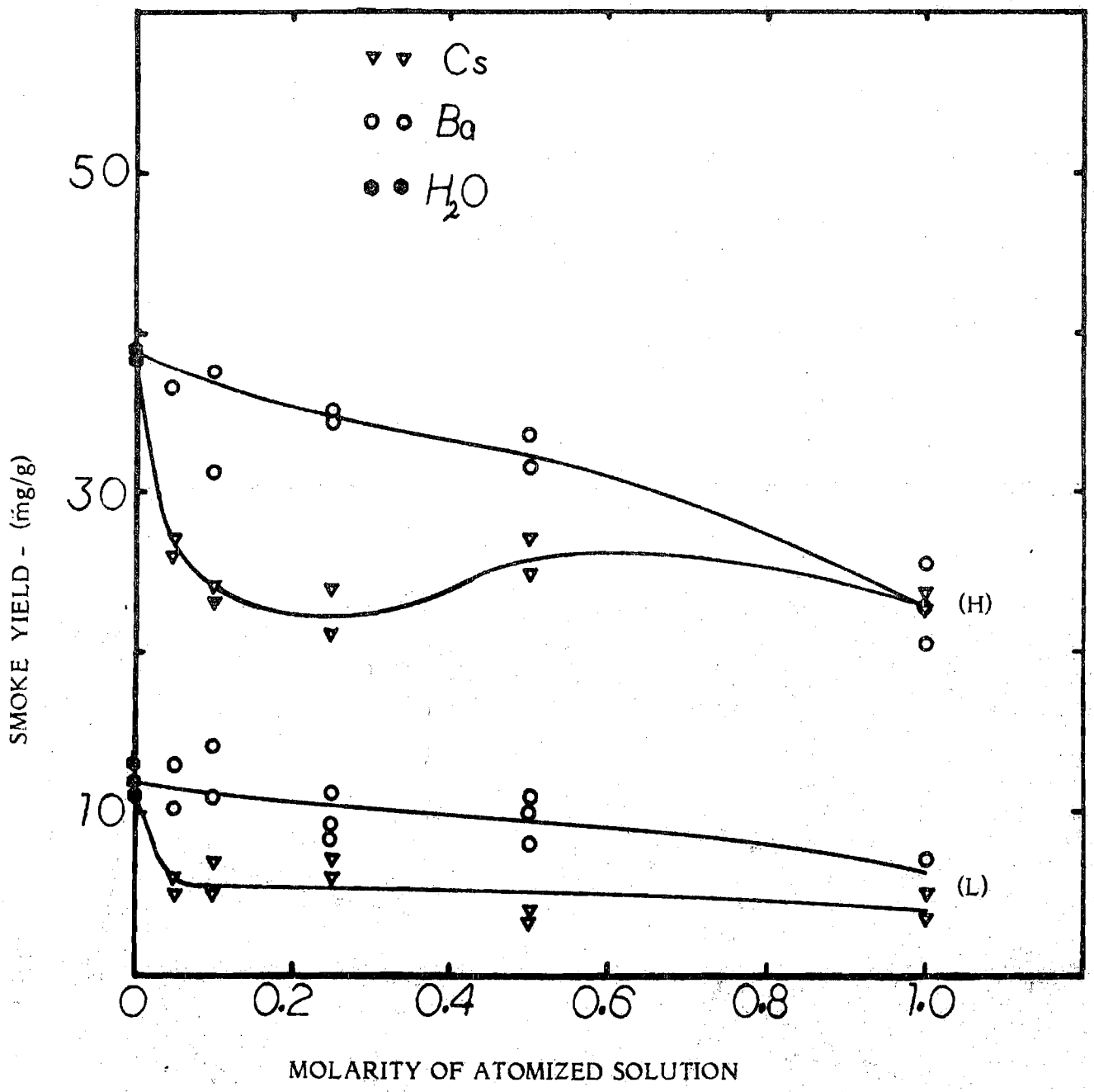

Figure 11. Effects of Ba (O) and Cs (▽) on the amount of smoke generated from polyethylene samples subjected to various external heating rates: (L) 92.7 watts, (H) 98.0 watts.

Table 5. Mean Smoke Particulate Diameters Determined From TEM*

Additive	Mean Smoke Particulate Size in the Flame (A)	Mean Smoke Particulate Size 35 cm Above the Flame (A)
Deionized water	218.0	292.8
CsCl solution	134.7	186.4
$BaCl_2$ solution	236.9	275.9

* Above results were obtained at 98 watts heating rate and additive concentration of 1.0 M.

If these hypotheses are correct, then OH radicals could have been readily produced in the experiments conducted in this program through the dissociation of the water used in the solution of the $BaCl_2$ additive. The latter suggestion does not exclude the possible production of OH radicals from other flame reactions and from the dissociation of water vapor produced in the flame. Considering the arguments presented above, it appears that the flames investigated in this program may have presented a situation where the production of OH radicals in the pyrolysis zone was higher than in corresponding flames with no additives. Therefore, one can argue that the increase in OH radical concentration in the pyrolysis region may have also resulted in increased oxidation of soot precursors such as unstable polycyclic aromatics and/or polyacetylenes[10,11]. The reduction in the concentrations of these soot precursors would result in reduced soot particle number density in the flame. Such a decrease can be deduced from analyses of the data in Fig. 8 and Table 5, where it is clearly shown that Ba addition resulted in the reduction in the smoke yield without considerably affecting the mean particle size. Consequently, the smoke particle number density was reduced by the addition of Ba. This effect was qualitatively observed in the TEM. Thus, the results obtained here are consistent with the previously advanced argument[8] as to the mode of action of Ba.

Analysis of additive investigation to date, indicate that alkali metals (i.e., Cs, K and Na) and the Ba additives reduce soot formation in polymer diffusion flames through entirely different mechanisms. The results suggest that the presence of Cs, K and Na in the flame results in electric charging of young soot particles. The resulting coulombic repulsion between the charged particles inhibits coagulation and agglomeration processes leading to the formation of a larger number (as compared to unseeded flame) of

smaller diameter soot particles. It appears that a large fraction of these smaller particles are oxidized upon passage through the flame region, resulting in a net reduction in soot yield.

Results obtained with Ba additives indicates that Ba additives reduce the total smoke yield while apparently not affecting coagulation and agglomeration processes. These trends can be explained using arguments advanced elsewhere[8] which suggest that Ba additives catalyze reactions that produce OH radicals in the flame. These OH radicals are expected to oxidize both soot precursors and young soot particles, resulting in a net reduction in the soot particle number density in the flame. This reduction is apparently responsible for the observed decrease in soot yield. To confirm this hypothesis, independent measurements of the dependence of OH concentration in the flame region upon the amount of added Ba should be conducted. Also, the nature of the reactions between OH radicals and compounds that are believed to be soot precursors would be investigated.

Finally, the results of this investigation suggest that all of the additives investigated in this study can potentially be used as smoke suppressants in polymer diffusion flames.

B-II. Investigation of Soot Formation in Opposed Flow Polymer Diffusion Flames.

In this task the mechanism of the suppression of soot by additives is being investigated. The general chronology of soot formation is now widely accepted although little agreement exists on the precise nature of the individual steps. During combustion, the burning polymer surface first melts.

A primary pyrolysis reaction in this melt liberates a gaseous fuel which travels through a region of increasing temperature towards the flame front. During this period the main pyrolysis occurs which first breaks down the fuel molecules to simpler species. These then react to form larger molecules, polycyclic aromatic hydrocarbons (PAHs) or polyacetylenes (PAs), some of which act as soot particle precursors, the exact nature of which are as yet unknown. Nucleation then occurs by mechanisms which may differ for different types of flames. The nuclei then grow into spherical soot particles or spheroids by a combination of small particle coagulation and surface deposition of large hydrocarbon molecules. The spheroids finally agglomerate to form the chain like soot aggregates observed in the smoke down-stream of the flame. In and beyond the flame front soot burn out competes with each of the steps in soot formation described above. Since the individual processes leading up to smoke formation are not well established, the mechanisms by which additives interfere in the soot formation process are open to speculation. It may, however, be expected that different classes of additives affect different steps in the process outlined above.

In order to investigate possible effects of selected additives on the individual steps of soot formation during the combustion of polymers, a burner was constructed which yields a stationary counter flow diffusion flame (CFDF) between a 1" diameter polymer rod and an oxidizer nozzle (see Fig. 12). A CFDF was chosen since this configuration can best be represented by a one-dimensional flame model. This burner has been

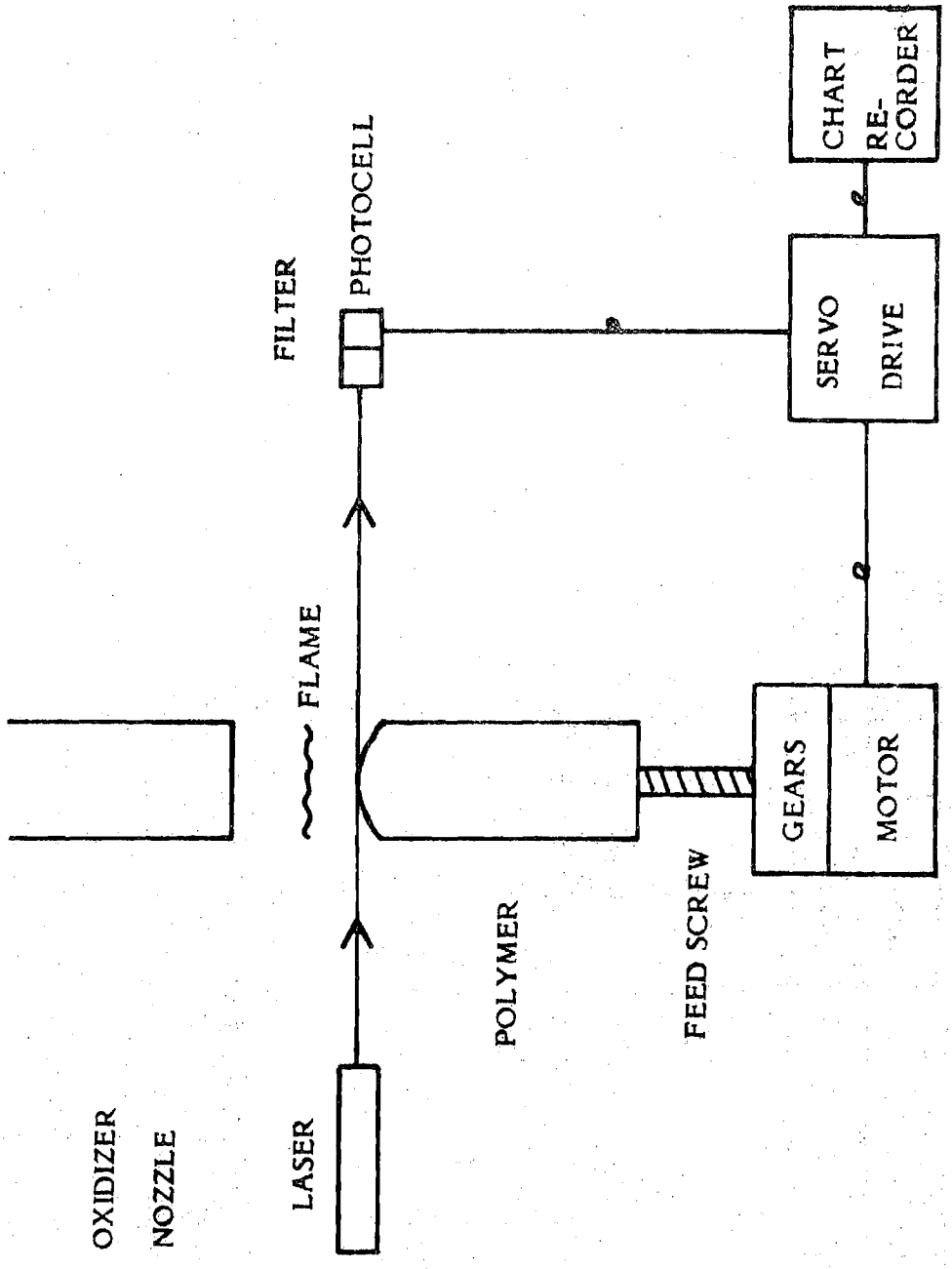

Figure 12. Schematic Representation of Burner System.

described in some detail in our Proposal Amendment dated April 5, 1981. Briefly, a low power (1 m watt) laser beam is allowed to graze over the burning surface of the polymer and falls on a photocell. The output from this cell maintains the rate at which the polymer is advanced equal to the burn rate and thus keeps the flame stationary in the laboratory frame of reference. The polymer advance rate and, therefore, its burn rate is continuously monitored. The burner is surrounded by a glass sleeve to exclude drafts which may interfere with flame stability. Slots are cut into the sleeve to permit unhindered passage of the laser beams. The flame thus produced is located within two millimeters of the burning surface because of the low velocity of the outgassed fuel. The only means of controlling the flame conditions in this arrangement is by adjusting the composition of the oxidizer flow. Since the gaseous fuel is liberated from its solid state by radiative heat transfer to the polymer the oxidizer composition also affects the fuel flow rate. This leads to the somewhat surprising result that an increase in oxygen content of the oxidizer flow increases soot formation. This can be explained by an increase in combustion intensity and thus heat transfer to the polymer due to the excess oxygen. Preheating the polymer by heating the burner has been shown to have only a minor effect.

The polymer samples used are polypropylene, polyethylene and polystyrene. Bars 1 1/4" x 1 1/4" x 6" are cast from granules under high pressure in heated picture frame molds in this laboratory. These are then machined into sample rods of 1" diameter and 3" length which fit the burner. Preliminary tests have shown that this burner provides a stable, horizontal

flat flame, which is located fairly close to the polymer surface with soot concentration increasing with radial distance from the polymer axis.

In order to increase the flexibility in achievable flame conditions a second burner has been designed to be used in conjunction with the one described above (see Fig. 13). This burner consists of a small container filled with the polymer under investigation and closed at the top with a porous plate. The vessel is heated externally until the polymer melts and gives off its volatile fuel. These gases undergo pyrolysis as they pass through the sintered plate above which they are met by an oncoming jet of oxidizer issuing from a nozzle which faces the sintered plate. This configuration results in a flat horizontal CFDF between the polymer vessel and the oxidizer nozzle. The polymer vessel has a side inlet which permits the addition of an inert gas or an additive carrying spray. Since this burner uses external heat to liberate the volatile fuel from the polymer, the fuel flow rate can be independently adjusted. The flame may, thus, be moved away from the porous surface by increasing the fuel gas velocity via the fuel flow rate. The flame position may, furthermore, be varied independently of the fuel feed rate by adding an inert gas such as nitrogen above the molten polymer. This results in an extended pyrolysis zone which lends itself to more precise measurements. The new burner also permits simpler injection of additives into the pyrolysis zone. A prototype of this burner has been assembled and preliminary tests have shown that the expectations of greater flexibility in the flame conditons for burner design has been born out.

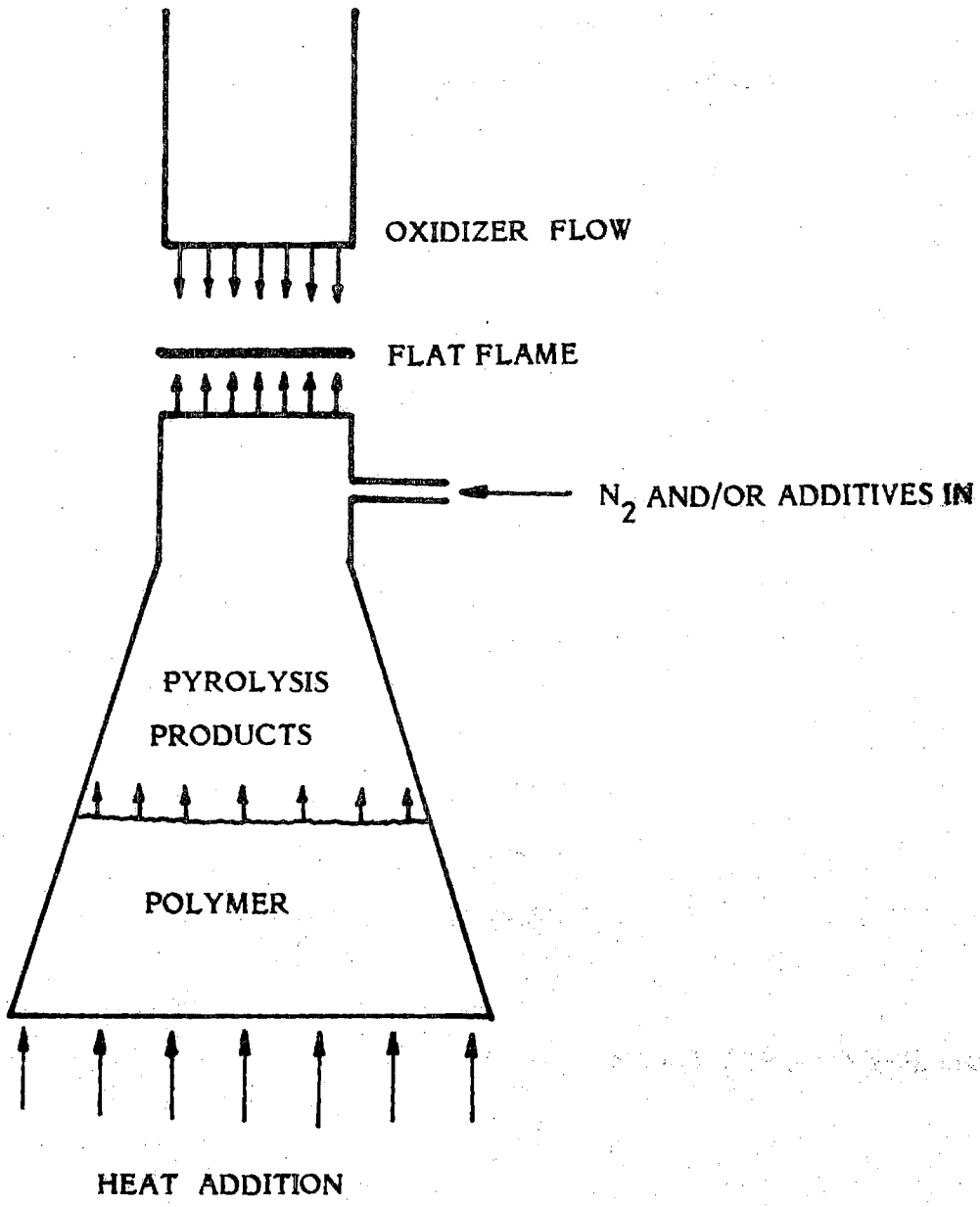

Figure 13. Schematic Representation of the Modified Opposite Flow Polymer Diffusion Flame Burner.

Analytical Methods. In order to differentiate between the individual steps in the mechanism of soot formation such as nucleation, surface growth and aggregation, the mean diameters and number densities of the spherical soot particles and their aggregates must be determined separately. Local soot mass loadings and the physical properties of the spheroids are to be measured in different parts of the flame using a specially designed suction probe which causes rapid quenching and is not easily blocked by soot deposits. This method is, however, not suitable for determining the degree of agglomeration since this process continues during sample collection and preparation.

Simultaneous in situ light scattering and absorbtion measurements are, therefore, being carried out at different locations in the flame in order to establish the mean diameters and number density distributions of the soot agglomerates throughout the diffusion flame. Local soot concentrations by volume are also obtained from the light absorbtion measurements. The required optical facility, as illustrated in Fig. 14 has been set up using funds kindly made available by Georgia Institute of Technology. The beam from a four watt argon ion laser is focused into the test section in the flame and passes through the flame onto a photomultiplier which measures the intensity of the transmitted light. A second photomultiplier is used to monitor the intensity of the beam scattered at any chosen angle to the incident beam. A system of lenses and apertures limits the solid angle over which scattered light is collected and eliminates radiation emanating from any part of the laser beam other than the test section under consideration.

HT - POWER SUPPLY L - LENS C - CHOPPER F - FILTER

M - MONOCHROMATOR S - SLIT O/S - OSCILLOSCOPE C/R - CHART RECORDER

PM - PHOTOMULTIPLIER O - OPTIC FIBER PSD - PHASE SENSITIVE DETECTOR

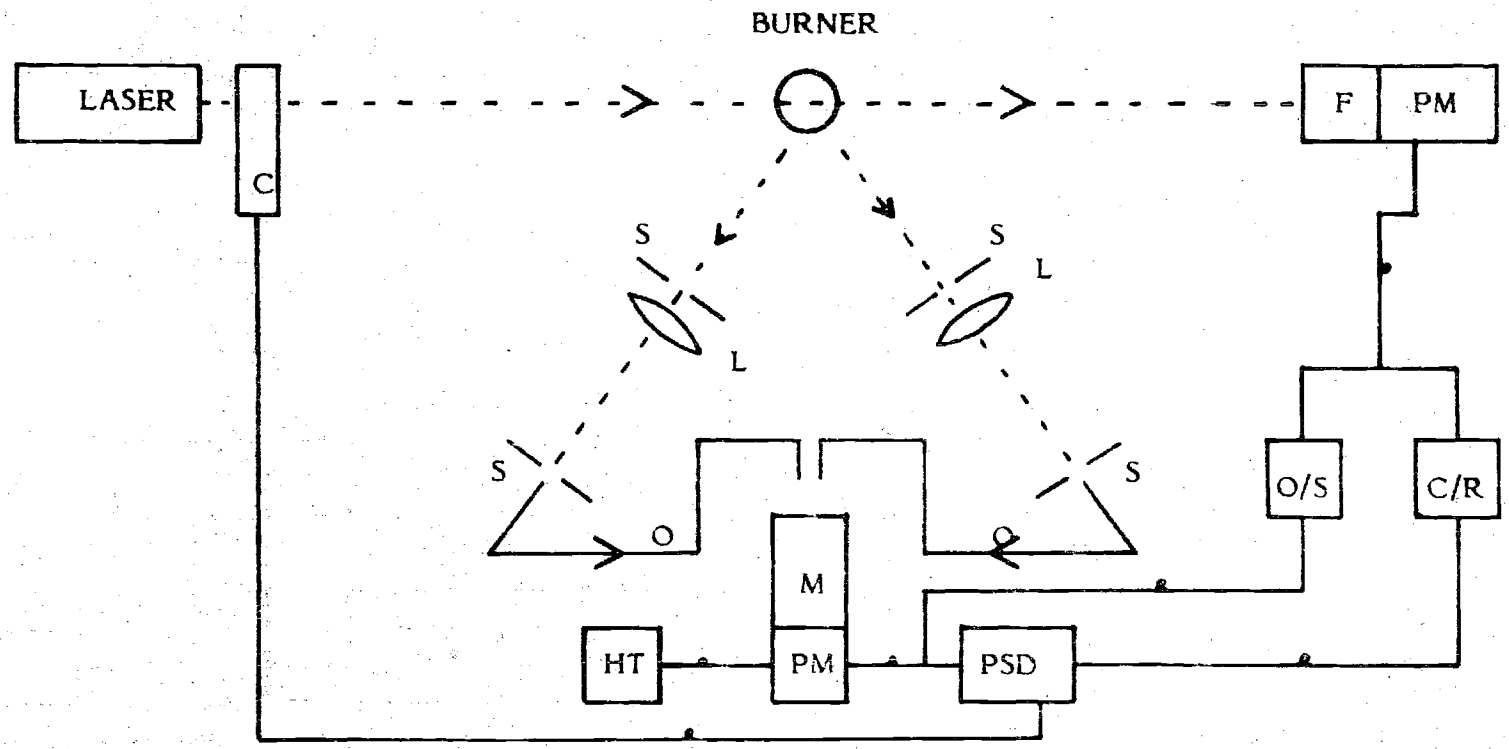

Figure 14. Optical Set-up.

The diameter of the focused beam along with the dimensions of the aperture limits the test volume from which light is received at any one time and, therefore, the 3-D resolution of the optical system to about 60 micron cubed. The direct light from the flame is reduced by a monochromator or narrow bandwidth interference filter centered about the wavelength of the laser. The remaining stray radiation is eliminated by placing a chopper into the incident beam and processing the output from the photomultipliers in a phase sensitive detector which only amplifies the part of the signal in constant phase with the chopper. The system, therefore, only registers light originating from the laser beam and disregards all other radiation as noise. White noise five orders of magnitude larger than the scattered signal can thus be eliminated. The signals from the scattering and transmission measurements are observed simultaneously on an oscilloscope and recorded on a chart recorder.

The Mie theory of scattering of electromagnetic radiation relates the diameter of spherical scatterers and their number density to the intensities of the transmitted and scattered beams as a function of the scattering angle. For scatterers of diameter less than the wavelength of the incident radiation the Rayleigh approximation can be used. This leads to a considerable simplification of the theory as the scattering intensity is no longer a function of the scattering angle. In that case the scattered intensity is proportional to ND^6 and the absorbed light to ND^3 where N is the number density and D the mean diameter of the scatterers. (A correction has to be introduced according to the distribution function of the diameters.) The

constants of proportionality can be eliminated by calibrating the system with gases of known scattering cross-sections such as oxygen, nitrogen and methane. Soot particles, in general, fall just within the Rayleigh regime. This will be confirmed by carrying out scattering measurements at different angles.* Since the Mie theory assumes spherical scatterers a small error is introduced because the soot agglomerates are not spheres. This departure from symmetry can be estimated by observing the depolarization ratio of the scattered beams.

Modelling Efforts. This study has been concerned with the development of a confined analytical-experimental approach that would enable us to determine the regions of soot formation/destruction in the flame in an effort to further existing understanding of the soot formation process. To achieve this goal, the theoretical modelling of the opposite flow polymer diffusion flame that is associated with the burners developed under this task has been undertaken. This modelling effort is related to the work of Wendt et al who used a gaseous fuel opposed flow diffusion flame to investigate NO_x formation. This study differs, however, from these investigations by the fact that the present modelling includes soot formation terms.

---

* Systems like these have been employed to measure particle diameter down to 10 nm. Signals from particles of smaller diameters become difficult to detect for the number of soot particles present in a typical flame over and above the background due to molecular scattering.

To date the necessary conservation equations have been developed and current efforts investigate the most efficient approach that would allow the use of these equations, in conjunction with appropriate measurements, in the determination of the distribution of the soot formation/destruction throughout the flame region.

Publications. The following are recent publications resulting from work conducted under this contract. The actual publications are collected in Appendix A.

1. Ndubizu, C. C. and Zinn, B. T., "Mechanisms of Soot Suppression by Alkali Metals in Polyethylene Diffusion Flames". In the Proceedings of the First (International) Specialists Meeting of The Combustion Institute, Bordeau, France, pp 592-597, July 1981.

2. Ndubizu, C. C. and Zinn, B. T., "Effects of Metallic Additives upon Soot Formation in Polymer Diffusion Flames". Accepted for Publication in Combustion and Flame.

3. Pasternak, M. and Zinn, B. T., "Studies of the Chemical Mechanism of Smoke Particulates Formation during the Combustion of Chlorinated Polymers". Accepted for Publication in Combustion Science and Technology.

4. Pasternak, M. and Zinn, B. T., "The Role of Polycyclic Aromatic Hydrocarbons (PAH) in the Formation of Smoke Particulates during the Combustion of Polymeric Materials". In the Proceedings of the 18th Symposium (International) on Combustion, The Combustion Institute, pp 91-99, 1981.

5. Pasternak, M. and Zinn, B. T., "Oxidation of Aromatic Species as a Competitive Chemical Pathway to the Major Process of Soot Formation". Published in Combustion and Flame 41, pp. 335-337, 1981.

SMOKE HAZARDS RESULTING FROM THE BURNING OF SHIPBOARD PAINTS

E. A. Powell and B. T. Zinn

Georgia Institute of Technology
School of Aerospace Engineering
Atlanta, GA 30332

Prepared for

Combustion and Fuels Branch
Naval Research Laboratory

under

Contract N00014-78-C-0432

Naval Research Laboratory
Washington, D. C.

Unclassified

URITY CLASSIFICATION OF THIS PAGE

REPORT DOCUMENTATION PAGE

REPORT SECURITY CLASSIFICATION: Unclassified	1b. RESTRICTIVE MARKINGS
SECURITY CLASSIFICATION AUTHORITY	3. OISTRIBUTION/AVAILABILITY OF REPORT: Approved for public release; distribution unlimited
). OECLASSIFICATION/OOWNGRAOING SCHEOULE	
PERFORMING ORGANIZATION REPORT NUMBER(S)	5. MONITORING ORGANIZATION REPORT NUMBER(S)
a. NAME OF PERFORMING ORGANIZATION: eorgia Institute of Technology, chool of Aerospace Engineering; 6b. OFFICE SYMBOL (If applicable)	7a. NAME OF MONITORING ORGANIZATION: Naval Research Laboratory
c. AOORESS (City, State and ZIP Code): Atlanta, Georgia 30332	7b. AODRESS (City, State and ZIP Code): Washington, DC 20375
8a. NAME OF FUNOING/SPONSORING ORGANIZATION; 8b. OFFICE SYMBOL (If applicable)	9. PROCUREMENT INSTRUMENT IDENTIFICATION NUMBER
c. AOORESS (City, State and ZIP Code)	10. SOURCE OF FUNOING NOS.

PROGRAM ELEMENT NO.	PROJECT NO.	TASK NO.	WORK UNIT NO.

1. TITLE (Include Security Classification) Smoke Hazards Result-ing from the Burning of Shipboard Paints

2. PERSONAL AUTHOR(S)
E. A. Powell and B. T. Zinn

3a. TYPE OF REPORT	13b. TIME COVERED	14. OATE OF REPORT (Yr., Mo., Day)	15. PAGE COUNT
Final	FROM _____ TO _____		93

6. SUPPLEMENTARY NOTATION
Contract monitored by Frederick W. Williams, Code 6180
Naval Research Laboratory

7. COSATI CODES			18. SUBJECT TERMS (Continue on reverse if necessary and identify by block number)	
FIELO	GROUP	SUB. GR.		
			Smoke	Light Scattering
			Combustion Products	Polymeric Materials
			Particle Size Analysis	Fire Hazards

9. ABSTRACT (Continue on reverse if necessary and identify by block number)

Investigations have been continued to evaluate the hazards due to smoke formation in shipboard fires. The physical properties of the smoke particulates generated during combustion were determined for two types of paints used by the Navy in ships and submarines. These were a chlorinated alkyd paint and an intumescent paint. The physical properties measured were particle size distribution and mean particle diameter, mass fraction of fuel converted to particulates, optical density, particle refractive index, and particulate volume fraction. The dependence of these properties on the temperature of the test-chamber atmosphere (room temperature to 300°C) and the mode of combustion (flaming or smoldering) was determined for both materials.

0. OISTRIBUTION/AVAILABILITY OF ABSTRACT	21. ABSTRACT SECURITY CLASSIFICATION
NCLASSIFIEO/UNLIMITEO ☒ SAME AS RPT. ☐ OTIC USERS ☐	Unclassified
2a. NAME OF RESPONSIBLE INOIVIOUAL	22b. TELEPHONE NUMBER (Include Area Code); 22c. OFFICE SYMBOL

D FORM 1473, 83 APR EOITION OF 1 JAN 73 IS OBSOLETE.

SECURITY CLASSIFICATION OF THIS PAGE

The results of this study indicate that both paints produce smoke with a log-normal particle size distribution during smoldering combustion in the room temperature tests. Optical measurements made during these tests show that both paints produce smoke particles with mean diameters which vary with time between 0.6 and 1.2 microns. Under these conditions the chlorinated alkyd paint produces pale yellow spherical liquid droplets, while the intumescent paint produces a mixture of light tan and white solid particles. For flaming combustion of the chlorinated alkyd paint, irregularly shaped aggregates of smaller soot particles with a mean aggregate diameter of about 1.2 microns are produced. For the intumescent paint flaming combustion is weak and intermittent, occurring only in tests conducted in air heated to 100°C or above. For flaming combustion of the chlorinated alkyd paint, mean particle diameter increases slightly as the temperature of the chamber atmosphere is increased. For nonflaming combustion of the intumescent paint increasing the ventilation air temperature greatly reduces the total amount of smoke produced and the resulting light obscuration. Under room temperature, nonflaming conditions, the light obscuration (optical density) obtained with the intumescent paint is much greater than that produced by burning an equal mass of chlorinated alkyd paint under the same conditions.

CONTENTS

Abstract

Investigations have been continued to evaluate the hazards due to smoke formation in shipboard fires. The physical properties of the smoke particulates generated during combustion were determined for two types of paints used by the Navy in ships and submarines. These were a chlorinated alkyd paint and an intumescent paint. The physical properties measured were particle size distribution and mean particle diameter, mass fraction of fuel converted to particulates, optical density, particle refractive index, and particulate volume fraction. The dependence of these properties on the temperature of the test-chamber atmosphere (room temperature to 300°C) and the mode of combustion (flaming or smoldering) was determined for both materials.

The results of this study indicate that both paints produce smoke with a log-normal particle size distribution during smoldering combustion in the room temperature tests. Optical measurements made during these tests show that both paints produce smoke particles with mean diameters which vary with time between 0.6 and 1.2 microns. Under these conditions the chlorinated alkyd paint produces pale yellow spherical liquid droplets, while the intumescent paint produces a mixture of light tan and white solid particles. For flaming combustion of the chlorinated alkyd paint, irregularly shaped aggregates of smaller soot particles with a mean aggregate diameter of about 1.2 microns are produced. For the intumescent paint flaming combustion is weak and intermittent, occurring only in tests conducted in air heated to 100°C or above. For flaming combustion of the chlorinated alkyd paint, mean particle diameter increases slightly as the temperature of the chamber

atmosphere is increased. For nonflaming combustion of the intumescent paint increasing the ventilation air temperature greatly reduces the total amount of smoke produced and the resulting light obscuration. Under room temperature, nonflaming conditions, the light obscuration (optical density) obtained with the intumescent paint is much greater than that produced by burning an equal mass of chlorinated alkyd paint under the same conditions.

INTRODUCTION

This report describes the efforts conducted for the Naval Research Laboratory under Contract No. N00014-78-C-0771 entitled "The Determination of the Smoke Hazards Resulting from the Burning of Shipboard Materials Utilized by the U. S. Navy." This work, which was performed during the period September 1, 1981 through August 31, 1983, was concerned with the evaluation of the hazards due to smoke formation in shipboard fires. Specifically, this research program is a continuation of work done during the previous three years to determine the physical and chemical properties of smoke particulates generated during the combustion of representatives of three classes of materials abundantly present on shipboard. In the present investigation, the same measurements were obtained for a fourth class of shipboard materials, namely, interior fire retardant paints. Two types of paint were investigated: (1) a chlorinated alkyd paint (as specified by DOD-E-24607) and (2) an intumescent paint (Ocean 9788). The aims of this investigation were: (1) the identification of conditions under which large quantities of smoke that would result in severe light obscuration are generated and (2) the identification of major toxic species which are associated with the smoke particulates generated during the combustion of these paints.

To pursue the objectives outlined above, the efforts of this research project have been divided into two major tasks. The first task is concerned with the measurements of the physical properties of the smoke particulates, while the second task deals with the chemical analysis of the combustion products. This report is concerned with the smoke physical properties only,

while the results of the chemical analysis is presented in a separate report.

This program has been directed by Dr. Ben T. Zinn in the School of Aerospace Engineering of the Georgia Institute of Technology. He was assisted by Dr. E. A. Powell who was responsible for the smoke physical properties work presented herein and Dr. R. F. Browner in the School of Chemistry who was responsible for the chemical analysis work.

EXPERIMENTAL FACILITIES

The smoke research program described herein has been conducted utilizing the following facilities which have been developed at the School of Aerospace Engineering, Georgia Institute of Technology: (1) a Combustion Products Test Chamber, (2) a Combustion Products Sampling System; and (3) an In Situ Optical Aerosol Measurement System.

The ventilated Combustion Products Test Chamber (CPTC) shown in Figure 1 is capable of simulating a wide variety of environmental conditions that may be encountered in actual fire situations. Specifically, the design of the CPTC permits easy control and measurement of the following variables during the combustion of small samples of materials: (1) the mode of combustion (i.e., flaming vs. smoldering combustion); (2) the sample radiant heating rate (up to 10 watts/cm^2); (3) the sample weight loss during the test; (4) the composition of the ventilating gas surrounding the sample; (5) the temperature of the ventilation gas (up to 650^{o}C) and; (6) an option to test the sample under either vertical or horizontal mounting. A complete description of the CPTC including operating procedures, can be found in References 1 through 3.

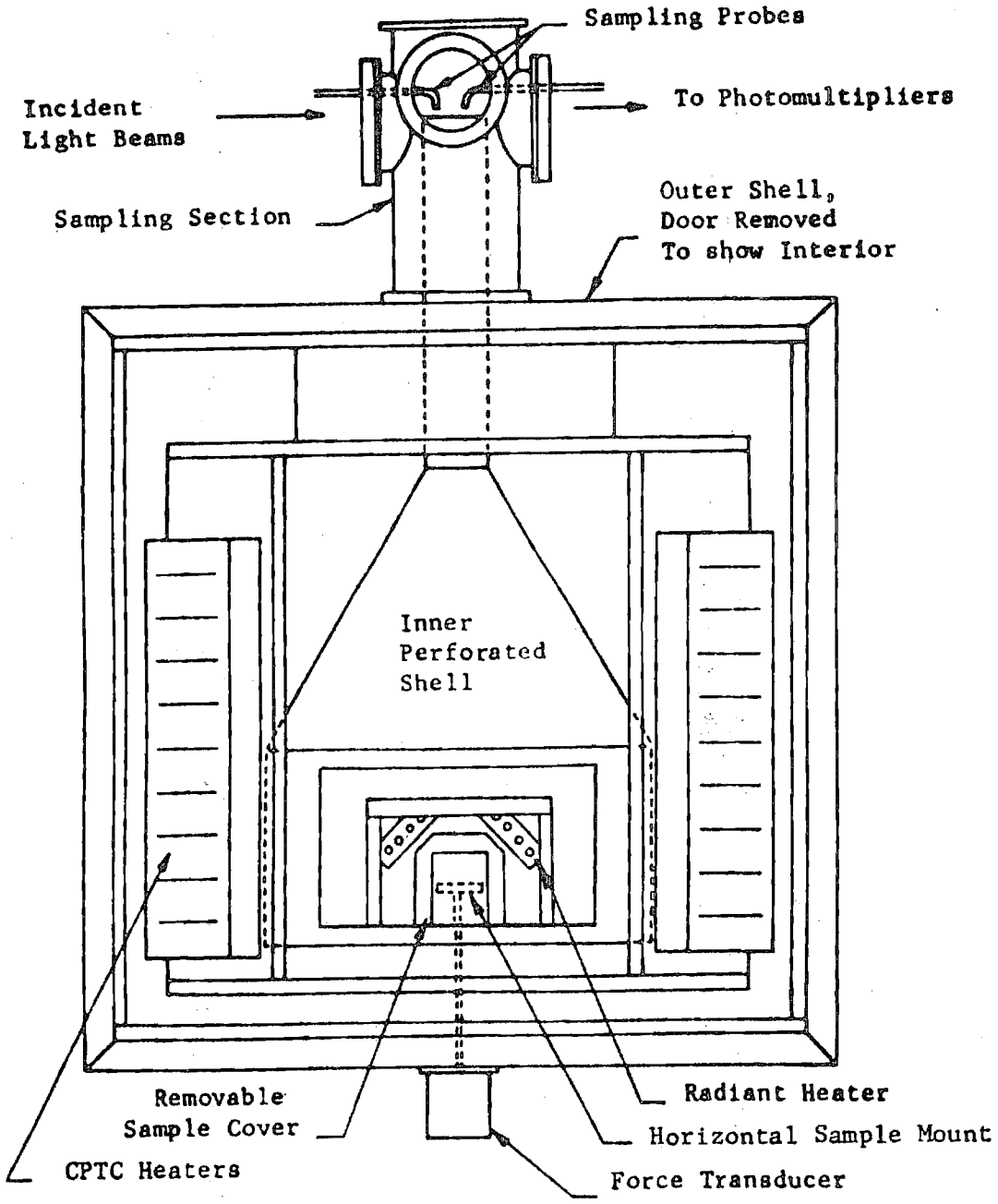

Figure 1. Combustion Products Test Chamber.

During testing, a Combustion Products Sampling System shown in Figure 2 is used to analyze smoke samples that are continuously withdrawn from the gases flowing from the CPTC. Information obtained by the Aerosol Sampling System includes particle size distributions and total particulate mass generated. Some of the collected smoke samples are also retained for chemical analysis. A description of the sampling system can also be found in References 1 and 2.

In addition to the data obtained by sampling techniques, an In Situ Optical Aerosol Measurement System is utilized to make simultaneous mean particle size and concentration measurements (Figure 3). With this optical smoke analysis system measurement of scattered blue-green laser light (λ = 0.488 μm) at forward angles of 5^{o} and 15^{o} provide time-resolved data describing the average size of the smoke particles. Measurement of transmitted red (λ = 0.633 μm) and blue-green laser lights provide the optical densities of the smoke at these two wavelengths. For nonabsorbing particles (usually produced by nonflaming combustion) the transmitted light measurements along with the mean particle size measurements also yield the refractive index and volume fraction of the smoke particles. For absorbing particles (i.e., soot) measurements of 90^{o}-scattered blue-green light intensities parallel to and perpendicular to the plane of polarization of the incident light beam (Figure 4) provide additional data necessary to determine the complex refractive index of the smoke particles. Details of the optical system are available in References 4 and 5.

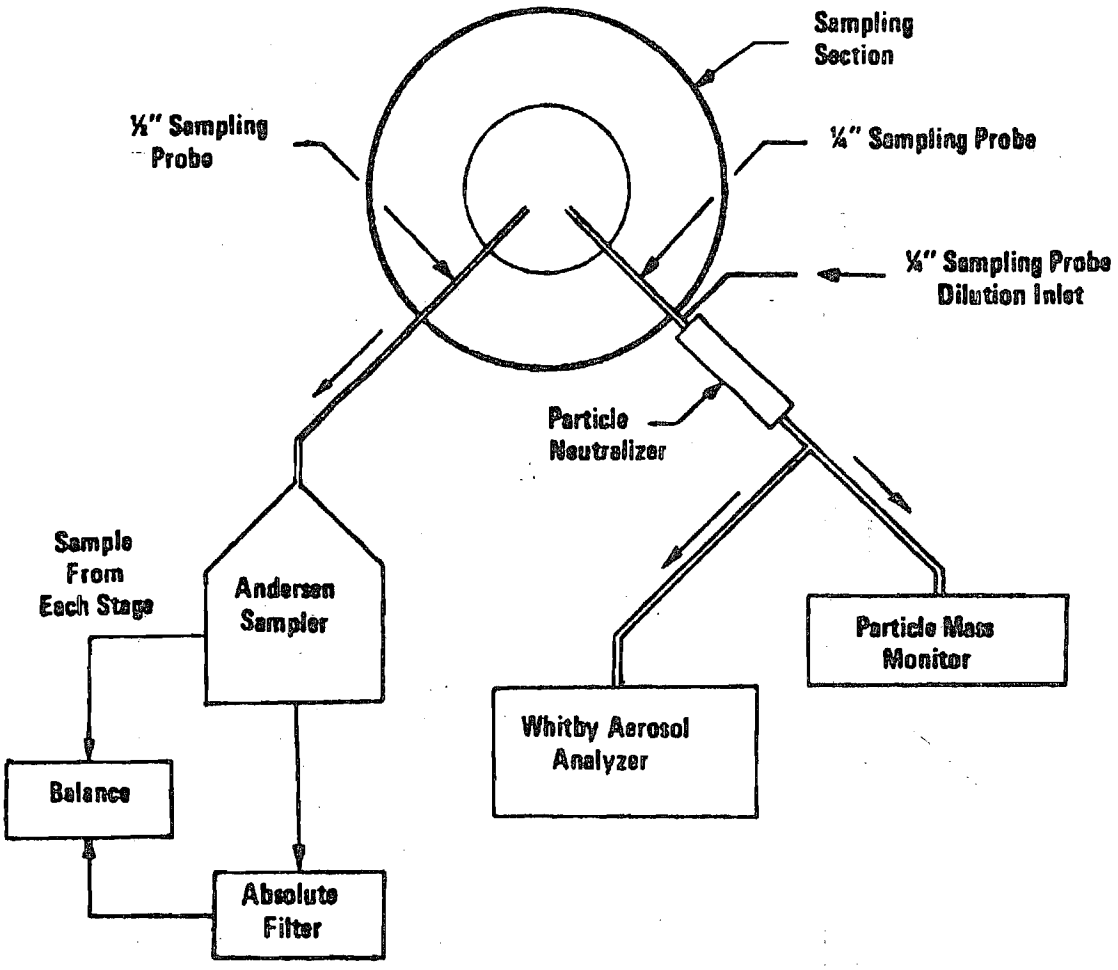

Figure 2. Combustion Products Sampling System.

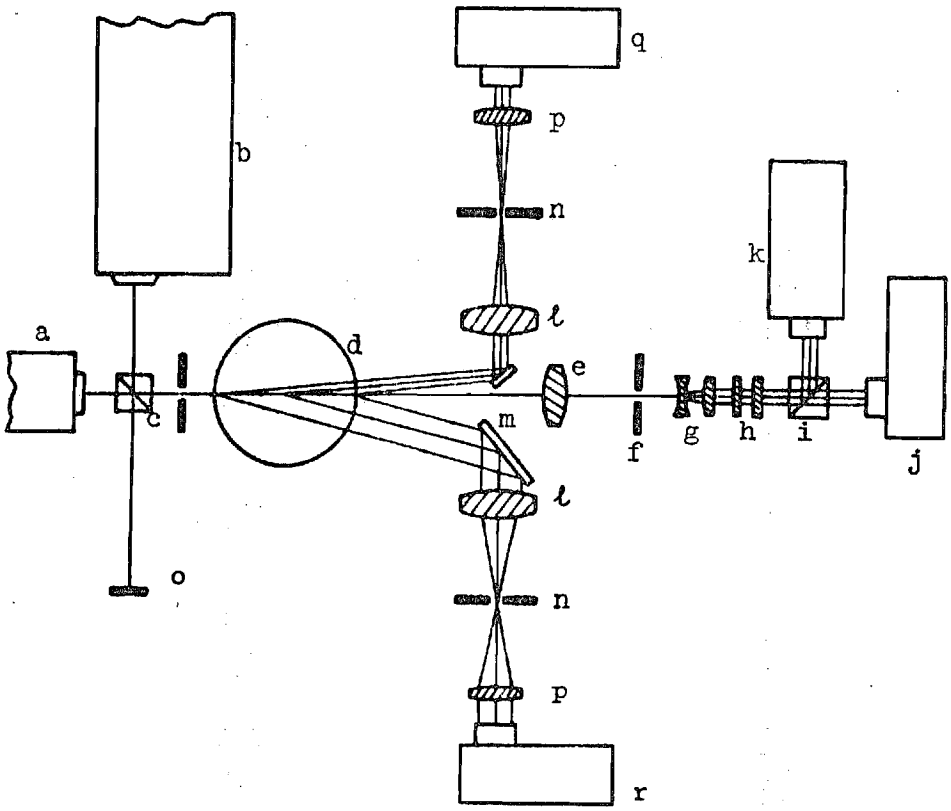

Figure 3. In situ optical aerosol measurement system:
(a) helium-neon laser, 5 mW
(b) argon-ion laser, 30 mW
(c) beam-combining cube,
(d) 11.4-cm-diam stack from the combustion products test chamber,
(e) objective lens,
(f) pinhole aperture,
(g) beam expander,
(h) neutral density filters,
(i) beam-splitter cube,
(j) transmitted blue-light detector,
(k) transmitted red-light detector,
(l) objective lenses,
(m) mirrors,
(n) pinhole apertures,
(o) light stop,
(p) collimating lenses,
(q) 5^{o}-scattering detector, and
(r) 15^{o}-scattering detector.

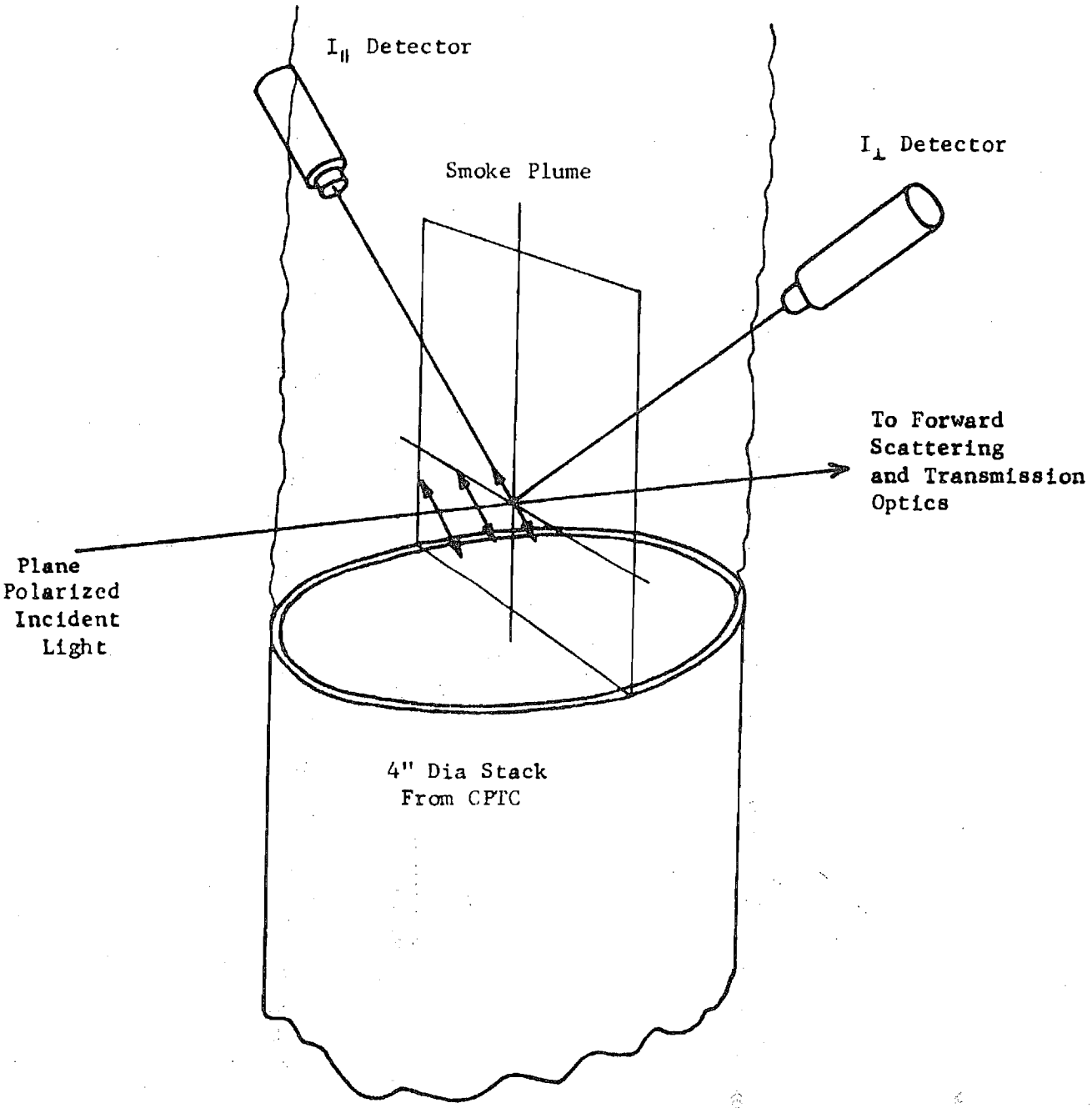

Figure 4. Optical system for 90°- scattering measurements.

An on-line data acquisition system utilizing a Hewlett-Packard 2100 mini-computer is being used for acquiring, reducing and plotting all of the optical data with the exception of the 90^{o}-scattering data which must be reduced using the CDC Cyber 730 computer at Georgia Tech's computer center.

TEST PROCEDURES AND CONDITIONS FOR SMOKE PHYSICAL PROPERTIES MEASUREMENTS.

This research program was concerned with the determination of the detailed physical properties of smoke particulates generated by burning two types of interior fire retardant paints which are being used or are being considered for use by the U. S. Navy aboard submarines. The first material to be tested, a chlorinated alkyd paint, was provided by the Navy. The second material, Ocean 9788 intumescent paint, was supplied by the manufacturer. The tests were performed by utilizing the Combustion Products Test Chamber (CPTC), the Aerosol Sampling System and the In Situ Aerosol Measurement System.

For tests conducted in room temperature ventilation gas, the physical analysis of the smoke particulates determined the following smoke properties: (1) the particle size distribution, (2) the mass fraction of fuel converted to particulates, (3) the evolution of the mean particle diameter with time, (4) the light obscuration by the particles (i.e., optical density), (5) the particle refractive index, and (6) the volume fraction (i.e., volume concentration) of the particles. For the tests conducted in hot ventilation gas, items (1) and (2) above were not determined since the Aerosol Sampling System can not be operated at high temperature. In addition the sample mass loss as a function of time was determined for most of the tests.

The dependence of the above quantities upon the following experimental conditions was determined: (1) the temperature of the test chamber atmosphere, and (2) the mode of combustion (i.e., flaming or

smoldering combustion). Thus the two paints were subjected to the test matrix shown in Table 1. All of the tests were conducted in the horizontal sample orientation, and in all of the tests the sample was exposed to a radiant heat flux of 5 W/cm^2. The particulate size distributions using cascade impactor sampling were determined for all room temperature tests. In the flaming tests, the pyrolysis products generated by exposure of the sample to the 5 W/cm^2 radiant flux were ignited by a small propane pilot flame. Finally, in all tests of the chlorinated alkyd paint the CPTC ventilation gas consisted of air flowing at a volumetric rate (before heating) of 425 liters per minute, while in all tests of the Ocean 9788 intumescent paint a lower flow rate of 142 liters per minute was used. Due to the decrease in density of the ventilation air during heating, the volumetric flow rate of the heated air during the high temperature tests was higher as shown in Table 1. Additional tests at 150°C and 200°C were also conducted for reasons to be discussed later. The flow rates for these extra tests are also given in Table 1 (Tests 7 and 8).

In the following sections of this report smoke particulate physical properties data will be presented for the fire retardant paints tested during this research program. Brief discussions of each of the measured parameters are given in Appendix A of Reference (6).

Table 1. Test Matrix for Interior Fire Retardant Paints

est	Radiant Flux (W/cm^2)	Ventilation Gas Temperature (^oC)	Mode of Combustion	Ventilation Gas Composition	Flow Rate of Heated Ventilation Gas (ℓ/min)	
					Chlorinated Alkyd	Intumescent
1	5.0	25	Nonflaming	Air	425	142
2	5.0	100	"	"	532	178
3	5.0	300	"	"	817	273
4	5.0	25	Flaming	"	425	142
5	5.0	100	"	"	532	178
6	5.0	300	"	"	817	273
7	5.0	150	Nonflaming	"	-	202
8	5.0	200	"	"	675	225

SMOKE PHYSICAL PROPERTIES DATA FOR CHLORINATED ALKYD PAINT

Description of Material and Sample Preparation

This paint conforms to the military specification (DOD-E-24607) for interior semigloss enamel based on chlorinated alkyd resin.[7] This enamel is formulated to provide a decorative coating or dry film which, although degraded by heat, will not spontaneously ignite in the event of exposure to fire. The color of the paint tested was Soft White, Formula No. 124. The chemical composition of this paint is given in Table 2 below.

Table 2. Composition of Chlorinated Alkyd Paint

Ingredient	Percent by Mass of Enamel
Barytes[1]	34.90
Titanium Dioxide	23.27
Chlorinated Alkyd Resin[2]	30.91
Paint Thinner (Petroleum Spirits)	9.97
Lead Naphthenate	0.39
Cobalt Naphthenate	0.16
Anti-Settling Agent	0.33
Anti-Skinning Agent	0.07

(1) Minimum of 98.0 percent barium sulfate.

(2) Chlorine, in the form of chlorinated dibasic acid, minimum of 4.2% by mass of enamel.

Regardless of color, the paint consists of 57.0-60.5 percent by mass pigments (primarily barium sulfate and titanium dioxide), 20.5-23.0 percent volatiles, and 18.5-21.0 percent nonvolatile vehicle (45% chlorinated dibasic acid). The density of the wet paint ranges from 1.73 to 1.80 kg/L.

Samples of the chlorinated alkyd paint were prepared by brushing onto 5.1 cm squares (2 in) of cold rolled steel substrate 0.79 mm (1/32 in.) thick. The average weight of the substrates was 19.0 g, which was just below the limit imposed by the force transducer. The substrates were first cleaned with acetone, then 10 thick coats of paint were applied with a small brush over a 17 day period with 1-4 days drying time between coats. The average dry mass of paint applied in this manner was 10.66 g with a standard deviation of 0.49 g. This yields an average dry film thickness of 2.3 mm based on a dry film density of 1.79 g/cm^3. Storage time under ambient laboratory conditions for these samples ranged from 2 weeks to 44 weeks.

Tests in Room Temperature Ventilation Air

Both flaming and nonflaming tests of the chlorinated alkyd paint have been conducted in room temperature ventilation air (25°C) with a radiant flux of 5 W/cm^2. For all of these tests the ventilation air flow rate was 425 L/min (15 CFM). The results of these tests are presented in Figures 5 through 9 and in Tables 3 and 4.

Curves of sample mass versus time for flaming and nonflaming combustion of the chlorinated alkyd paint samples are presented in Figure 5. Peak mass loss rates obtained from these curves are given in Table 3. These curves show that significant mass loss due to pyrolysis begins about 2

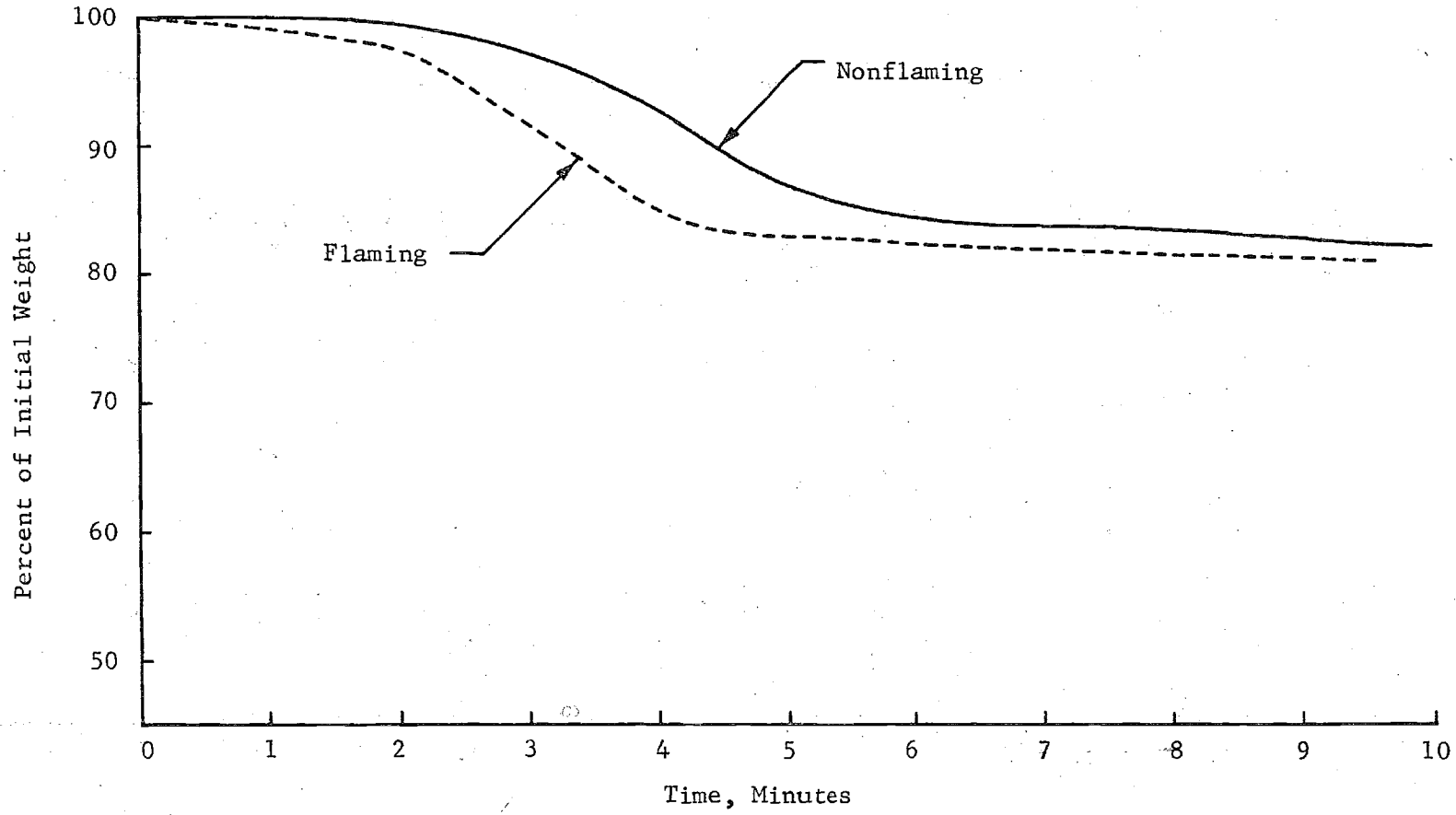

Figure 5. Sample weight losses for flaming and nonflaming combustion of chlorinated alkyd paint exposed to a radiant flux of 5 W/cm^2 in room temperature ventilation air (25^{o}C).

Table 3. Sample Weight Loss Data for Chlorinated Alkyd Paint on Steel Substrate.

Mode	Ventilation Air Temperature (^{o}C)	Radiant Flux (W/cm^2)	Peak Mass Loss Rate (mg/cm^2-s)	Char Residue (Percent of Initial Weight)
NF	25	5.0	0.40	82.1
NF	100	5.0	0.40	81.2
F	25	5.0	0.58	80.8
F	100	5.0	0.82	79.7
F*	200	5.0	0.57	78.5
F	300	5.0	1.12	77.4
F*	300	5.0	1.40	77.7

* Spontaneous flaming ignition occurred during a "nonflaming" test (i.e., no pilot flame).

minutes after the sample is first exposed to the radiant heat flux. For the nonflaming mode, a peak mass loss rate of about 0.4 mg/s-cm^2 occurs after about 4 minutes of exposure. For flaming combustion, the peak mass loss rate is about 50% greater and occurs about a minute earlier than for the nonflaming mode. For both flaming and nonflaming conditions, slightly more than 80% of the initial sample mass remains as char, with slightly less char remaining in the flaming case. This is not surprising, since about 75% of the dry paint consists of nonvolatile inorganic pigments. The char residues for both nonflaming and flaming tests are shown in Figure 6. In both cases the residue has a thin, brittle, white surface skin with large cracks revealing black flaky char layers underneath. Some swelling of the char occurs during combustion with a maximum char thickness of about 6 mm. In Figure 6 it is seen that the residue left after flaming combustion also has more cracks in the surface skin than the residue left after nonflaming combustion, and it also has numerous small blisters in the surface skin along the edge of the largest cracks. It is likely that these blisters are due to higher local surface temperatures associated with the flaming combustion of pyrolysis gases issuing from these cracks.

Smoke particle size distributions were obtained using the cascade impactor for both flaming and nonflaming combustion of the chlorinated alkyd paint samples at the radiant flux of 5 W/cm^2. These size distributions are shown in Figure 7 as cumulative curves generated by plotting the percentage of particulate weight having particle diameters less than a given particle size versus the particle size on log-normal probability coordinates. In both cases, a straight line gives a good fit to the cascade impactor data

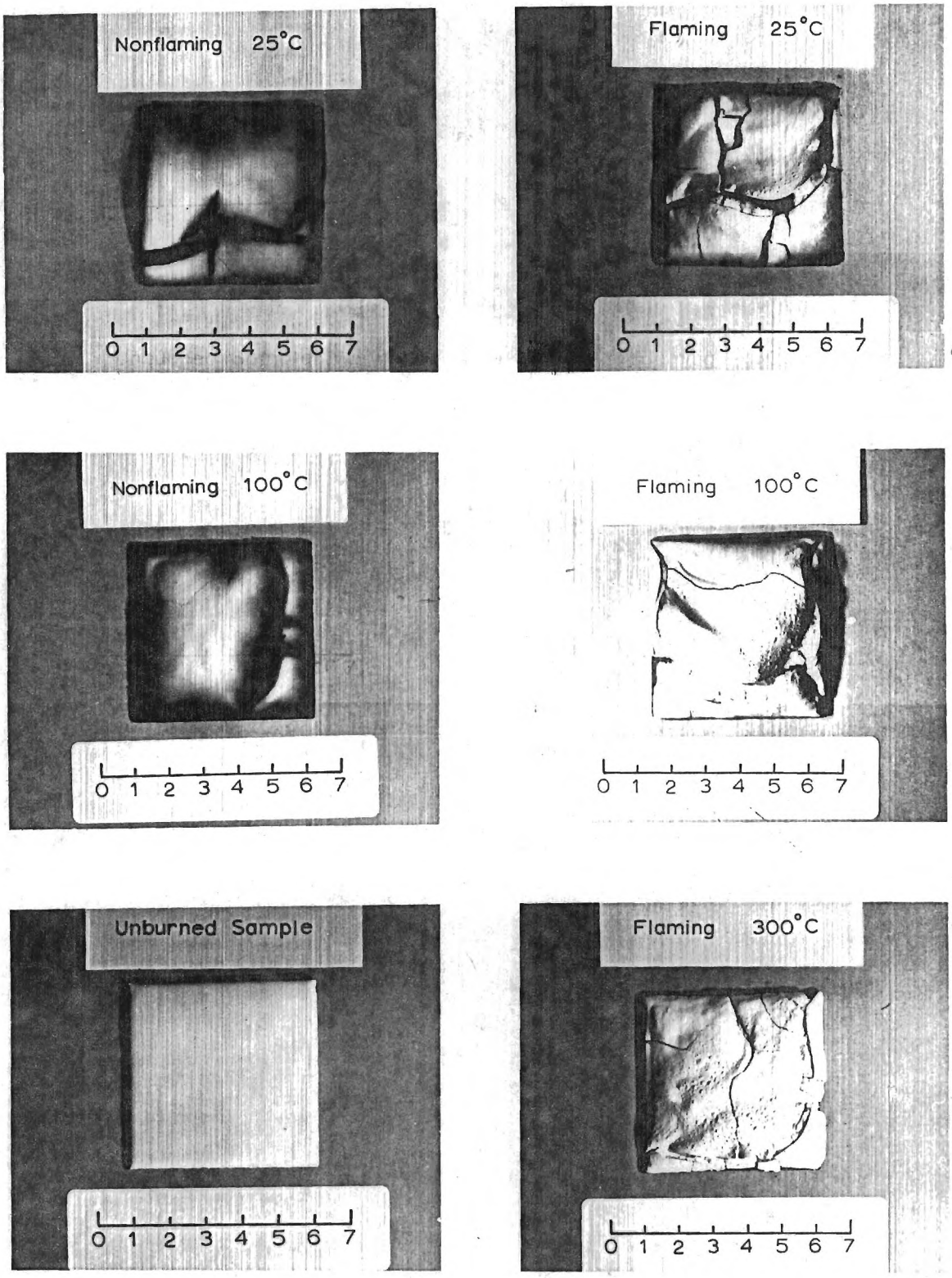

Figure 6. Char Residues for Chlorinated Alkyd Paint Tests.

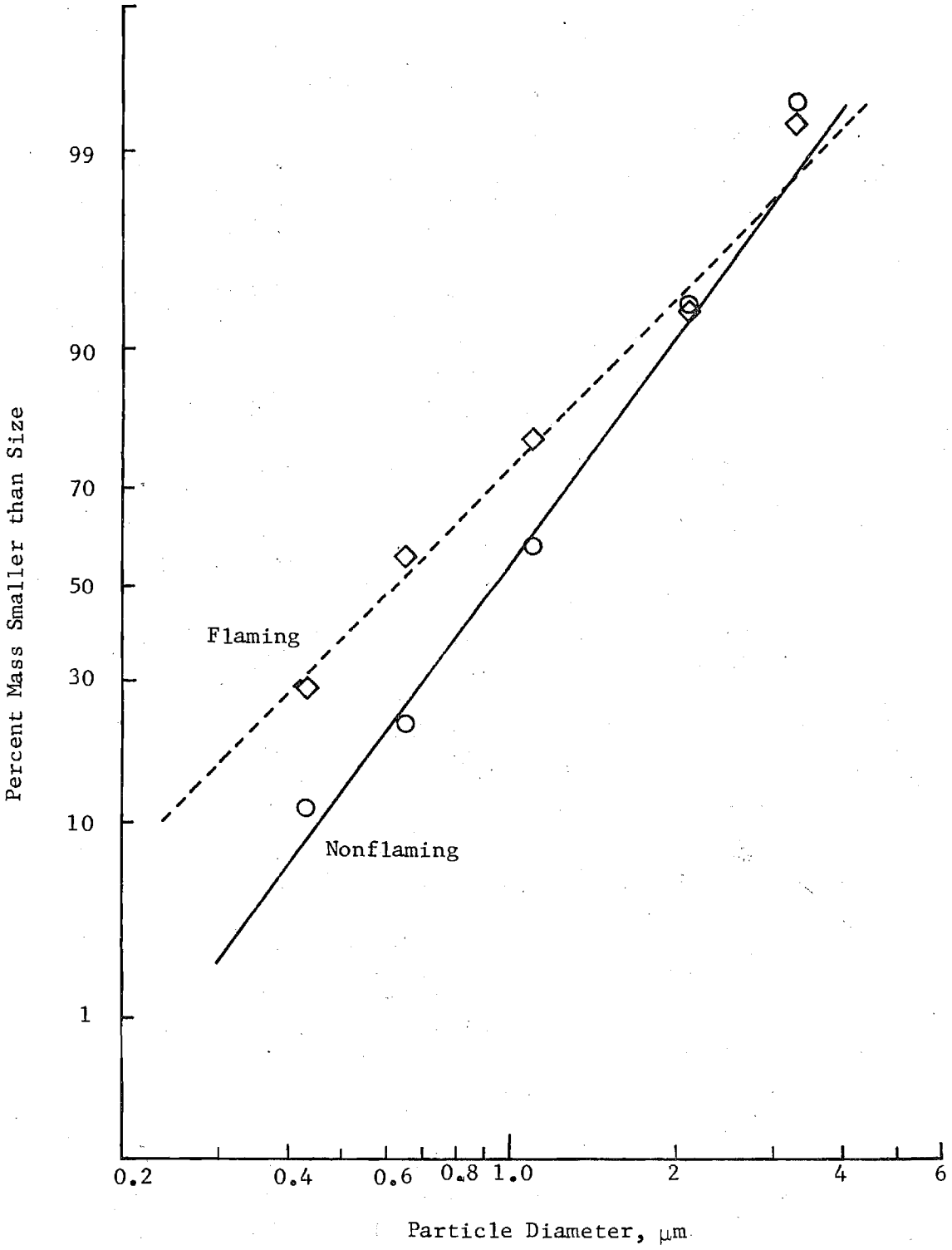

Figure 7. Smoke particle size distributions for flaming and nonflaming chlorinated alkyd paint exposed to a radiant flux of 5 W/cm^2 in room temperature ventilation air (25°C).

(plotted points), which indicates that the size distribution is log-normal for both flaming and nonflaming modes. The mass median diameters (D_{MMD}) and standard deviations (σ_g) obtained from these curves are given in Table 4. For nonflaming combustion the particulates consist of pale yellow spherical liquid droplets with a mass median diameter of about 0.9 micron. Here the total mass of particulates collected on the cascade impactor was about 13 mg, with about 1.5 mg collected on the absolute filter ($<.43\ \mu m$) and the last impactor stage ($.43 - .65\ \mu m$) and about 4.5 mg on each of the next two impactor stages ($.65-1.1\ \mu m$ and $1.1 - 2.1\ \mu m$). Less than 1 mg of these particles were larger than 2.1 μm. For flaming combustion black sooty particulates were collected with a mass median diameter of about 0.6 micron. This size distribution determination is less accurate than that for the nonflaming mode, because the total mass of particulates collected was only about 4 mg, of which about 1 mg each was collected on the absolute filter ($< .43\ \mu m$) and the last two impactor stages ($.43 - .65\ \mu m$ and $.65 - 1.1\ \mu m$). Smaller amounts were collected (0.6 mg and 0.3 mg) on the next two stages ($1.1 - 2.1\ \mu m$ and $2.1 - 3.3\ \mu m$). Traces of soot particles were detected visually on the impactor plates for sizes greater than 3.3 μm, but the quantities collected were too small to detect by weighing (<0.02 mg per stage). These results indicate that the particle size distribution obtained for flaming combustion of the chlorinated alkyd paint is considerably broader than that obtained for nonflaming combustion, even though the value of D_{MMD} is smaller in the flaming case.

Sampling data was also used to determine the fraction of the sample mass loss converted to particulates (Γ) for the room temperature tests. These values of Γ, which are given in Table 4, show that for nonflaming combustion under 5 W/cm^2 radiant flux about 11% of the total mass loss appears as particulates, while for flaming combustion under similar conditions slightly less than 4% of the mass loss is converted to soot particles.

The in situ optical system was used to obtain mean particle diameters (D_{32}) and optical densities produced by flaming and nonflaming combustion of the chlorinated alkyd paint samples. A comparison of mean particle sizes for flaming and nonflaming combustion is given in Figure 8, while the corresponding optical densities are given in Figure 9.

Figure 8 shows that for nonflaming combustion in room temperature ventilation air, the mean particle diameters vary between 0.7 and 1.1 microns during the initial stages of pyrolysis and average about 0.85 micron during the time of maximum optical density. This latter value is in very good agreement with the mass median diameter obtained by cascade impactor sampling (Table 4). During the later stages of pyrolysis the mean particle diameter decreases gradually to below 0.4 μ m as a result of the rapidly declining rate of production of condensible pyrolysis products. For flaming combustion, the mean particle diameters are nearly constant throughout the test, ranging between 1.1 and 1.2 microns. The mean diameter obtained optically (D_{32}) is nearly twice that obtained by particle sampling (D_{MMD}) for flaming combustion. This discrepancy is probably due to the nonspherical shape of the soot particle agglomerates produced under flaming combustion.

Table 4. Smoke Properties Data for Chlorinated Alkyd Paint

Mode	T (^{o}C)	Radiant Flux (W/cm^2)	Γ	D_{MMD} (μm)	σ_g	OD_{max} Blue	(m^{-1}) Red	D_{32}^{+} (μm)	Time to Peak OD (min)
NF	25	5.0	.113	0.94	1.77	0.90	0.79	0.84	4.9
NF	100	5.0	-	-	-	0.54	0.44	0.82	4.1
F	25	5.0	.037	0.63	2.16	0.84[a]	0.70[a]	1.17	3.5[a]
F	100	5.0	-	-	-	1.25[b]	1.03[b]	1.20	1.8[b]
F*	200	5.0	-	-	-	0.79[a]	0.62[a]	1.21	2.4[a]
F	300	5.0	-	-	-	1.46	1.17	1.29	0.9
F*	300	5.0	-	-	-	2.06	1.67	1.26	1.1

* Spontaneous flaming ignition occurred during a "nonflaming" test (i.e., no pilot flame)

+ Average of data points near OD_{max}.

a Second of two peaks.

b First of two peaks.

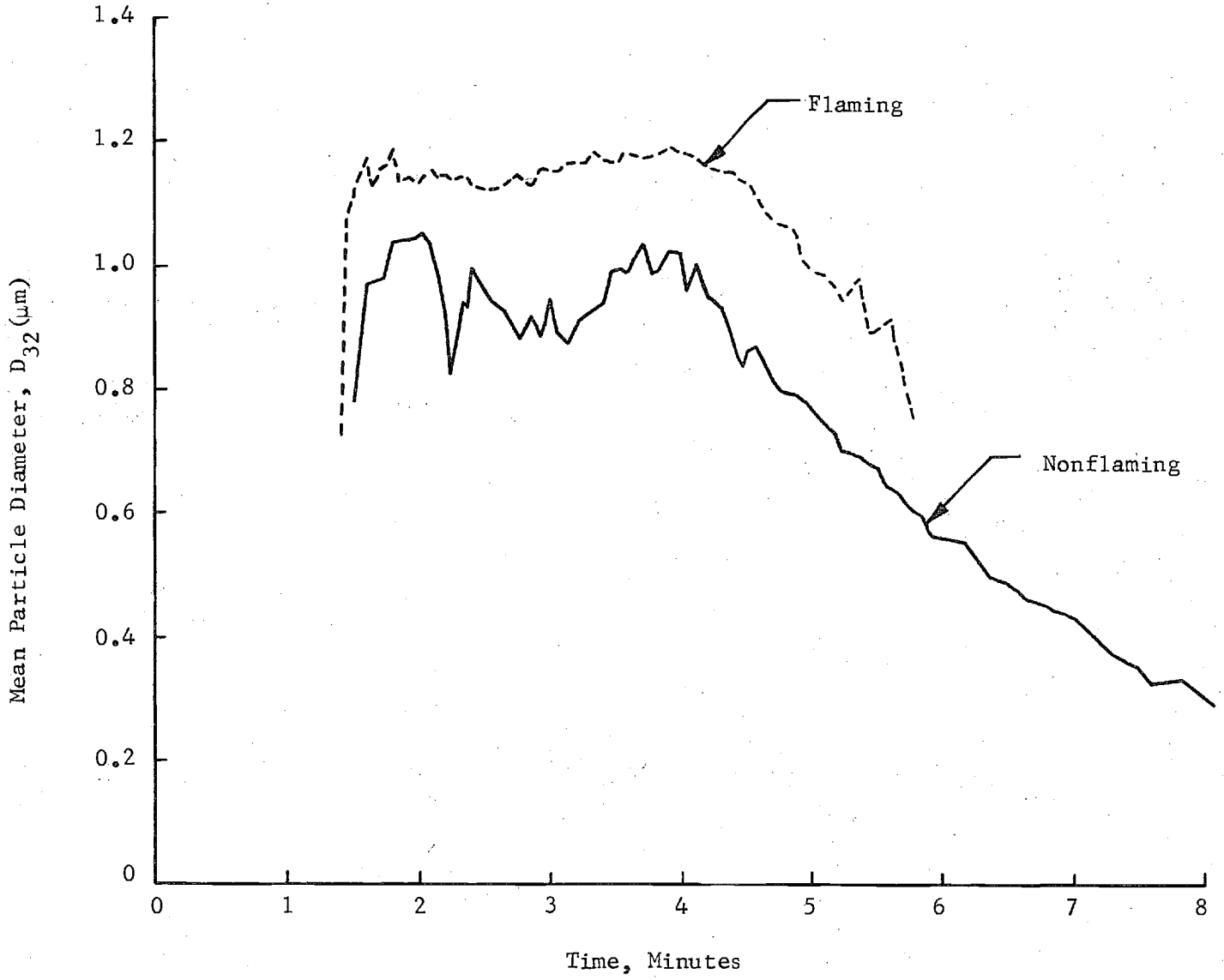

Figure 8. Smoke mean particle diameters for flaming and nonflaming combustion of chlorinated alkyd paint exposed to a radiant flux of 5 W/cm^2 in room temperature ventilation air (25°C).

Figure 9 shows that for nonflaming combustion in room temperature ventilation air, the optical density at the blue-green argon line (.488 μm) rises smoothly to a peak of about 1.0 m^{-1} about five minutes after initiation of exposure and then smoothly declines. For flaming combustion peak optical density is somewhat lower and occurs earlier in the test. Furthermore, the curves of optical density versus time exhibit two pronounced peaks; the second of these occurring after about 3.5 minutes and reaching about 0.85 m^{-1}.

Tests in Heated Ventilation Air

Results of tests of chlorinated alkyd paint samples conducted in hot ventilation air are shown in Figs. 10, 12 and 13 for nonflaming combustion and in Figs. 11, 14 and 15 for flaming combustion. In each figure the room temperature data are also shown for comparison. High temperature data are also given in Tables 3 and 4. In all flaming tests a small propane pilot flame was maintained throughout the test, and the radiant heat flux was 5 W/cm^2 for all tests. For ventilation air temperatures of 200°C and above, the chlorinated alkyd paint samples ignited spontaneously (i.e., without the pilot flame), therefore nonflaming data was not obtained for the highest ventilation gas temperature.

Figure 10 and Table 3 show that, for nonflaming combustion of the chlorinated alkyd paint, heating the ventilation air to 100°C causes pyrolysis to begin earlier but has little or no effect on the peak mass loss rate (0.4 mg/cm^2-s). This moderate increase in ventilation air temperature also results in a slight increase in the total mass of pyrolysis products evolved as

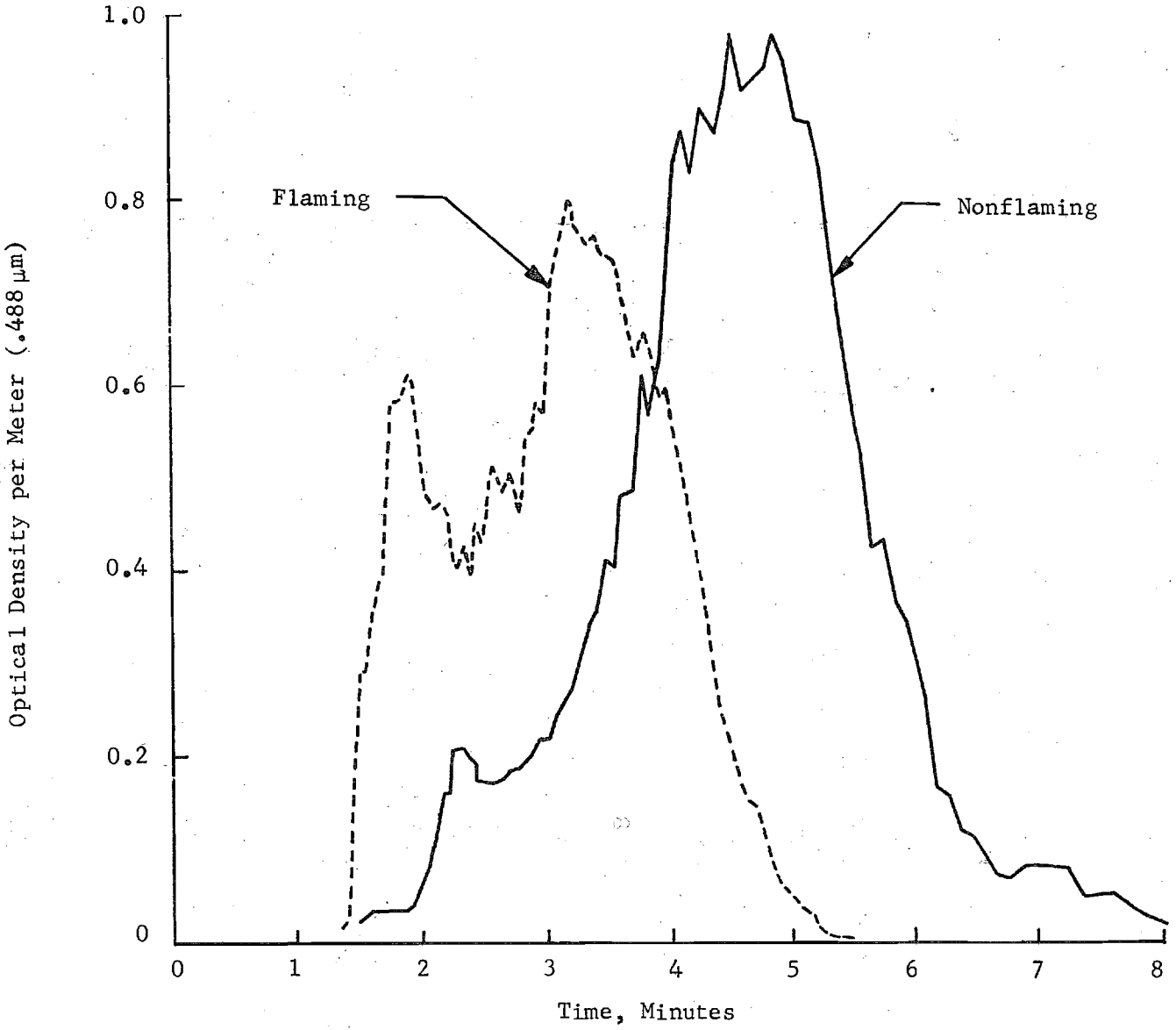

Figure 9. Smoke optical densities for flaming and nonflaming combustion of chlorinated alkyd paint exposed to a radiant flux of 5 W/cm^2 in room temperature ventilation air (25^{o}C).

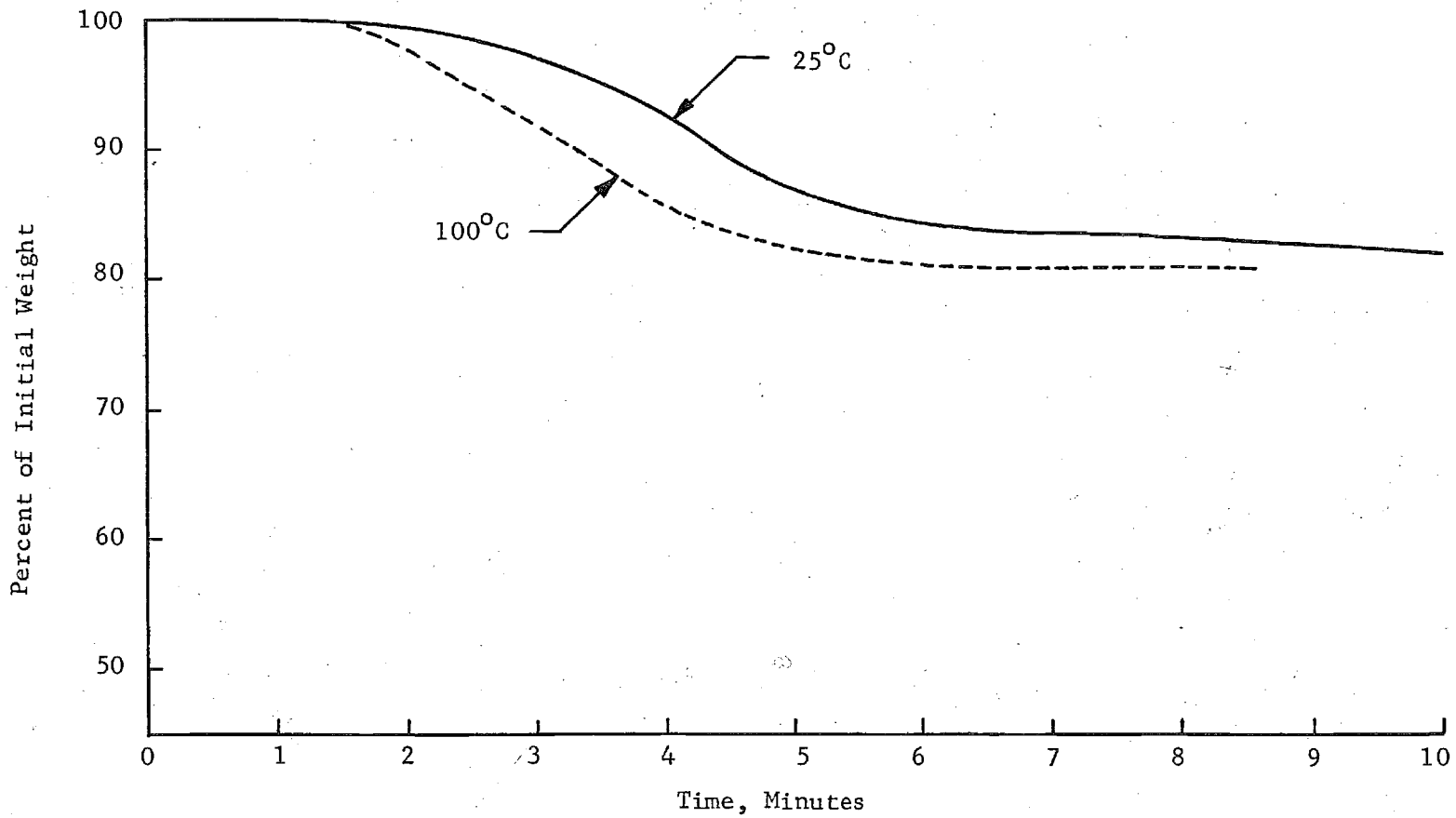

Figure 10. Effect of ventilation air temperature on sample weight loss for nonflaming combustion of chlorinated alkyd paint exposed to a radiant flux of 5 W/cm^2.

reflected in the slight decrease in the amount of char residue. On the other hand, Table 3 and Fig. 11 show that for flaming combustion of the chlorinated alkyd paint, increasing the ventilation air temperature results in a significant increase in peak mass loss rate. For flaming tests in 300°C air the peak mass loss rate (1.1 mg/cm^2-s) was nearly twice that obtained in the room temperature flaming tests. The peak mass loss rate also occurs earlier at elevated ventilation air temperatures. For 300°C ventilation air, half of the mass loss has occurred by 1.3 minutes after initiation of exposure, while about 3.2 minutes are required for a similar mass loss to occur in the room temperature environment. Also heating the ventilation air for the flaming tests resulted in further small reductions in the percentage of initial mass remaining as char. In each of the flaming tests the pilot flame and radiant heating were maintained for ten minutes. The results of the flaming tests are consistent with increased convective heat transfer to the samples from the hot ventilation gas which results in increased pyrolysis rates and greater amounts of material pyrolyzed.

Mean particle diameters for nonflaming tests of chlorinated alkyd paint conducted in room temperature and 100°C atmospheres are compared in Figure 12. It is seen that this moderate amount of heating has a pronounced effect on the shape of the curve of mean particle diameter (D_{32}) vs time. In contrast to the relatively constant values of D_{32} followed by a gradual decline obtained in room temperature air, at 100°C there is an initial sharp peak in D_{32} of nearly 1.4 microns followed by a short plateau at about 1.0 μm followed by a rapid decline in particle size. In both cases the maximum optical density occurs shortly after the beginning of the final

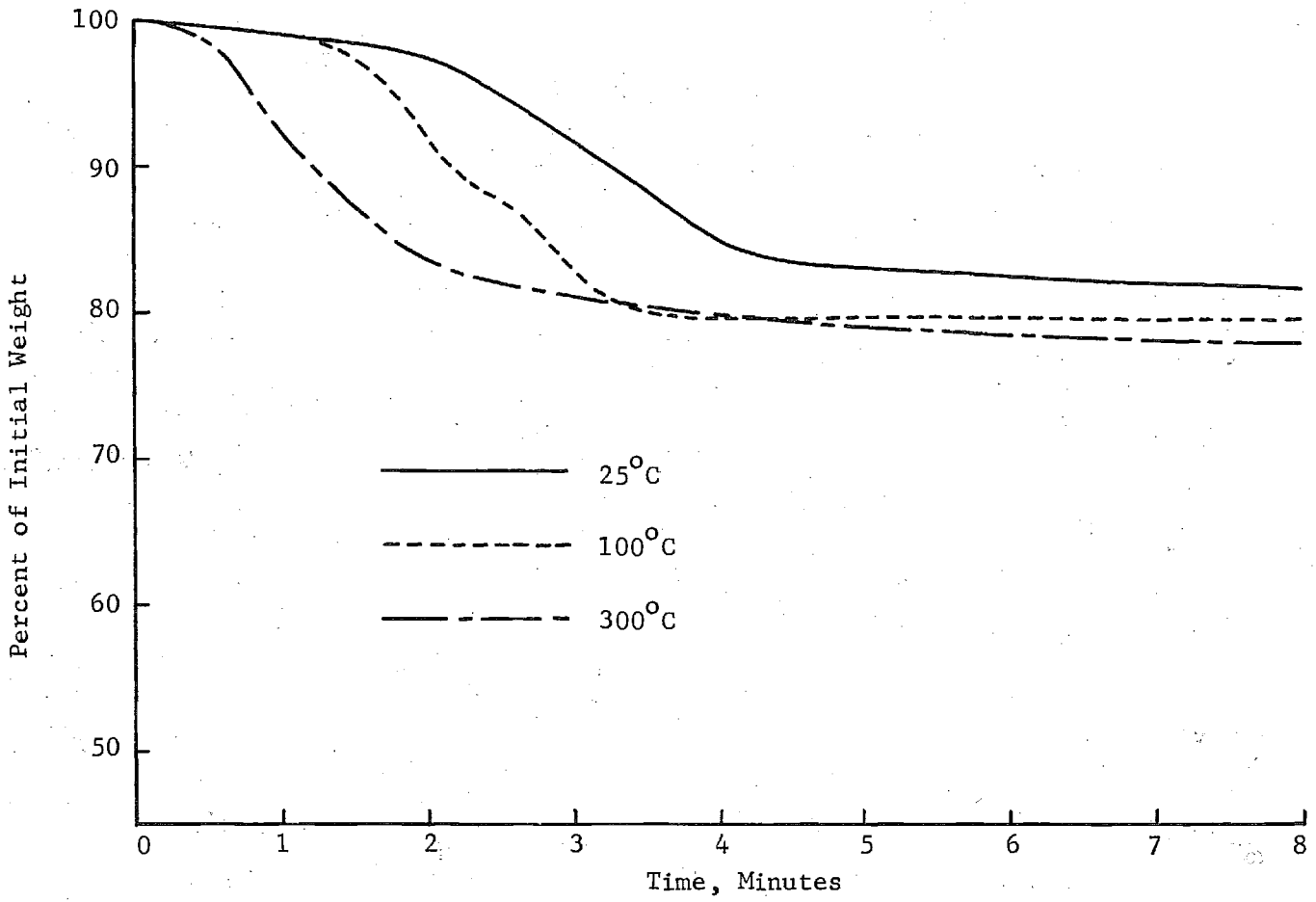

Figure 11. Effect of ventilation air temperature on the sample weight loss for flaming combustion of chlorinated alkyd paint exposed to a radiant flux of 5 W/cm^2.

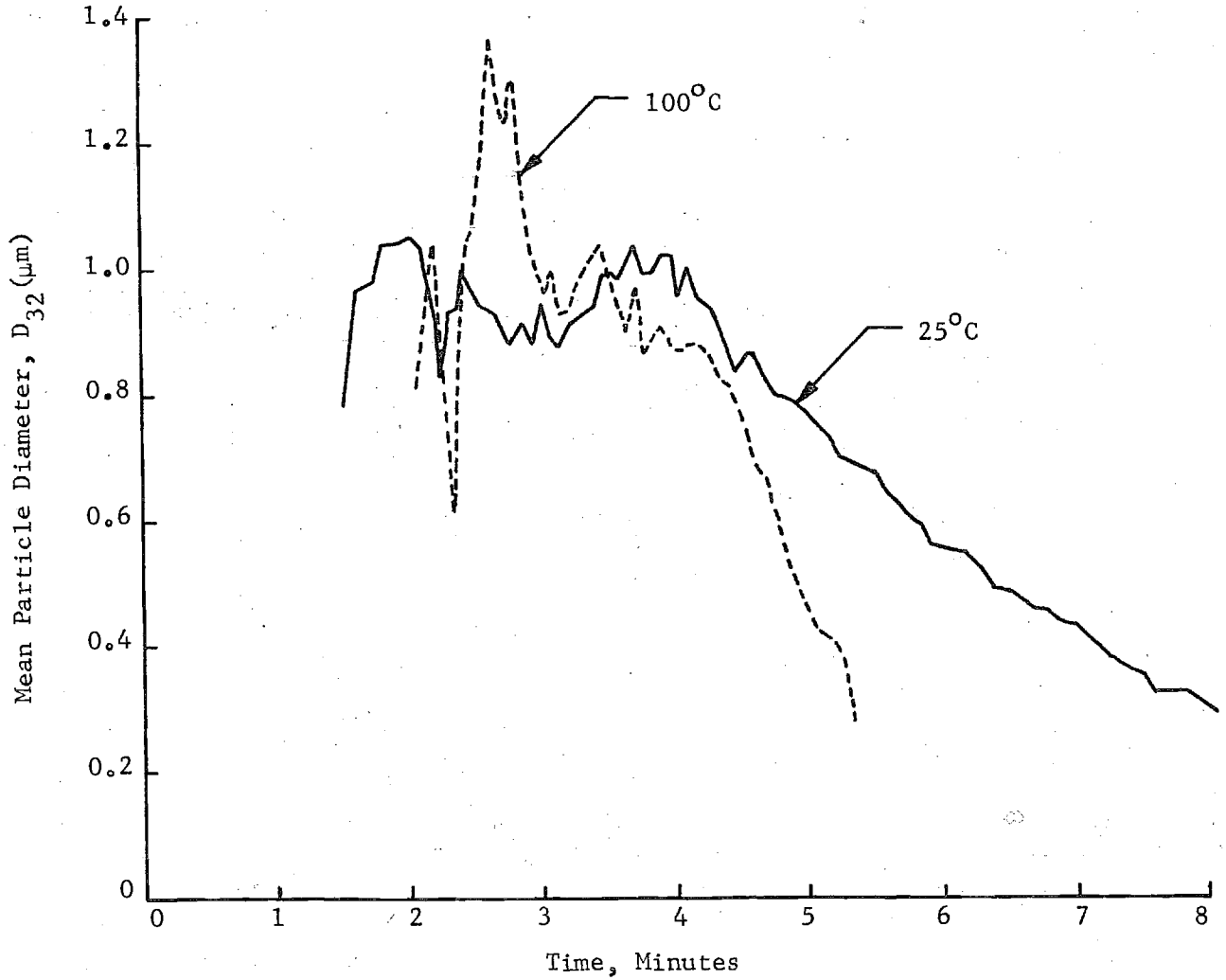

Figure 12. Effect of ventilation air temperature on the smoke mean particle diameter for nonflaming combustion of chlorinated alkyd paint exposed to a radiant flux of 5 W/cm^2.

decline in D_{32}. Although the shapes of the curves are different, moderate increases in environmental temperature have little effect on the mean particle diameters obtained near the time of peak optical density (Table 4). It should also be noted that the sharp peak in particle size for the 100°C test occurs at a time when the optical density, and hence the particle volume fraction, is relatively low. Even though pyrolysis begins earlier at 100°C than at room temperature, particulate light scattering is detected later in the higher temperature test due to the suppressed condensation of the more volatile pyrolysis products.

The effect of environmental temperature upon optical density (λ = .488 μm) during nonflaming tests of the chlorinated alkyd paint is shown in Fig. 13. The curves in Fig. 13 are based on directly measured values, while the corresponding peak optical densities (λ = .488 μm and .633 μm) given in Table 4 have been corrected for the higher ventilation air flow rates due to the expansion of the ventilation air during the constant pressure heating process. The curves of optical density versus time for the two temperatures are similar in shape, but the peak optical density at 100°C is roughly half that obtained in the room temperature test. The peak optical density also occurs slightly earlier in the hotter ventilation air. These trends are consistent with reduced condensation of pyrolysis products and increased heat transfer to the sample as the ventilation air temperature increases.

Figure 14 shows the effect of ventilation air temperature upon the mean particle diameters obtained during flaming combustion of the chlorinated alkyd paint. For tests in room temperature (25°C), 100°C and 300°C air, the pilot flame was ignited at t = 0, but the ignition of the sample

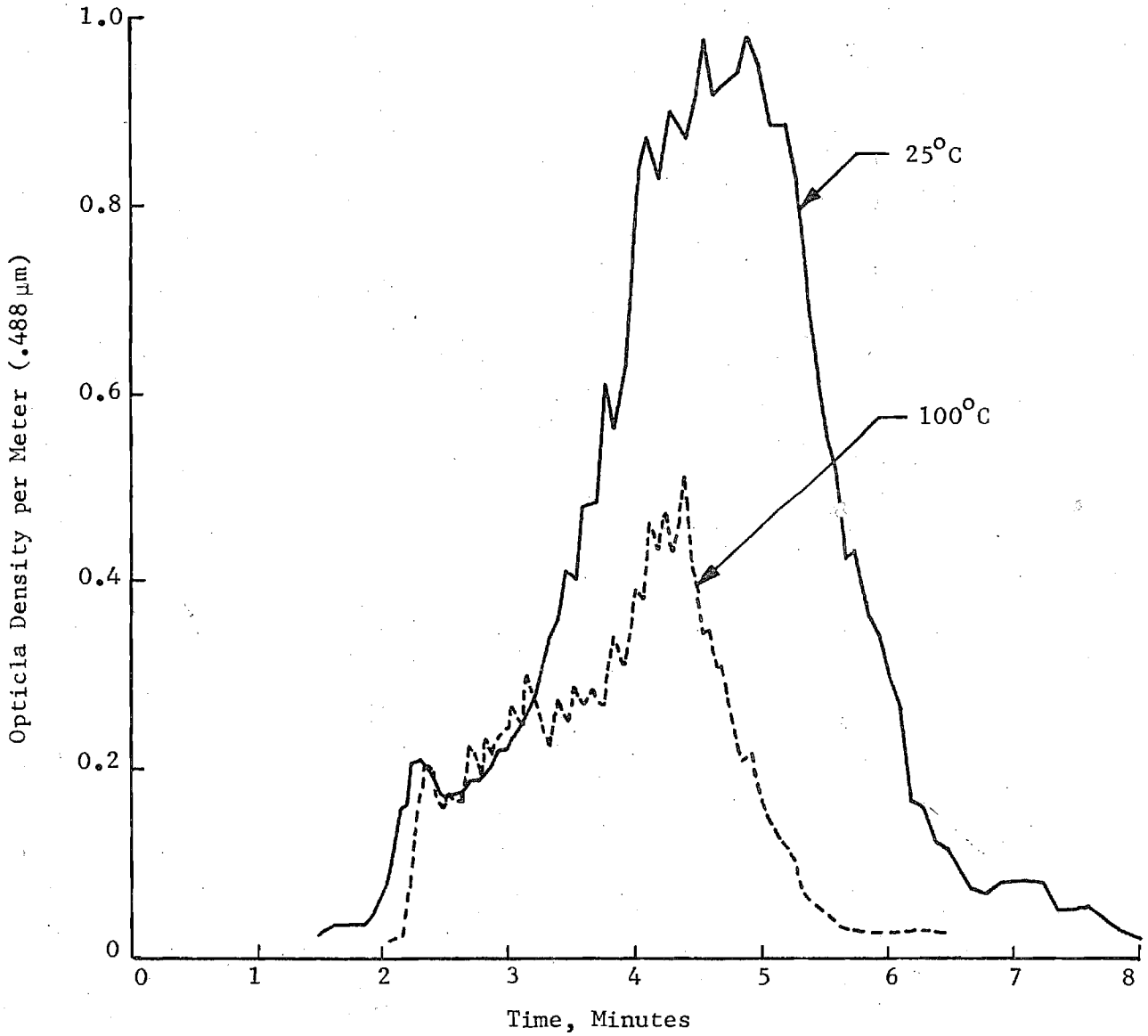

Figure 13. Effect of ventilation air temperature on the smoke optical density for nonflaming combustion of chlorinated alkyd paint exposed to a radiant flux of 5 W/cm^2.

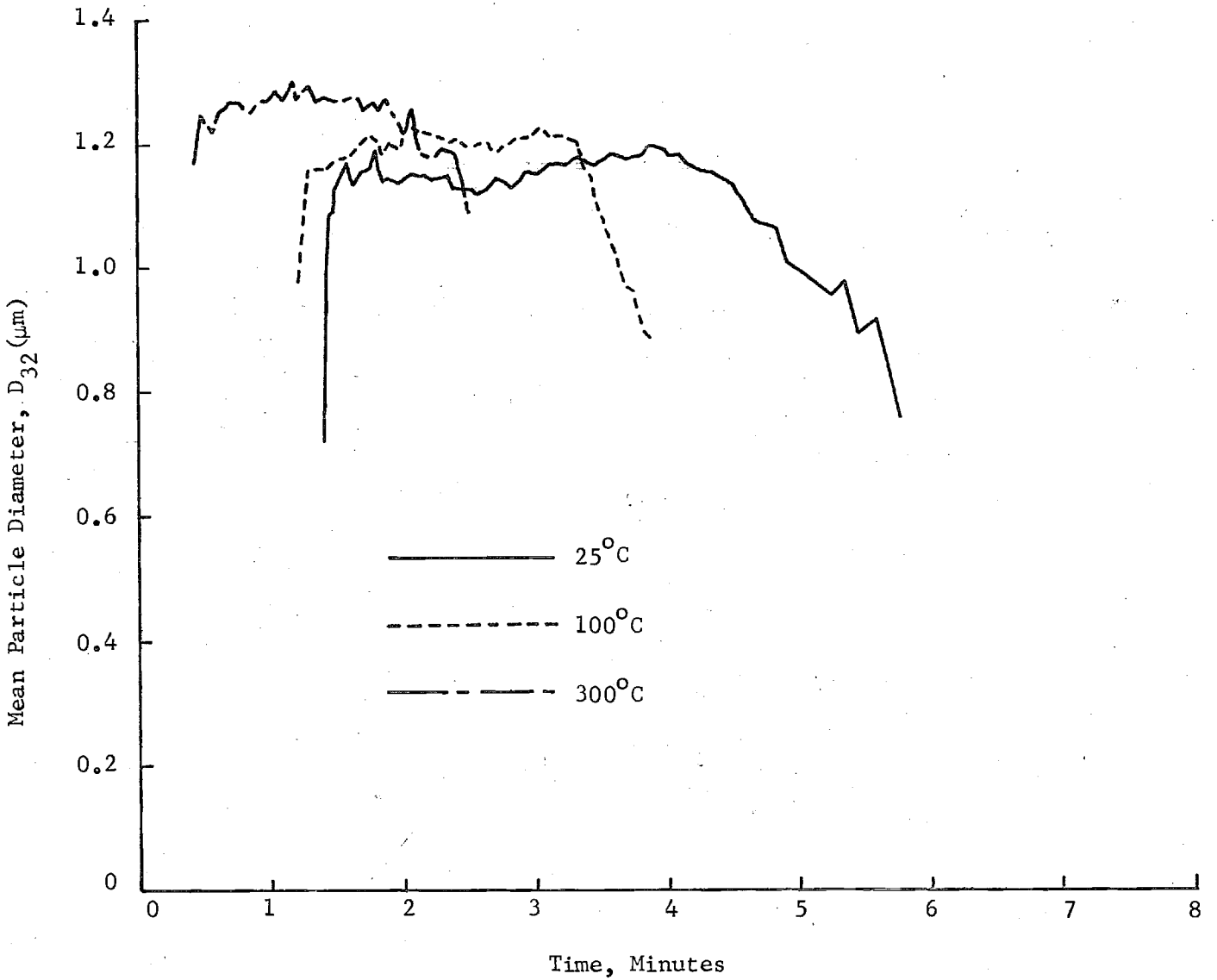

Figure 14. Effect of the ventilation air temperature on the smoke mean particle diameter for flaming combustion of chlorinated alkyd paint exposed to a radiant flux of 5 W/cm^2.

was delayed until sufficient pyrolysis products were evolved to form a combustible mixture. As expected this ignition delay becomes shorter as the environmental temperature is increased as evidenced by the sharp rise in light scattering and particle size exhibited at the beginning of each curve shown in Fig. 14. These curves and the data in Table 4 also show a small but definite trend of increasing mean particle diameter D_{32} as the ventilation air temperature is increased. This behavior has been observed to various degrees for a variety of polymeric materials.[3,6,8] It has been demonstrated experimentally that increasing the temperature of gaseous diffusion flames generally leads to greater quantities of soot and larger soot agglomerates produced within the flame.[9] This is expected to enhance further agglomeration processes in the smoke plume, which accounts for the larger particle sizes observed.

Curves of optical density variation with time for flaming combustion of the chlorinated alkyd paint samples at different ventilation air temperatures are presented in Fig. 15. The optical density peaks generally occur at earlier times as the environmental temperature increases, and the directly measured peak values of optical density are not significantly influenced by temperature. However when the dilution effect due to the increase of the volumetric ventilation flow rate with temperature is taken into account, the peak optical density ($\lambda = .488\ \mu m$) at 100°C is about 50% higher than at room temperature, while the corresponding increase in peak optical density at 300°C is about 75% (Table 4). For the room temperature and 100°C tests there were always two prominent optical density peaks with considerable variations in peak heights from one test to another. Thus the

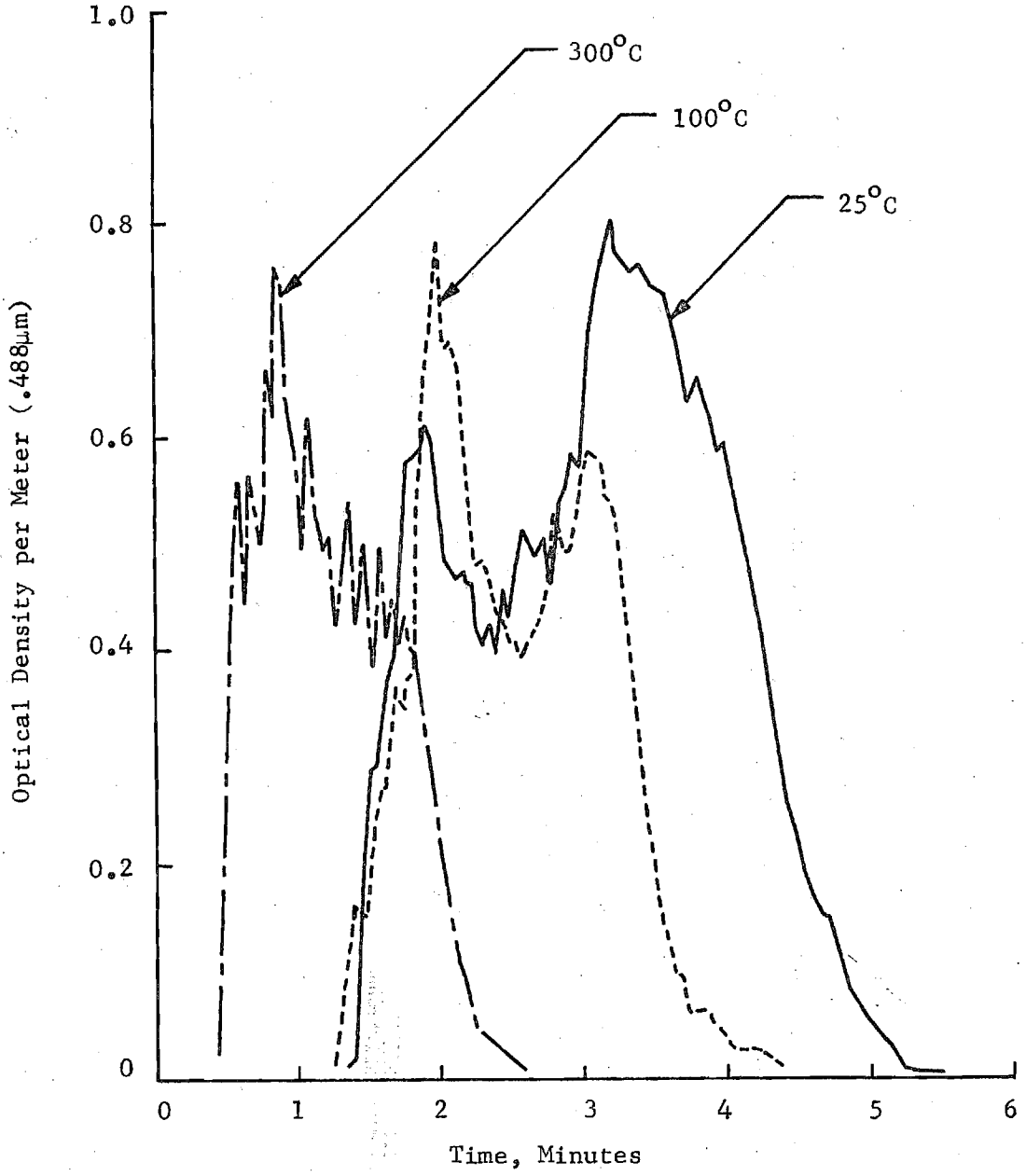

Figure 15. Effect of ventilation air temperature on the smoke optical density for flaming combustion of chlorinated alkyd paint exposed to a radiant flux of 5 W/cm^2.

OD_{max} values given in Table 4 are averages of the largest peak values over a number of replicate tests. The second peak generally predominated in the room temperature tests, while the first peak was more prominent in the 100°C tests. At 300°C the second peak was either absent or much smaller than the main peak. It thus appears that the two optical density peaks arise from different physico-chemical mechanisms, one which is enhanced by increasing temperature (first peak) and one which is suppressed by increasing temperature (second peak).

Smoke Particle Refractive Index and Volume Fraction

For nonflaming tests of the chlorinated alkyd paint, measurement of the ratio of optical densities, OD_R/OD_B, and the 90-degree scattering ratio, $I_{\parallel}/I_{\perp}$, were used to determine the refractive index of the smoke particles. For each test, it was initially assumed that the particles were nonabsorbing ($k = 0$), and the measured values of $I_{\parallel}/I_{\perp}$ in blue-green light ($\lambda = .488$ μm) along with the previously determined values of D_{32} were used to calculate the corresponding refractive index n_B. Measured OD_R/OD_B values were also used to obtain the refractive index, assuming that $k = 0$ and that n does not vary significantly with wavelength.

Values of n_B determined from the 90°-degree scattering data for a test in room temperature air reveal considerable variations in refractive index with time during a test, as shown by the solid curve in Fig. 16. For this case refractive index exhibits a gradual rise from values just below 1.30 to a maximum of nearly 1.375 followed by a gradual decline. Such variations in refractive index indicate corresponding variations in the chemical

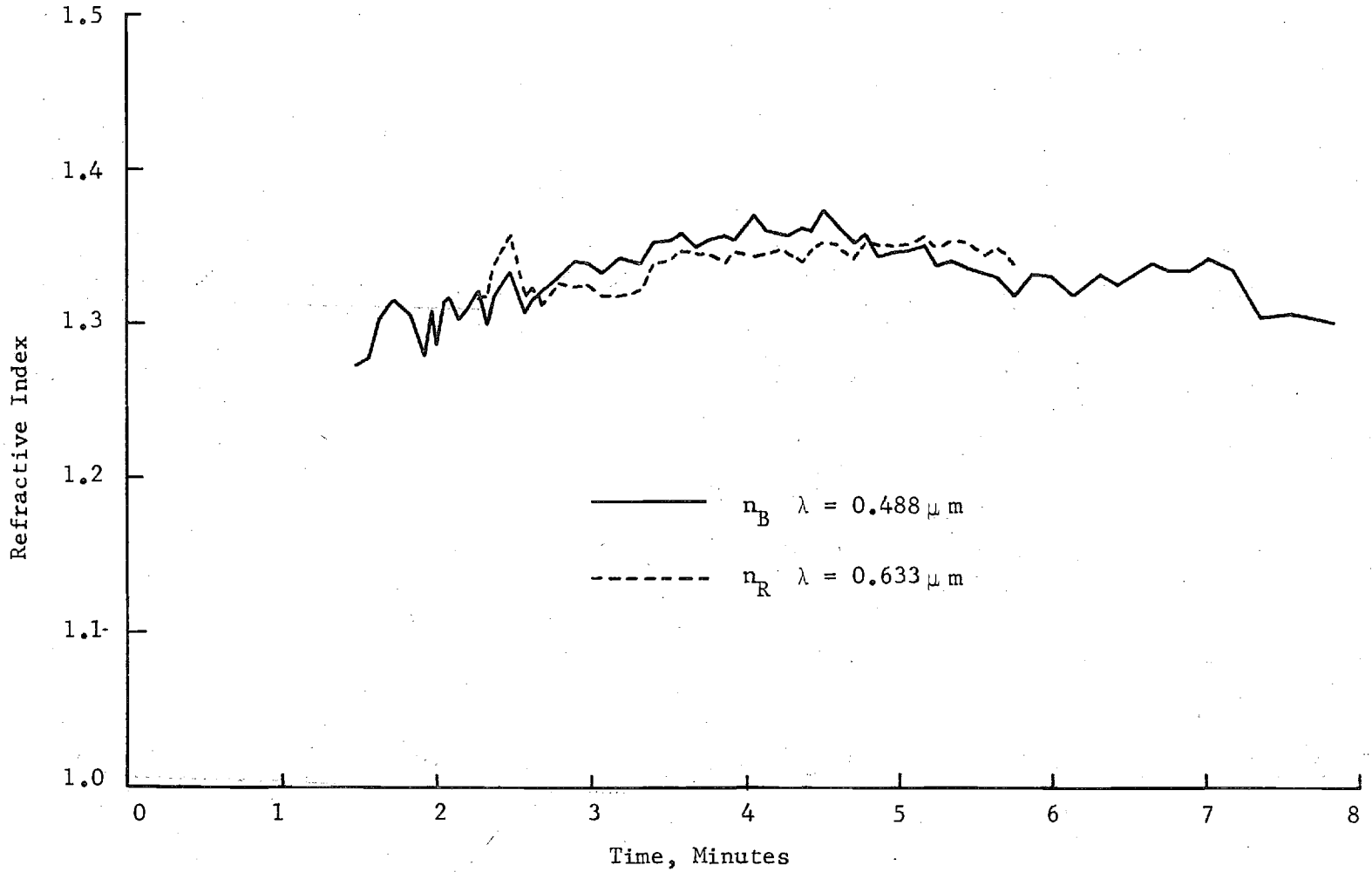

Figure 16. Variation of smoke particle refractive index during nonflaming combustion of chlorinated alkyd paint exposed to a radiant flux of 5 W/cm^2 in room temperature ventilation air (25^{o}C).

composition of the smoke particles (presumed to be mixtures of liquid organic compounds) during the nonflaming test. Near the time of peak optical density, the 90-degree scattering data gave an average value of n_B of 1.355 (Table 5), while the optical density ratio yielded a smaller value, $n_R = n_B = 1.338$. Assuming slightly absorbing particles did not resolve this discrepancy, as the Mie theory gave no solution for positive values of k. On the other hand, allowing n to vary with wavelength (with k = 0) successfully fitted both sets of data by calculating n_R from the measured OD_R/OD_B values using the n_B values obtained previously from the $I_{\parallel}/I_{\perp}$ data. As shown in Fig. 16 (dashed curve), the refractive index in red light (λ = .633 μm) is slightly smaller than the refractive index in blue-green light (λ = .488 μm) for the middle portion of the test, and it exhibits similar variations with time during this period. The average value of n_R at peak optical density was $n_R = 1.343$.

Refractive index values were also measured for smoke particles produced under nonflaming combustion in ventilation air at 100°C. Under the assumption of nonabsorbing particles (k = 0) variations in refractive index were again observed as the test proceeded. The refractive index measured during the time of maximum optical density was 1.314 (λ = .488 μm), which was somewhat lower than the corresponding value measured under room temperature conditions (Table 5). The refractive index in red light (λ = .633 μm) was only slightly larger (n_R = 1.319) than the values in blue-green light. Both of these values are lower than would be expected for the higher boiling organic compounds that would be expected to condense in the higher temperature atmosphere (Reference 6, Appendix B).

Table 5. Smoke Refractive Index, Volume Fraction, and Total Volume for Chlorinated Alkyd Paint.

Mode	Ventilation Air Temperature (°C)	Radiant Flux (W/cm^2)	Refractive Index m_B(NF) or m_s(F)	η_v	Peak Volume Fraction (ppm)	Specific Total Particle Volume (cm^3/g)	$\frac{\Gamma}{\Gamma_{25}}$
NF	25	5.0	1.355-0.0i	-	0.42	0.040	1.00
NF	100	5.0	1.417-0.095i	-	0.26	0.017	0.42
F	25	5.0	1.152-0.107i	0.259	0.76	0.054	1.00
F	100	5.0	1.173-0.123i	0.294	1.09	0.043	0.76
F*	200	5.0	1.154-0.109i	0.262	0.79	0.047	0.78
F	300	5.0	1.144-0.101i	0.245	1.43	0.050	0.79
F*	300	5.0	1.149-0.105i	0.254	1.95	0.047	0.75

* Spontaneous flaming ignition occurred during a "nonflaming" test (i.e., no pilot flame).

To investigate the possibility that the particles produced in the 100°C nonflaming tests absorb as well as scatter light (i.e. $k \neq 0$), plots of $I_{\parallel}/I_{\perp}$ and OD_R/OD_B as a function of mean particle diameter D_{32} were constructed. A typical plot for a 100°C test is shown in Fig. 17. By assuming reasonable values of the complex refractive index m_B, good curve fits were obtained using the Mie theory for various portions of the 90°-scattering data. For example, $m_B = 1.422 - 0.10i$ gave a good fit for D_{32} less than 0.85 μm, which includes the data obtained around the time of peak optical density (between 2.5 and 5.5 minutes after start of test). For larger particles ($D_{32} > 0.85$ μm), which were produced during the first 2.5 minutes of the test, $m_B = 1.414 - 0.085i$ gave a better fit. The theoretical curves corresponding to these values of m_B are shown in the upper plot of Fig. 17.

In order to fit the optical density ratios (OD_R/OD_B) plotted in the lower part of Fig. 17, it was necessary to allow the complex refractive index m to vary with wavelength. A fairly good fit for particles smaller than 0.85 μm was obtained using $m_B = 1.422 - 0.10i$ (obtained from $I_{\parallel}/I_{\perp}$ data) and $m_R = 1.343 - 0.17i$. The theoretical curve obtained with this combination of refractive indices is also shown in the lower plot of Fig. 17.

The curve fits and data shown in Fig. 17 indicate a strong possibility that moderately absorbing particles are produced by nonflaming combustion of the chlorinated alkyd paint in air heated to 100°C. Although m_R and m_B are assumed to be constants during the curve fitting process, the actual values probably vary with time during the test which may account for the scatter of the experimental data values around the theoretical curves. Such refractive index variations would indicate variations in the chemical

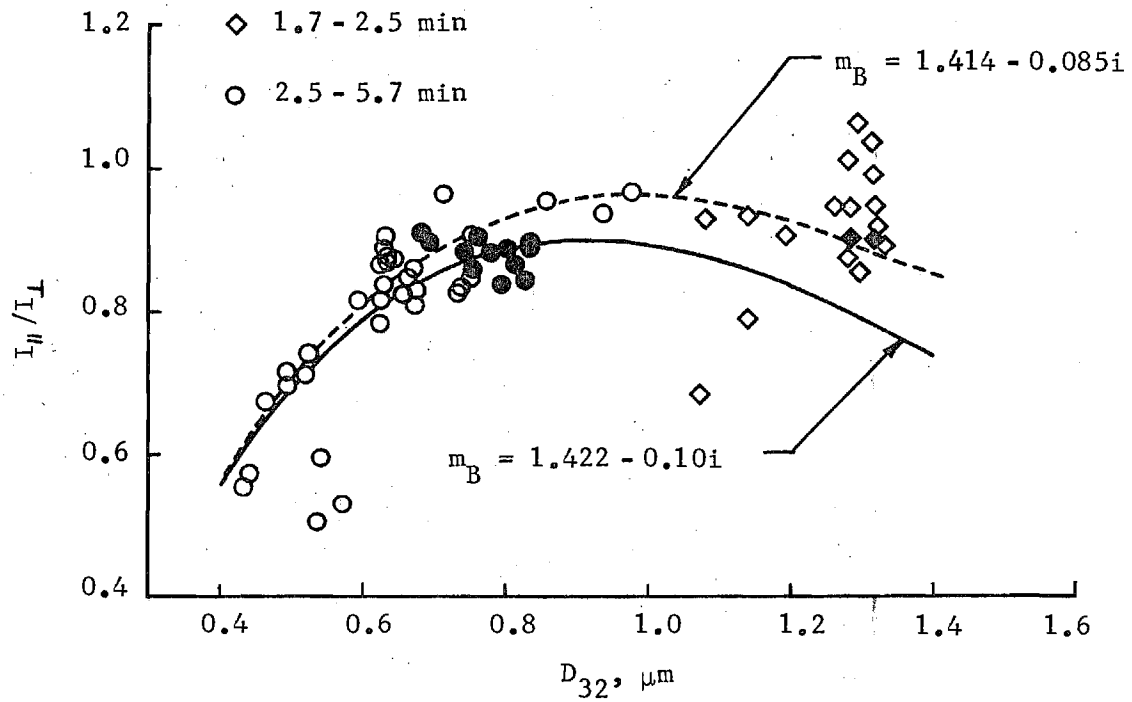

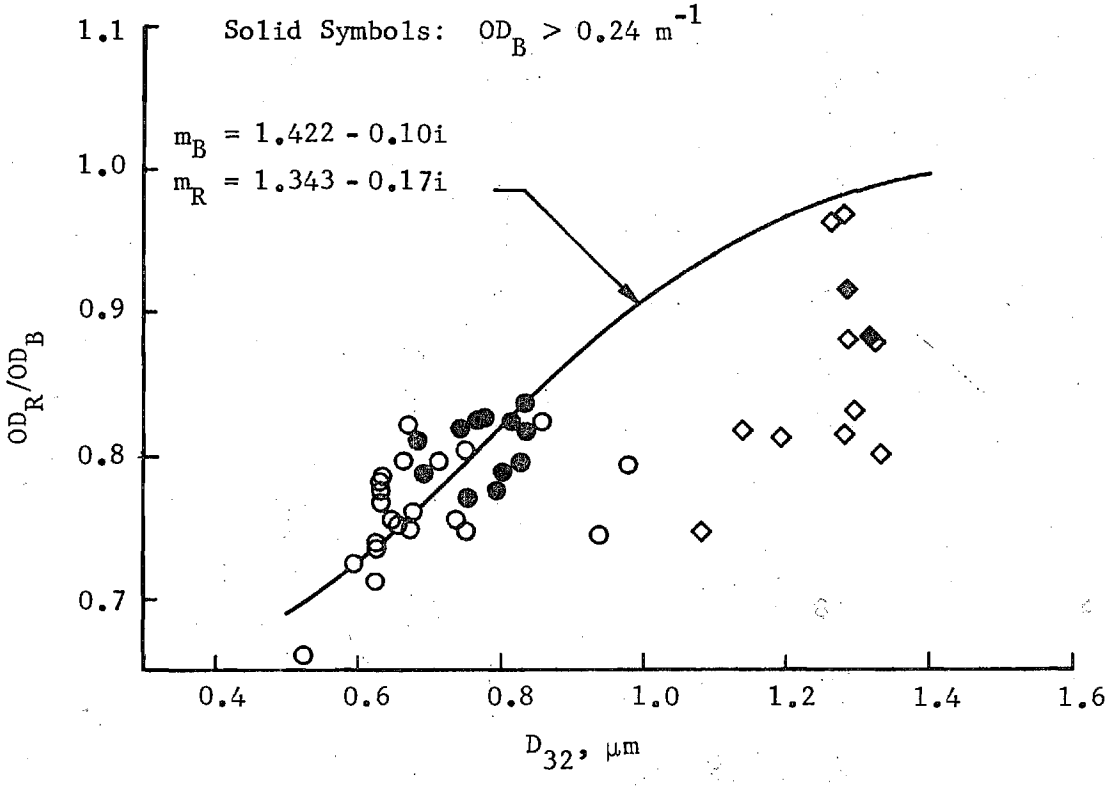

Figure 17. Optical density ratios and 90°-scattering ratios for nonflaming combustion of chlorinated alkyd paint exposed to a radiant flux of 5 W/cm^2 in 100°C ventilation air.

compositions of the smoke particles during various stages of the pyrolysis process.

Particulate volume fractions for the nonflaming tests of the chlorinated alkyd paint samples are shown in Fig. 18. The volume fractions for the room temperature test were computed using the refractive index values given in Fig. 16, which were obtained from the 90°-scattering data assuming nonabsorbing particles. The corresponding curve for the $100^{\circ}C$ test was obtained using a constant value of the complex refractive index ($m = 1.422 - 0.10i$, moderately absorbing particles) determined by the curve fitting procedure illustrated in Fig. 17. Volume fractions for the $100^{\circ}C$ test were also computed assuming nonabsorbing particles; for most of the test these values ranged from 4% to 18% lower than those calculated using the complex refractive index. The shapes of the curves of volume fraction versus time and their dependence on ventilation air temperature are similar to those of the optical density curves given in Fig. 13. This shows that the optical density of the smoke is determined principally by its concentration and that variations in particle size and refractive index only play secondary roles. Peak volume fractions for these tests are given in Table 5.

For the case of flaming combustion of the chlorinated alkyd paint samples, the soot particles produced are highly absorbing, and the determination of the complex refractive index directly from the measured values of OD_R/OD_B and $I_{\parallel}/I_{\perp}$ is difficult and unreliable. Figure 19 shows measured values of $I_{\parallel}/I_{\perp}$ and OD_R/OD_B plotted versus D_{32} for a typical flaming test of the chlorinated alkyd paint conducted in room temperature air. Also plotted in Fig. 19 are curves of $I_{\parallel}/I_{\perp}$ and OD_R/OD_B vs D_{32} which

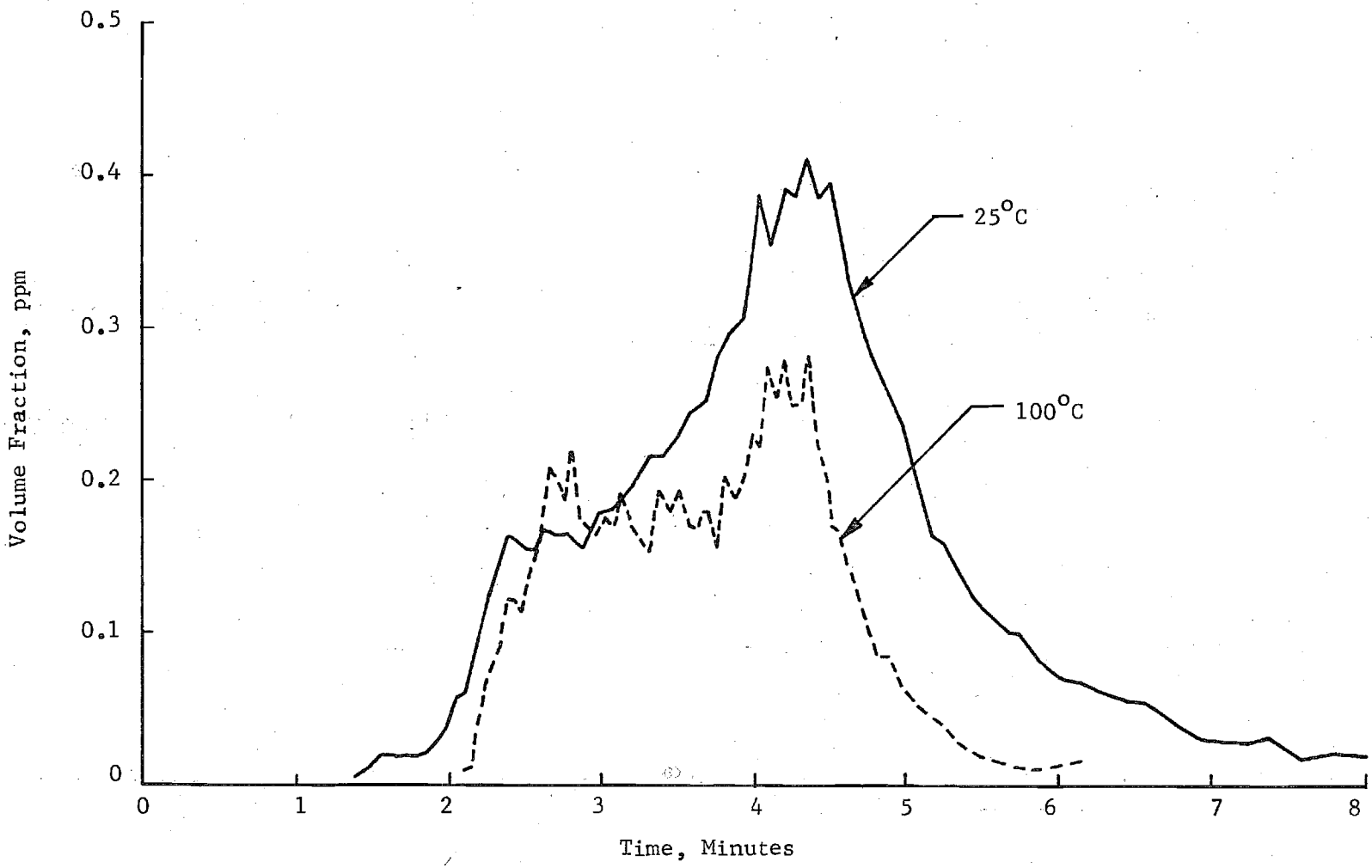

Figure 18. Effect of ventilation air temperature on the particulate volume fraction for nonflaming combustion of chlorinated alkyd paint exposed to a radiant flux of 5 W/cm^2.

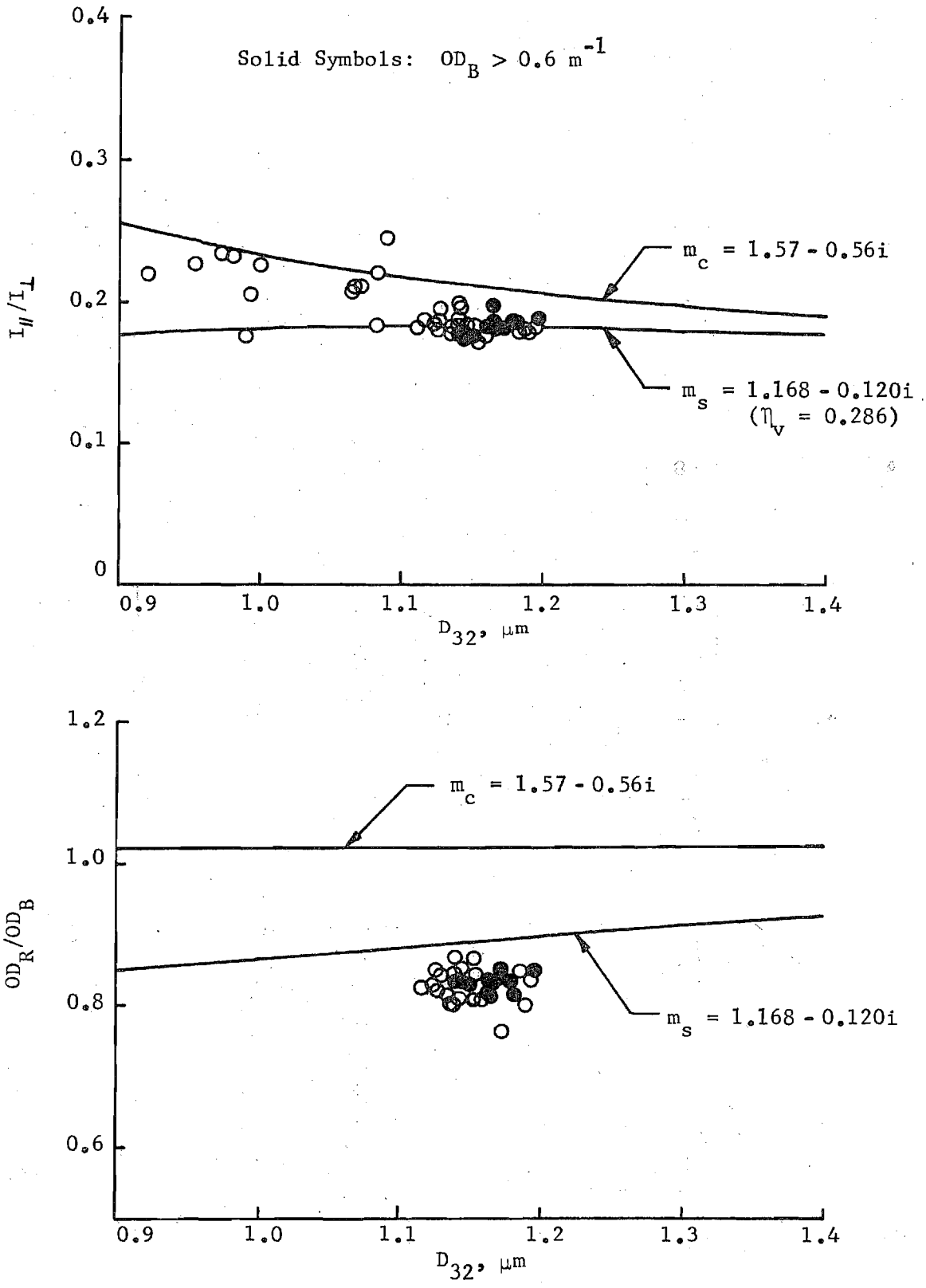

Figure 19. Optical density ratios and 90°-scattering ratios for flaming combustion of chlorinated alkyd paint exposed to a radiant flux of 5 W/cm^2 in room temperature ventilation air (25°C).

were calculated using the Mie scattering theory for spheres with m = 1.57 - 0.56i. The measured values of $I_{\parallel}/I_{\perp}$ are seen to cluster about 0.18 which is about 12% below the theoretical values. In addition, the measured optical density ratios lie about 20% below the Mie curve for these smoke particles. Similar discrepancies between theoretical and measured values of $I_{\parallel}/I_{\perp}$ and OD_R/OD_B were also obtained for flaming tests conducted in heated ventilation air.

In a recent paper by Santoro, et al.[10] it was shown that similar discrepancies between experimental observations and the Mie theory for polydispersions of absorbing spheres can be resolved. There it was concluded that the loosely packed, low-density soot agglomerates have an effective refractive index m_s that is significantly reduced below the refractive index m_c of the particulate material of which they are composed. This downward scaling of the refractive index was applied to the interpretation of the data shown in Fig. 19 by using the Lorentz-Lorenz formula to relate m_s and m_c as a function of f_v[10,11], the fraction of the optical mean "particle" volume that is actually occupied by the particulate material. Using m_c = 1.57 - 0.56i, measured values of $I_{\parallel}/I_{\perp}$ and D_{32} yield a unique value of $m_s = n_s - ik_s$ from which f_v can also be determined. The best fit to the $I_{\parallel}/I_{\perp}$ data shown in Fig. 19 is given by m_s = 1.168 - 0.120i for which f_v = 0.286. Using this same value of m_s, the Mie theory gives significantly lower values of OD_R/OD_B which are only about 7% above the experimental data (Fig. 19). Although this small remaining discrepancy may be due in part to variations in the effective refractive index with wavelength, it is also within the expected experimental error.

Effective refractive indices were also obtained from the flaming tests in heated ventilation air; these are given in Table 5 along with the corresponding values of η_v. For these tests values of η_v were between 0.24 and 0.30 with the largest values occurring at 100°C; however, the effect of environmental temperature upon η_v appears to be weak. Therefore, for all of the flaming tests of the chlorinated alkyd paint an average value of η_v = 0.264 was obtained for which the corresponding effective refractive index is m_s = 1.155 - 0.110i. Thus the soot particulates produced by flaming combustion of the chlorinated alkyd paint appear to be very loose, low-density aggregates of smaller primary soot particles which occupy slightly more than 25% of the optical mean volume as determined from the forward scattering measurements. The effective complex refractive index of these agglomerates (both n_s and k_s) is much smaller than the complex refractive index customarily used for the bulk particulate material.

Volume fractions for flaming combustion of the chlorinated alkyd paint samples were calculated using the downward scaled complex refractive index (m_s) values given in Table 5. These curves for ventilation air temperatures of 25°C, 100°C and 300°C are presented in Fig. 20 where the data has been corrected to the standard flow rate of 425 l/min to eliminate the dilution effect at high temperatures. The peak volume fractions are also given in Table 5; these values exhibit the same trend with increasing ambient temperature as the optical density. Again smoke concentration appears to be the primary factor influencing the light-obscuring properties of the smoke produced by flaming combustion of this material. For comparison volume fractions were also computed based on the complex

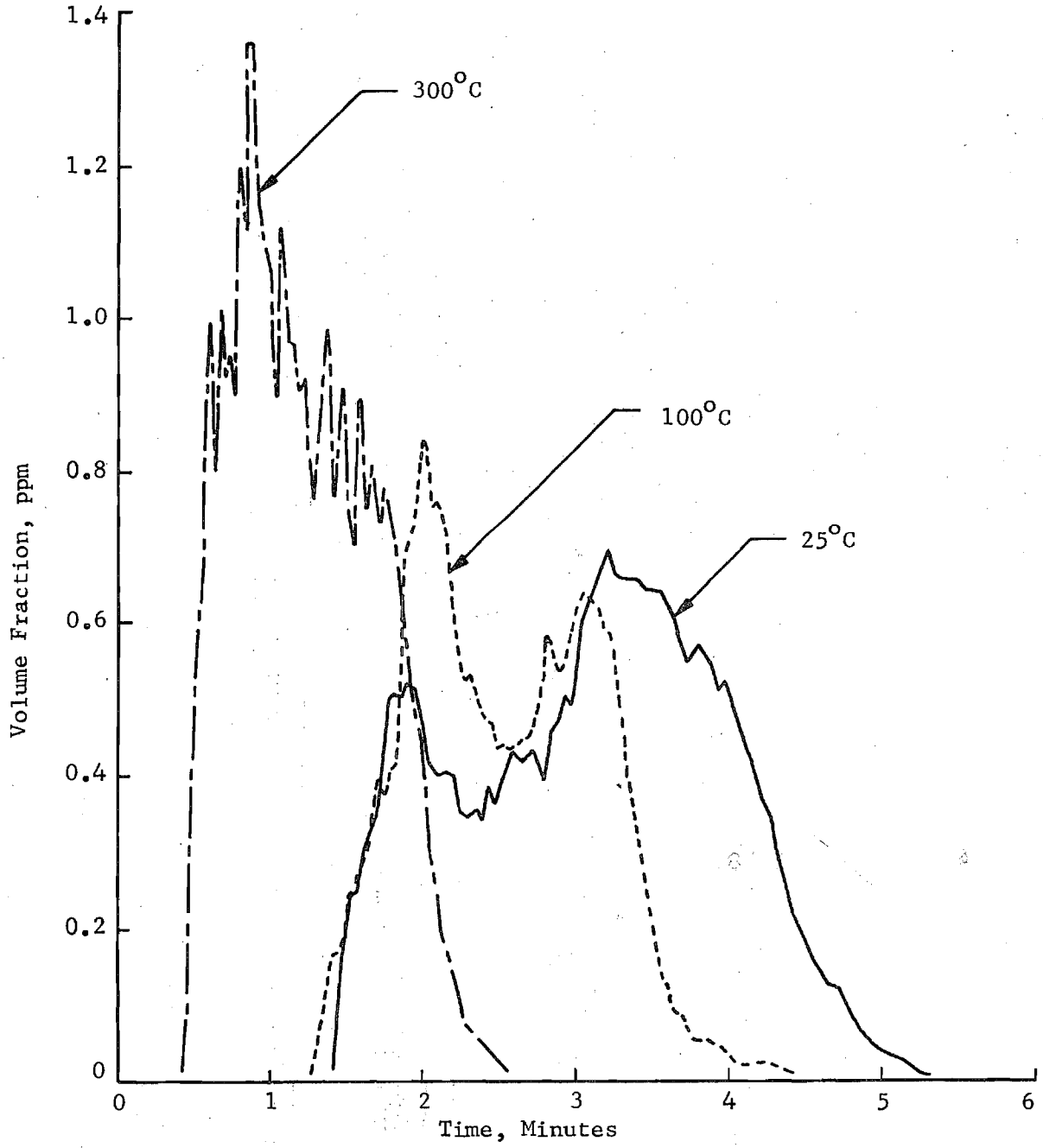

Figure 20. Effect of ventilation air temperature on the particulate volume fraction for flaming combustion of chlorinated alkyd paint exposed to a radiant flux of 5 W/cm^2.

refractive index, m_c = 1.57 - .56i, of the bulk particulate material. Significant differences in the calculated volume fractions were found; peak values obtained using the bulk refractive index averaged about 17% lower than those determined using the effective refractive index.

Values of the total particulate volume were obtained by integrating the volume fraction curves in Figs. 18 and 20 with respect to time. These values were then normalized by dividing by the unburned sample weight to yield a specific total particulate volume (i.e., total particulate volume per unit mass of material burned). Values of the specific total particulate volume (STPV) for both flaming and nonflaming modes are also given in Table 5. For nonflaming combustion, the STPV, like the peak volume fraction, decreases markedly as the ambient temperature is increased. At 100°C the STPV is less than half of that obtained at room temperature. On the other hand, for flaming combustion of the chlorinated alkyd paint samples the STPV is rather insensitive to the ventilation air temperature as seen from Table 5. The average STPV value obtained for all of the flaming tests is nearly 0.05 cm^3/g. This result is surprising considering the much stronger effect of temperature upon the peak height and shape of the curves of volume fraction vs time; however, a close inspection of the curves shown in Fig. 20 reveals that the area under each of the three curves is roughly the same.

Although no sampling data were available for elevated temperatures, the effect of ambient temperature on Γ was estimated from the optical data. These data are also given in Table 5 for both flaming and nonflaming combustion, where Γ is normalized with respect to the corresponding room

temperature value. The Γ values for the nonflaming combustion mode follow the same trend with increasing ventilation air temperature as the specific total particulate volume. For flaming combustion, however, the Γ values estimated for the tests conducted at 100°C and above are all roughly 75% of the corresponding room temperature value.

With the assumption of a particulate density $\rho_p = 1.3$ g/cm^3 for smoke particles produced by nonflaming combustion and $\rho_p = 2.0$ g/cm^3 for soot produced by flaming combustion, the total particulate mass was estimated from the optically determined total particulate volume. For the room temperature tests, the optically determined values of the total particulate mass were then compared with the corresponding values estimated by particulate sampling. For nonflaming combustion, assuming spherical particles, the optically determined particulate masses were about 2.5 times as large as the particulate masses estimated by sampling. Similar discrepancies have been obtained with previously tested materials such as PVC-nitrile rubber and PVC cable jacket material.[8] Possible sources of this discrepancy are uncertainties in the particulate density and complex refractive index, losses in the sampling system, and departures of the size distribution from that assumed in reducing the optical data. For flaming combustion, the total particulate mass was estimated from the optically determined particulate volume obtained using the downward scaled (effective) refractive index by multiplying it by the factor η_v, which represents the fraction of the optical volume occupied by the particulate material. The total particulate masses obtained in this manner average about 3.8 times larger than the corresponding masses obtained by particulate

sampling. However, when the refractive index of the bulk particulate material (i.e., $m_c = 1.57 - 0.56i$) is used and the η_v correction is not applied (i.e. the particles are assumed to be compact spheres), the discrepancy between the total particulate masses is much larger; here the optical particulate mass averages about 11.6 times the mass obtained by sampling. This latter discrepancy is consistent with previous results for flaming tests of PVC-nitrile rubber, PVC cable jacket, and hydraulic fluid[8] in which refractive index downscaling and η_v corrections were not used. It appears from the above results that the nonspherical shape and high void fraction typical of soot agglomerates obtained during flaming combustion accounts for most of the particulate mass discrepancy, while the remaining discrepancy is probably due to the same effects as noted above for nonflaming combustion.

Values of the specific total particulate volume (STPV) given in Table 5 can be used to estimate the smoke volume concentration and optical density for a known quantity of chlorinated alkyd paint burning in a confined space. The STPV value is first multiplied by the total mass of dry paint originally present in the compartment to obtain the total volume of the smoke particulates produced during combustion. Assuming that all of the smoke is uniformly distributed throughout the compartment, the volume fraction φ is next obtained by dividing the previous result by the compartment volume. To obtain the optical density the following formula is used:

$$OD_B = 0.651 \bar{Q}_{ext}(D_{32}, m_B) \varphi / D_{32}$$

where D_{32} is obtained from Table 4, m_B (effective) is obtained from Table 5, and $\bar{Q}_{ext}$ is calculated using the Mie scattering theory. As an example, consider a 10 ft x 10 ft bulkhead (9.29 m^2) covered with 5 coats of chlorinated alkyd paint (approximately 2 kg/m^2) burning in a 25,000 ft^3 (708 m^3) space. The weight of the unburned polymer in this case is 18.6 kg. From Table 5 the worst nonflaming case occurs for a 5.0 W/cm^2 radiant flux in room temperature air, for which the STPV is about 0.040 cm^3/g, while only slightly more particulates (0.050 cm^3/g) are produced for a typical flaming case which occurs in 25°C-300°C air. The worst case values of optical volume fraction are 1.05 ppm for nonflaming combustion and 1.31 ppm for flaming combustion, while the corresponding values of optical density (blue) are 2.7 m^{-1} and 1.4 m^{-1} respectively. From this example, it is clear that greater light obscuration occurs under nonflaming conditions than for flaming combustion. For the nonflaming case the light attenuation is severe, amounting to about 0.2% of the incident light transmitted over a one meter optical path length. It is unlikely that such large amounts of the chlorinated alkyd paint will undergo nonflaming combustion in an actual fire, however, since the radiant flux would have to be supplied by flaming combustion of neighboring materials. Thus flaming combustion of the paint would be expected to occur, especially if the ambient temperature rises above 200°C. In this case the light obscuration is much less severe, amounting to a 4% transmission of blue light over a one meter optical path length.

SMOKE PHYSICAL PROPERTIES DATA FOR INTUMESCENT PAINT

Description of Material and Sample Preparation

The intumescent paint tested was No. 9788 Fire Retardant Paint which is manufactured by Ocean Chemical Co. of Savannah, Georgia specifically for marine applications. Upon exposure to heat or flame this paint swells rapidly to form a thick porous char which insulates and protects the substrate from the fire environment. The Ocean 9788 intumescent paint is an oil-based material which is about 70% solids by weight. It has a wet density of 1.222 g/cm^3, and it dries to form a film with a density of 1.673 g/cm^3. The chemical composition of this paint is proprietary and thus was not available. The color of the paint used in these tests was white.

Samples of the Ocean 9788 intumescent paint were prepared by brushing onto 5.1 cm squares (2 in) of cold rolled steel substrate 1.19 mm (3/64 in) thick. The average weight of the substrates was 29.5 g. The substrates were first cleaned with acetone, then 3 liberal coats of paint were applied with a small brush over a 12 day period with a 1-day drying time between the first and second coats. The average dry mass of paint applied in this manner was 1.63 g with a standard deviation of 0.14 g. This yields an average dry film thickness of 0.378 mm (0.015 in), which is close to the recommended thickness. Storage time under ambient laboratory conditions for these samples ranged from 7 weeks to 56 weeks.

One of the samples was exposed to the flame of a Bunsen burner to observe the intumescent behavior. After about 20-30 seconds of heating in

the flame, the paint began to darken and blister, followed by rapid vertical swelling and expansion of the char. This was accompanied by a slight lateral contraction. The char thickness ranged from about 22 mm in the center to about 27 mm along one edge. The surface had a nodular texture with a scale of about 2 mm. Cutting into the char revealed a fragile cellular structure; light, dry and brittle in the outer layers and somewhat tacky in the layers adjacent to the substrate.

Tests in Room Temperature Ventilation Air

Tests of the Ocean 9788 intumescent paint have been conducted in room temperature ventilation air (25°C) with a radiant flux of 5 W/cm^2. Tests were run either with a propane pilot flame or without the pilot flame in order to study the smoking behavior of the paint under both flaming and nonflaming modes of combustion. However, due to the fire retardant nature of this paint, flaming combustion never occurred in the room temperature tests. Therefore, all of the room temperature tests were essentially conducted under nonflaming conditions with only slight differences due to the presence of the small propane pilot flame. For all of these tests the ventilation air flow rate was 142 L/min (5 CFM). The results of these tests are presented in Figures 21 through 24 and Tables 6 and 7.

For the intumescent paint samples it was impossible to obtain weight loss data during the test due to disturbances caused by the rapidly swelling char which contacted the pilot burner tube and its igniter wire. However an average mass loss rate was calculated based on the initial and final weights

and the time interval over which significant quantities of smoke were being evolved (based on optical density measurements). For the room temperature tests, this average mass loss rate ranged from 0.05 to 0.08 mg/cm^2-s (Table 6). The mass of the char residue, expressed as a percentage of the initial sample mass, was also obtained for the room temperature tests. These values (Table 6) ranged between 55% (with pilot flame) and 58% (no pilot flame). The black char residues obtained in the room temperature tests of the intumescent paint are shown in Figure 21. The coarsely nodular, porous surface texture of the thick char layer is readily seen in these photographs. The white patch near one edge of the char obtained in the test with the pilot flame was caused by direct impingement of the pilot flame upon the char, burning off some of the carbonaceous material and leaving a white residue.

Smoke particle size distributions were obtained using the cascade impactor for room temperature nonflaming tests of the Ocean 9788 intumescent paint exposed to a 5 W/cm^2 radiant flux both with and without the pilot flame. These size distributions are shown in Figure 22 as cumulative curves generated by plotting the percentage of particulate weight having particle diameters less than a given particle size versus the particle size on log-normal probability coordinates. In both cases, a straight line gives a good fit to the cascade impactor data (plotted points), which indicates that the size distribution is log-normal. The mass median diameters (D_{MMD}) and standard deviations (σ_g) obtained from these curves are given in Table 7. For nonflaming combustion without the pilot flame, the particulates consist of a mixture of white and light tan or beige solid particles with a mass median diameter of about 0.6 micron. Here the total

Table 6. Sample Weight Loss Data for Intumescent Paint on Steel Substrate.

Mode	Ventilation Air Temperature (^{o}C)	Radiant Flux (W/cm^2)	Average Mass Loss Rate (mg/cm^2-s)	Char Residue (Percent of Initial Weight)
NF	25	5.0	0.050	57.8
NF	100	5.0	0.19	54.9
NF	150	5.0	0.21	52.5
NF	200	5.0	0.84	56.4
NF	300	5.0	-	50.8
NF*	25	5.0	0.081	55.1
NF*	100	5.0	0.28	54.8
NF/F	100	5.0	0.12	56.4
NF*	300	5.0	0.3	44.7
NF/F	300	5.0	0.24	45.5

* Pilot burner on, but no flaming ignition.

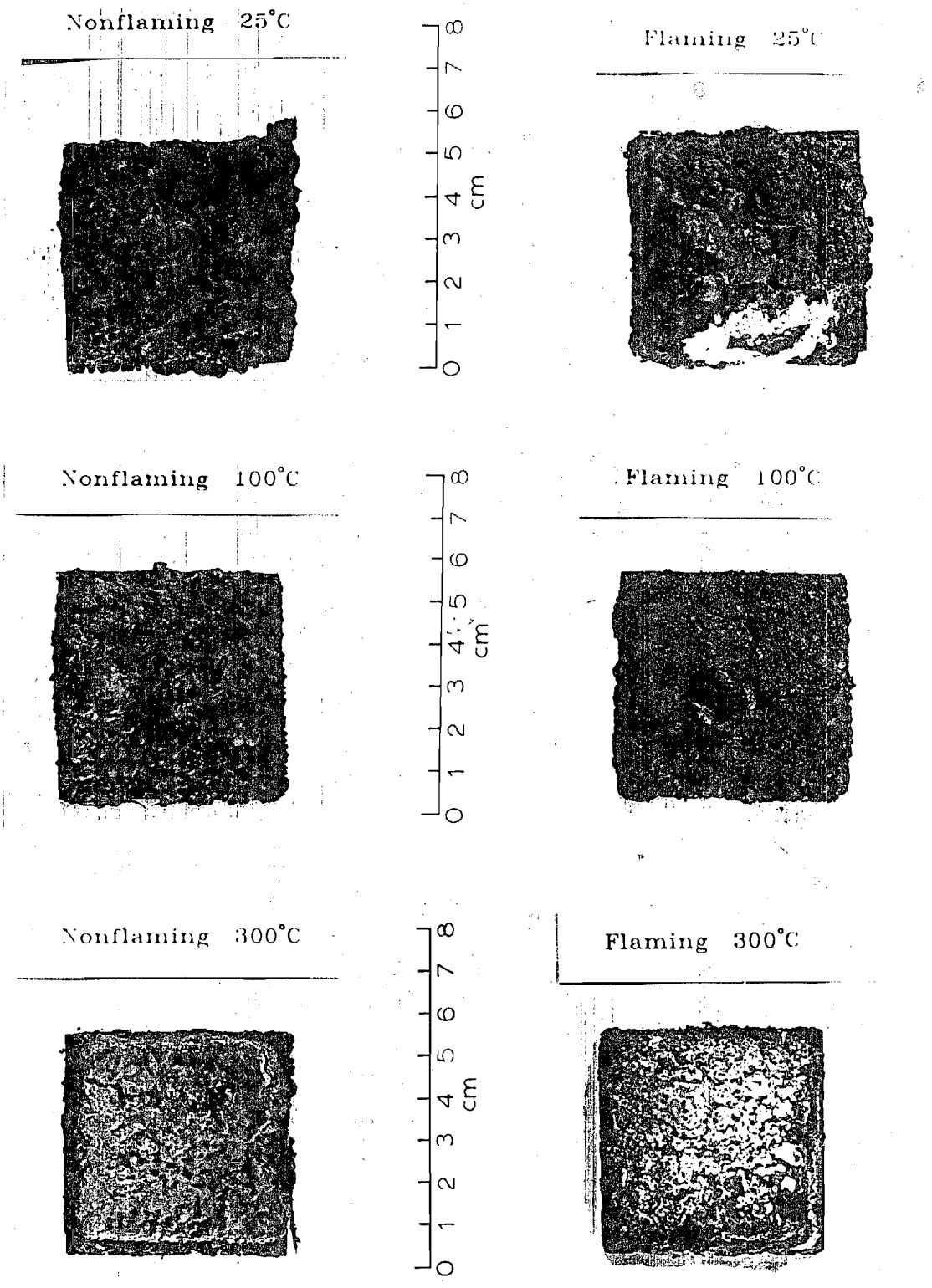

Figure 21. Char Residues for Intumescent Paint Tests.

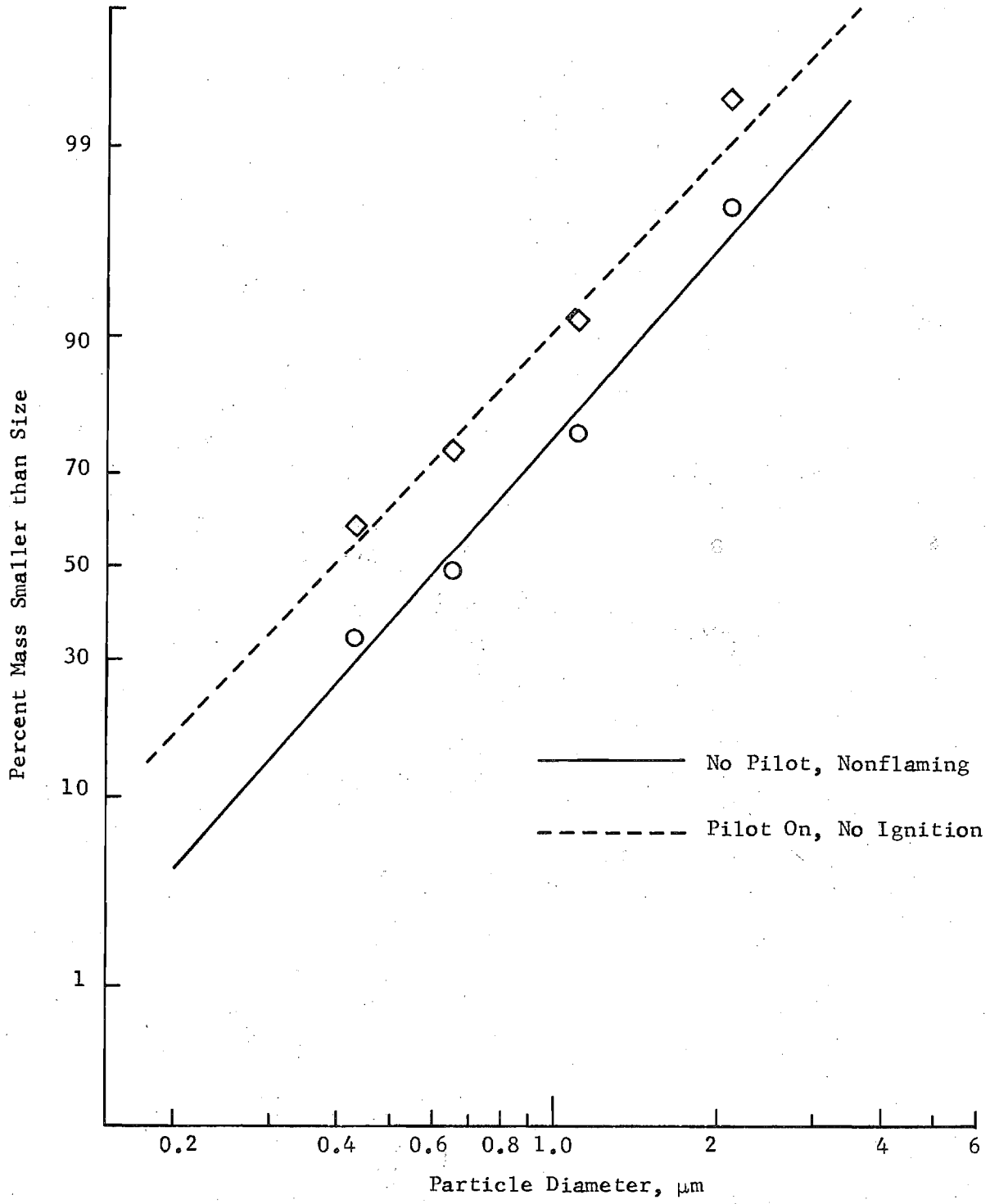

Figure 22. Smoke particle size distribution for nonflaming combustion of intumescent paint exposed to a radiant flux of 5 W/cm^2 in room temperature ventilation air (25°C).

Table 7. Smoke Properties Data for Intumescent Paint.

Mode	T (^{o}C)	Radiant Flux (W/cm^2)	Γ	D_{MMD} (μm)	σ_g	OD_{max} Blue	(m^{-1}) Red	D^{+}_{32} (μm)	Time to Peak OD (min)
NF	25	5.0	0.11	0.61	1.96	0.57	0.42	0.70	3.4
NF	100	5.0	-	-	-	0.71	0.61	0.80	3.0
NF	150	5.0	-	-	-	0.40	0.33	0.50	3.0
NF	200	5.0	-	-	-	0.14	0.06	0.63[a]	2.2
NF	300	5.0	-	-	-	< 0.10	< 0.10	b	-
NF*	25	5.0	0.09	0.39	2.06	0.45	0.32	0.58	4.0
NF*	100	5.0	-	-	-	0.30	0.18	0.73	3.0
F	100	5.0	-	-	-	0.13	0.11	1.18	4.8
NF*	300	5.0	-	-	-	0.48[c]	0.25[c]	b	1.6
F	300	5.0	-	-	-	0.08	-	1.34[a]	4.3[a]

* Pilot burner on, but nonflaming mode.

\+ Average of data points near OD_{max}.

a At peak scattering rather than OD_{max}.

b No measureable scattering in one or both angles.

c Narrow peak without corresponding scattering.

mass of particulates collected on the cascade impactor was only 6.6 mg (.43 μm - 2.1 μm), while about 3.5 mg were collected on the absolute filter (<.43 μm). The particles collected on the cascade impactor plates were examined under a microscope at 30X; they appeared as small agglomerates (about 1 mm across) of fine white solid particles. The sample on the filter appeared to consist of a fine light tan or beige powder. For the test conducted with the pilot flame, flaming ignition did not occur, but a mass median diameter of only about 0.4 micron was obtained. Here the total mass of particulates collected was only 9.8 mg of which about 59% were collected on the absolute filter (<.43 μm). The visual appearance of the particulates collected was the same as the case without the pilot flame.

The sampling data was also used to determine the fraction of the sample mass loss converted to particulates (Γ) for the room temperature tests. These values of Γ, which are given in Table 7, show that between 9% and 11% of the total mass loss appears as particulates for nonflaming combustion of the Ocean 9788 intumescent paint under 5 W/cm^2 radiant flux.

The in situ optical system was used to obtain mean particle diameters (D_{32}) and optical densities produced by nonflaming combustion of the intumescent paint samples. A comparison of mean particle sizes obtained with a radiant flux of 5 W/cm^2, both with and without the pilot flame, is given in Figure 23, while the corresponding optical densities are given in Figure 24.

Figure 23 shows that for nonflaming combustion of the Ocean 9788 intumescent paint a sharp peak in smoke mean particle size occurs shortly

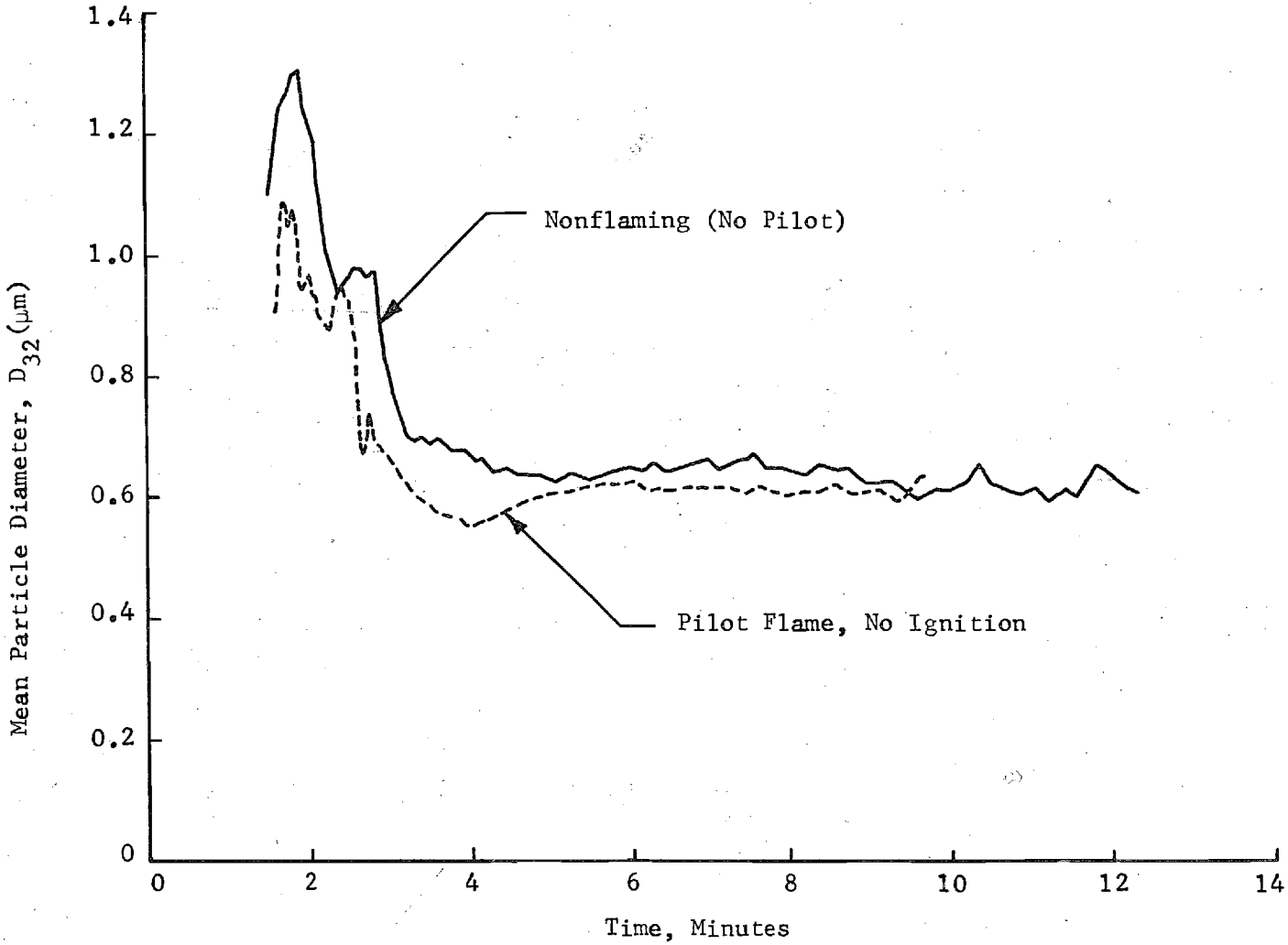

Figure 23. Smoke mean particle diameters for nonflaming combustion of intumescent paint exposed to a radiant flux of 5 W/cm^2 in room temperature ventilation air (25°C).

after pyrolysis begins. For the case without the pilot flame, the maximum value of D_{32} is about 1.3 microns, while D_{32} peaks at about 1.1 microns when the pilot flame is lit. In both cases, smoke mean particle size decreases rapidly during the next two minutes and then levels off to relatively constant values between 0.6 and 0.7 micron for the remainder of the test. Although the pilot flame does not initiate flaming combustion in these room temperature tests, it has a small effect on mean particle size as evidenced by the slightly smaller values of D_{32} obtained with the pilot flame on. Perhaps this is due to a small fraction of the smoke particulates which pass directly through the pilot flame and experience some degree of evaporation or combustion.

The smoke optical densities at the blue-green argon line (.488 μm) for nonflaming combustion of the intumescent paint samples in 25°C ventilation air are presented in Figure 24. Here the optical density rises rapidly between two and three minutes after initiation of radiant exposure and reaches a modest peak of about 0.5 - 0.6 m^{-1} lasting about one minute. Thereafter a much slower decline in light obscuration occurs. For the case with the pilot flame, the optical densities are slightly smaller, which is consistent with the smaller mean particle size.

Comparison of Figures 23 and 24 reveals that the sharp D_{32} peak occurs while the optical density is very low, which implies that the number density and volume fraction of these larger particles is relatively small. These curves also show that as the optical density is rapidly increasing, the mean particle diameter is rapidly decreasing, and the peak optical density occurs just as D_{32} is leveling off to a nearly constant value. Values of D_{32}

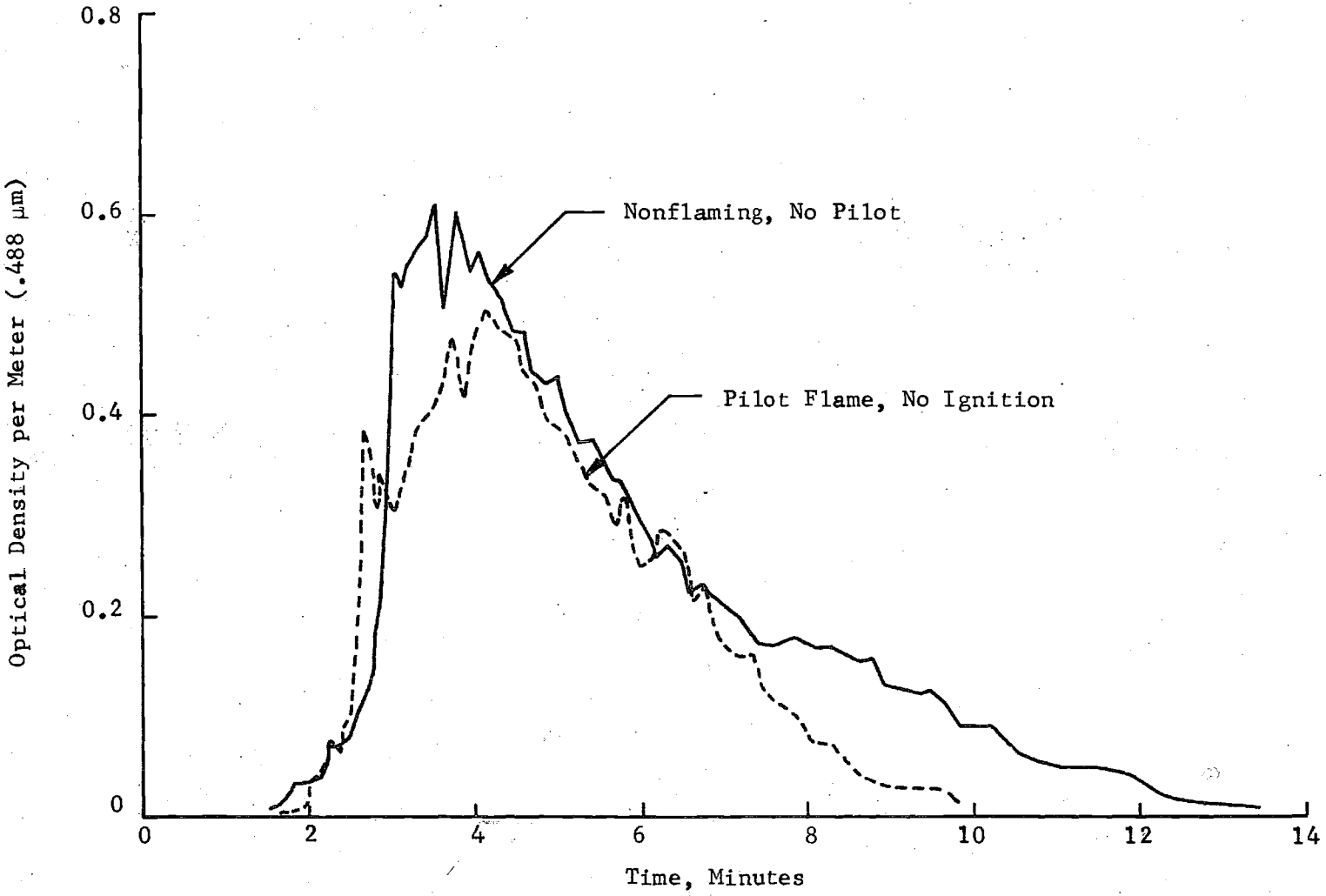

Figure 24. Smoke optical densities for nonflaming combustion of intumescent paint exposed to a radiant flux of 5 W/cm^2 in room temperature ventilation air (25°C).

corresponding to the peak optical densities are given in Table 7. These optical mean particle diameters (D_{32}) range from 15% (no pilot) to 50% (with pilot) larger than the corresponding mass median diameters (D_{MMD}) obtained by cascade impactor sampling. Aside from experimental errors, part of this discrepancy may be due to nonspherical shape of the solid particles generated by nonflaming combustion of this paint.

Tests in Heated Ventilation Air

A series of tests in heated ventilation air was conducted for the Ocean 9788 intumescent paint samples both with and without the pilot flame. For the nonflaming tests (no pilot flame), data was obtained at ventilation air temperatures of 100°C, 150°C, 200°C and 300°C. For high temperature tests with the pilot flame, the ventilation air was heated to 100°C and 300°C. For these last two test conditions, a brief period of flaming combustion was usually observed. The results of these tests are presented in Figure 21, Figures 25 through 28, and Tables 6 and 7.

As seen in Table 6, increasing the ventilation air temperature under nonflaming conditions to 100-150°C increased the average mass loss rate by a factor of four, while a further increase in air temperature to 200°C yielded another fourfold increase in average mass loss rate. With the exception of the 200°C test, increasing the ventilation air temperature (25°C - 300°C) for nonflaming conditions resulted in a small but steady decrease in the percentage of initial mass remaining as char. For tests with the pilot flame, average mass loss rate again increases with air temperature,

but the amount of increase is considerably less than in the nonflaming tests. This is opposite to what is expected, since the pilot flame and any flaming combustion of pyrolysate gases should increase the heat transfer to the polymer surface resulting in greater mass loss rates. However, the errors incurred in estimating the average mass loss rate in the absence of instantaneous weight loss data are expected to be significant and may account for this discrepancy. For the 300°C tests with the pilot flame the amount of char remaining is considerably less (about 45%) than for the corresponding nonflaming test (about 51%).

Char residues obtained from the high temperature tests of the Ocean 9788 intumescent paint are also shown in Figure 21. For the nonflaming tests there are considerable variations in the thickness and surface topography of the char layers, but there appears to be little correlation of these variations with temperature. These variations in char appearance are probably due to variations in some other factor such as paint film thickness, age of sample, or humidity of ventilation air. On the other hand, for cases in which flaming combustion occurred the chars obtained exhibited definite characteristic features. In the locations on the surface where flamelets were observed, the char was much darker than the surrounding surface. In some cases the intumescence was enhanced by the localized flamelets to produce columnar features; the largest such char column observed was about 15 mm in diameter and about 7 mm high. In addition a moderate coating of white material covered most of the surface, which had the same nodular texture as in the nonflaming tests.

Particle size and optical density data obtained from tests of Ocean 9788 intumescent paint samples conducted in hot ventilation air are shown in Figure 25 and 26 for nonflaming combustion and in Figures 27 and 28 for flaming combustion. In the figures for nonflaming combustion the room temperature data are also shown for comparison; however, this could not be done for flaming combustion since flaming ignition never occurred in the room temperature tests. High temperature data are also given in Tables 6 and 7. In all flaming tests a small propane pilot flame was maintained over the sample throughout the test, and the radiant flux was 5 W/cm^2 for all tests.

The effect of increasing the ventilation air temperature upon mean smoke particle diameter, D_{32},for nonflaming tests of the intumescent paint is shown in Figure 25. For tests at 100°C and 150°C, the curves of D_{32} versus time are qualitatively similar to that for the room temperature test, but the particle sizes obtained during the last half of the 10 minute exposure period (where D_{32} is nearly constant) are somewhat smaller for the higher temperature tests (about 0.5 μm). Furthermore, there is a pronounced dip in the D_{32} curve to about 0.3 μm for the 150°C test (t = 3.5 minutes) which does not appear at the lower temperatures. For the 200°C test, measurable quantities of smoke particulates were obtained only for a very brief period about two minutes after initial exposure, during which D_{32} dropped rapidly from about 0.9 μm to 0.4 μ m. At each temperature the largest particles occurred in the initial stages when the optical density was low. For the test conducted at 300°C without the pilot flame, no light scattering or absorption by smoke particulates was detected. Table 7 shows that for

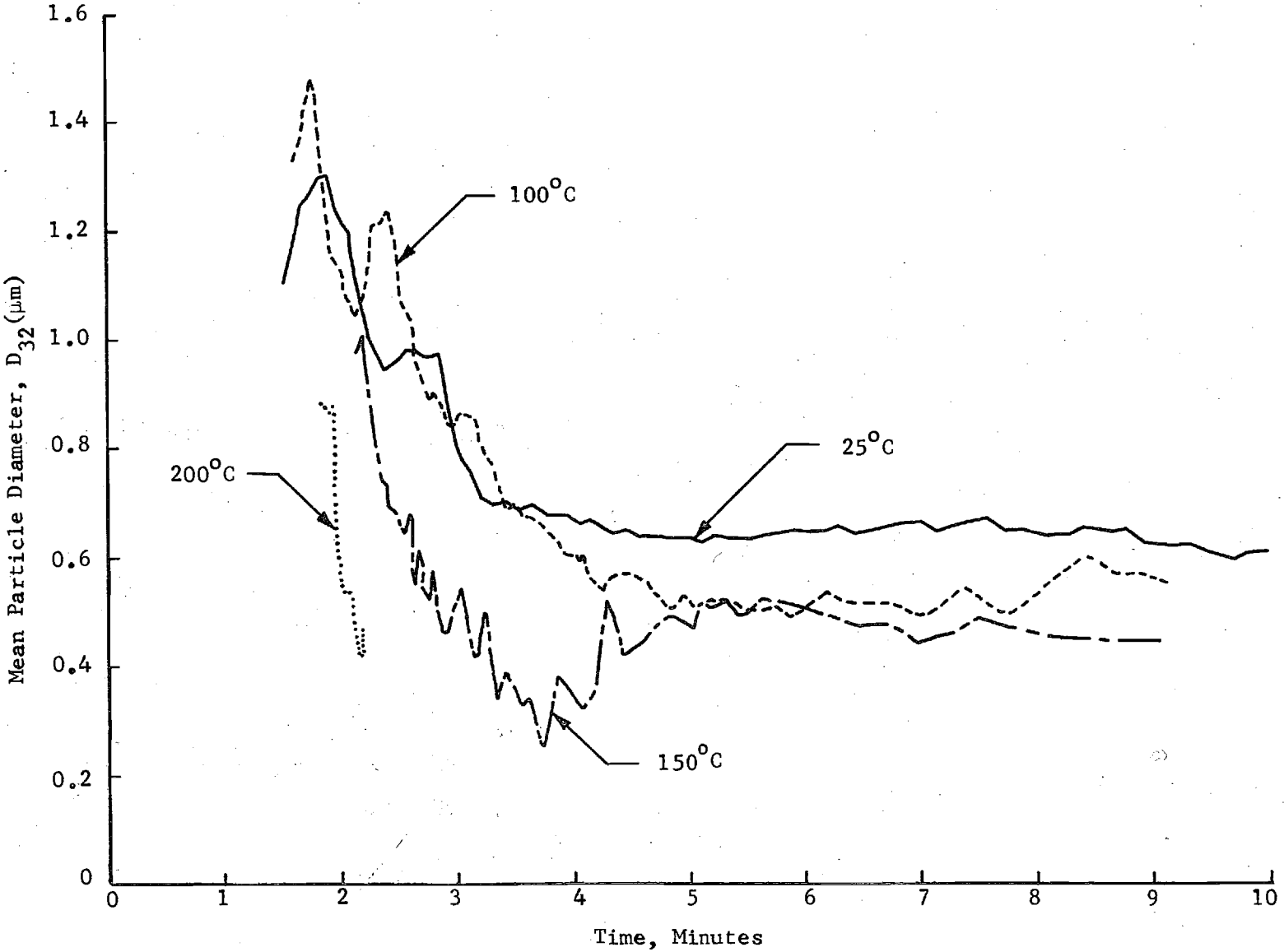

Figure 25. Effect of ventilation air temperature on the smoke mean particle diameter for nonflaming combustion of intumescent paint exposed to a radiant flux of 5 W/cm^2.

ambient temperatures of 25°C - 150°C, the value of D_{32} at the time of maximum optical density ranges from 0.5 - 0.8 μm.

The effect of ventilation air temperature upon smoke optical density (.488 μm wavelength) for nonflaming combustion of the intumescent paint is presented in Figure 26. Increasing the ambient temperature is seen to have a dramatic effect on optical density. At 100°C the peak in optical density is considerably higher and occurs earlier than at room temperature, and the decline in optical density following the peak is much more rapid at the higher temperature. In contrast, further moderate increases in ambient temperature greatly reduce the peak optical density and the time interval during which measurable light obscuration occurs. Part of this reduction in optical density shown in Figure 26, which gives directly measured values, is due to the increased dilution of the smoke particulates by the higher volumetric flow rate of the heated ventilation air (Table 1). The values of peak optical density given in Table 7 have been corrected for this effect; they reflect more accurately the decline in smoke production as the ambient temperature is raised above 100°C.

The effect of increasing temperature on optical density as shown in Figure 26 and Table 7 is probably due to the combined effects of increased pyrolysis rate and reduced condensation of pyrolysate vapors. Increasing the ambient temperature from 25°C to 100°C apparently accelerates the pyrolysis reactions without significantly reducing the condensation process which produces particulates, thus the peak optical density increases and the width of the peak narrows. This indicates that the boiling point of the particulates exceeds 100°C. The dramatic reduction in optical density

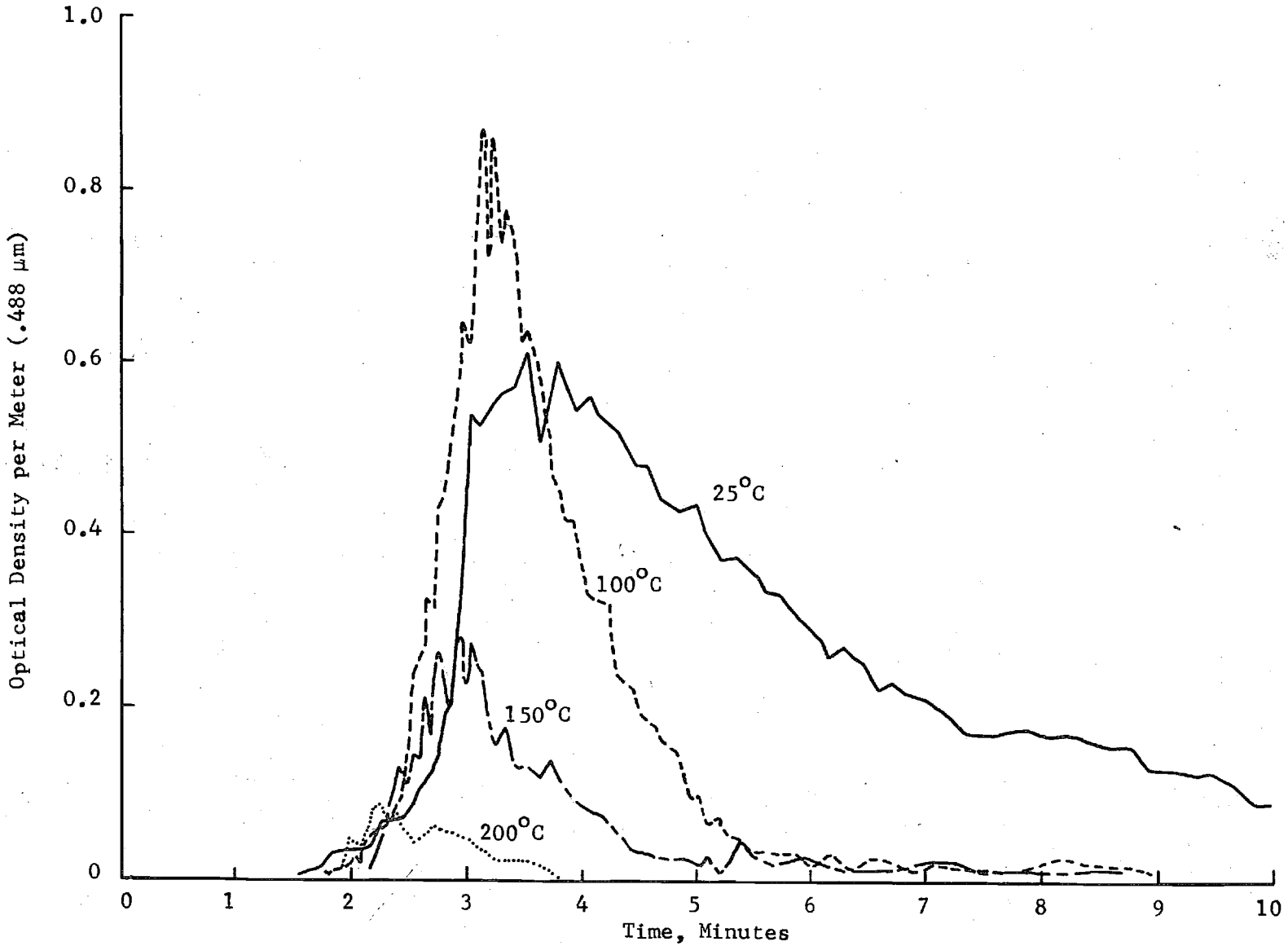

Figure 26. Effect of ventilation air temperature on the smoke optical density for nonflaming combustion of intumescent paint exposed to a radiant flux of 5 W/cm^2.

obtained with increases in temperature above 100°C indicates that suppressed condensation of pyrolysis vapors is then the dominant factor. Thus most components of the smoke particulates produced by nonflaming combustion of the intumescent paint probably have boiling points between 150°C and 200°C. The absence of measurable smoke particulates at temperatures above 300°C indicate that virtually none of the components of the smoke particulates have boiling points exceeding 300°C. This eliminates the possibility that the solid particles collected by cascade impactor sampling and filtration consist of inorganic pigment materials which have much higher vaporization temperatures.

At elevated ambient temperatures it was possible under certain conditions to obtain flaming combustion of the Ocean 9788 intumescent paint. Figures 27 and 28 give the results of three tests conducted in 100°C ventilation air in which the propane pilot flame was used. In Test A flaming ignition did not occur, and in Test B nonflaming smoke was detected shortly after one minute and flaming ignition occurred about two minutes later. In Test C the smoking behavior of the paint sample was similar to Test B, but the onset of pyrolysis and flaming ignition were both delayed by about two minutes.

The variations of mean smoke particle diameter with time during these flaming tests are shown in Figure 27. The variation in D_{32} during the initial nonflaming phase is similar to that observed in similar tests conducted without the pilot flame (Figure 25). The onset of flaming combustion is marked by a sudden increase in D_{32} from 0.5 - 0.6 μm (nonflaming) to about 1.2 μm. This is also accompanied by a sudden

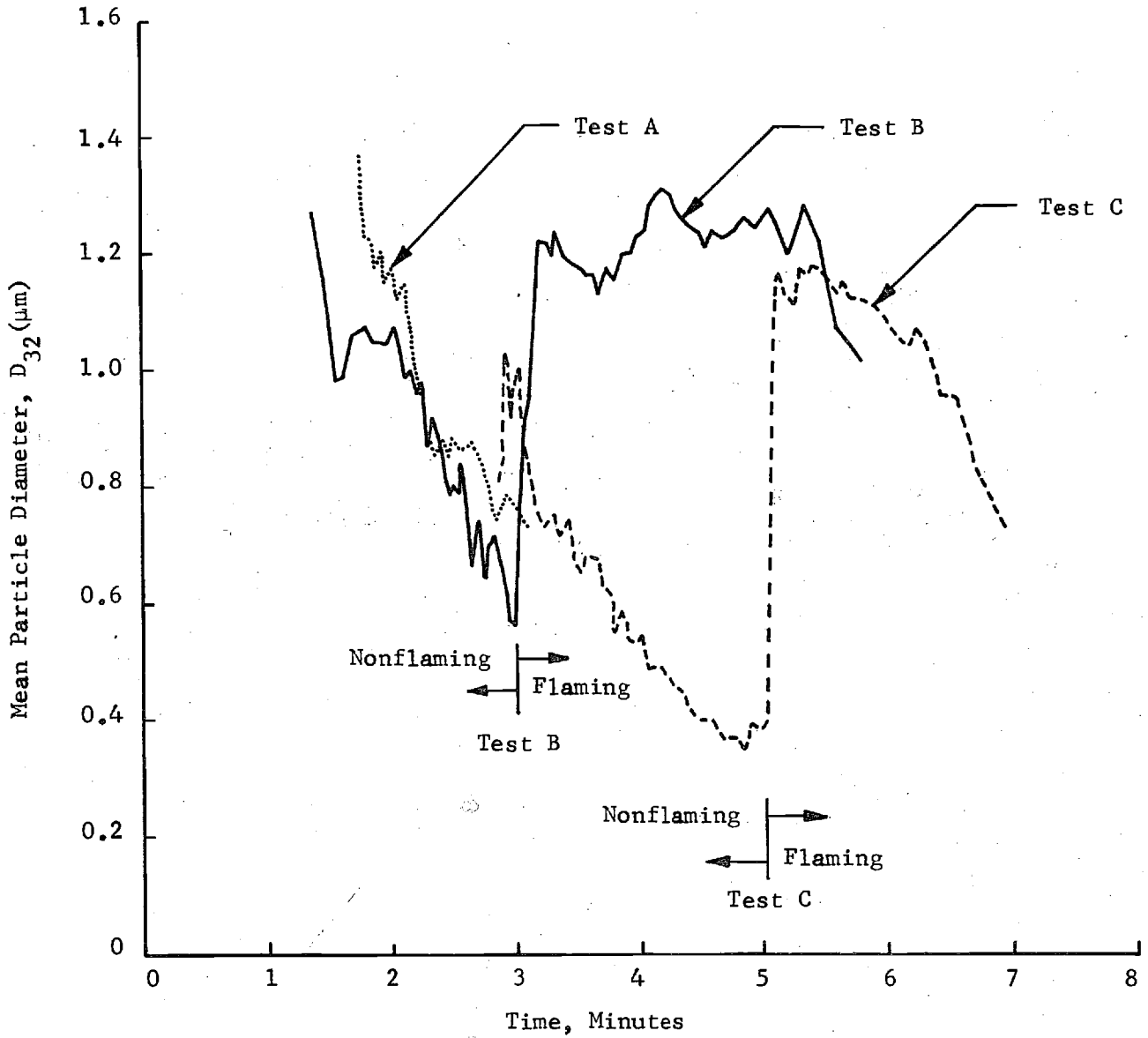

Figure 27. Smoke mean particle diameters for flaming combustion of intumescent paint exposed to a radiant flux of 5 W/cm^2 with pilot flame in heated ventilation air at 100°C.

decrease in the 90°-scattering ratio, $I_{\parallel}/I_{\perp}$, to the low values consistent with the highly absorbing, black, soot agglomerates produced by flaming combustion. For Test B the flaming phase lasted about 2 1/2 minutes. Visual observations during these tests indicated that flaming combustion was intermittent or flickering and was highly localized to specific regions of the sample surface.

Optical density variations (.488 μm wavelength) for the same three 100°C tests are shown in Figure 28. These curves show that optical density for Test B declined rapidly shortly after flaming ignition, while a low peak was obtained after ignition in Test C. In both tests the optical density observed during flaming combustion was about half of that obtained during the earlier nonflaming phase.

Three tests were conducted in 300°C ventilation air with the pilot flame lit. As in the 100°C tests, brief periods of localized intermittent flaming combustion accompanied by light soot production were observed. In only one of these tests, however, were the light scattering and attenuation signals from this soot sufficiently strong to yield values of mean smoke particle size and optical density. In this test (Table 7) the mean particle size D_{32} measured at peak scattering was somewhat larger than that obtained at 100°C, while the peak optical density obtained at 300°C was considerably less than that observed at 100°C. These tests also indicate that the duration and extent of flaming combustion of the Ocean 9788 intumescent paint is considerably less at high ambient temperature (300°C) than at intermediate ambient temperature (100°C). This behavior is quite different from the chlorinated alkyd paint for which spontaneous ignition occurs at elevated ambient temperatures. These differences are probably due to the complex

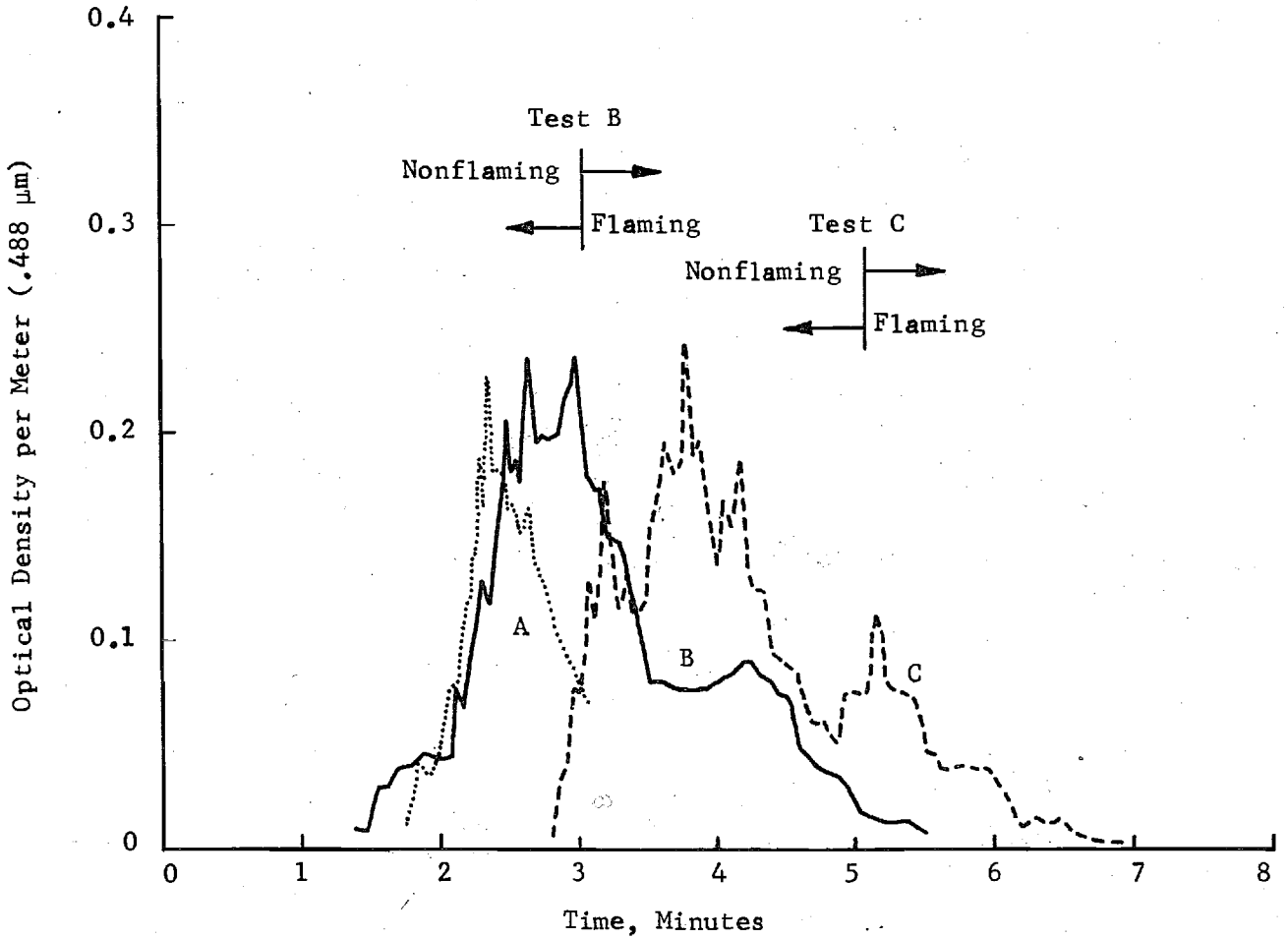

Figure 28. Smoke optical densities for flaming combustion of intumescent paint exposed to a radiant flux of 5 W/cm^2 with pilot flame in heated ventilation air at 100°C.

physical and chemical processes involved in the intumescence and pyrolysis of the Ocean 9788 paint.

Smoke Particle Refractive Index and Volume Fraction

For nonflaming tests of the Ocean 9788 intumescent paint, measurement of the ratio of optical densities, OD_R/OD_B, and the 90-degree scattering ratio, $I_{\parallel}/I_{\perp}$, were used to estimate the complex refractive index of the smoke particles. Values of the refractive index determined from these measurements under the assumption of nonabsorbing particles for these tests were often lower than expected for smoke particles (less than 1.3), which usually indicates that the smoke particles absorb as well as scatter light ($k > 0$). Thus the curve fitting technique which was used in determining the complex refractive index for smoke particles produced in tests of the chlorinated alkyd paint in heated ventilation air was also used to determine the refractive index n and absorption index k for smoke produced by the intumescent paint. For each of the nonflaming tests, measured values of $I_{\parallel}/I_{\perp}$ and OD_R/OD_B were plotted versus D_{32}. Values of n and k were then estimated from the Mie theory curve which best fits the plotted data.

Typical plots for nonflaming tests at room temperature are shown in Figure 29, while the corresponding data at 100°C are given in Figure 30. For the room temperature tests, Fig. 29 shows that no single theoretical curve of $I_{\parallel}/I_{\perp}$ versus D_{32} fits the plotted points, which vary steeply over a narrow range in D_{32}. This indicates that the complex refractive index varies considerably during the test, particularly near the time of peak optical density. The curve corresponding to $m_B = 1.306 - .0114i$ best fits the average of the $I_{\parallel}/I_{\perp}$ and OD_R/OD_B data near peak optical density (solid circles) and

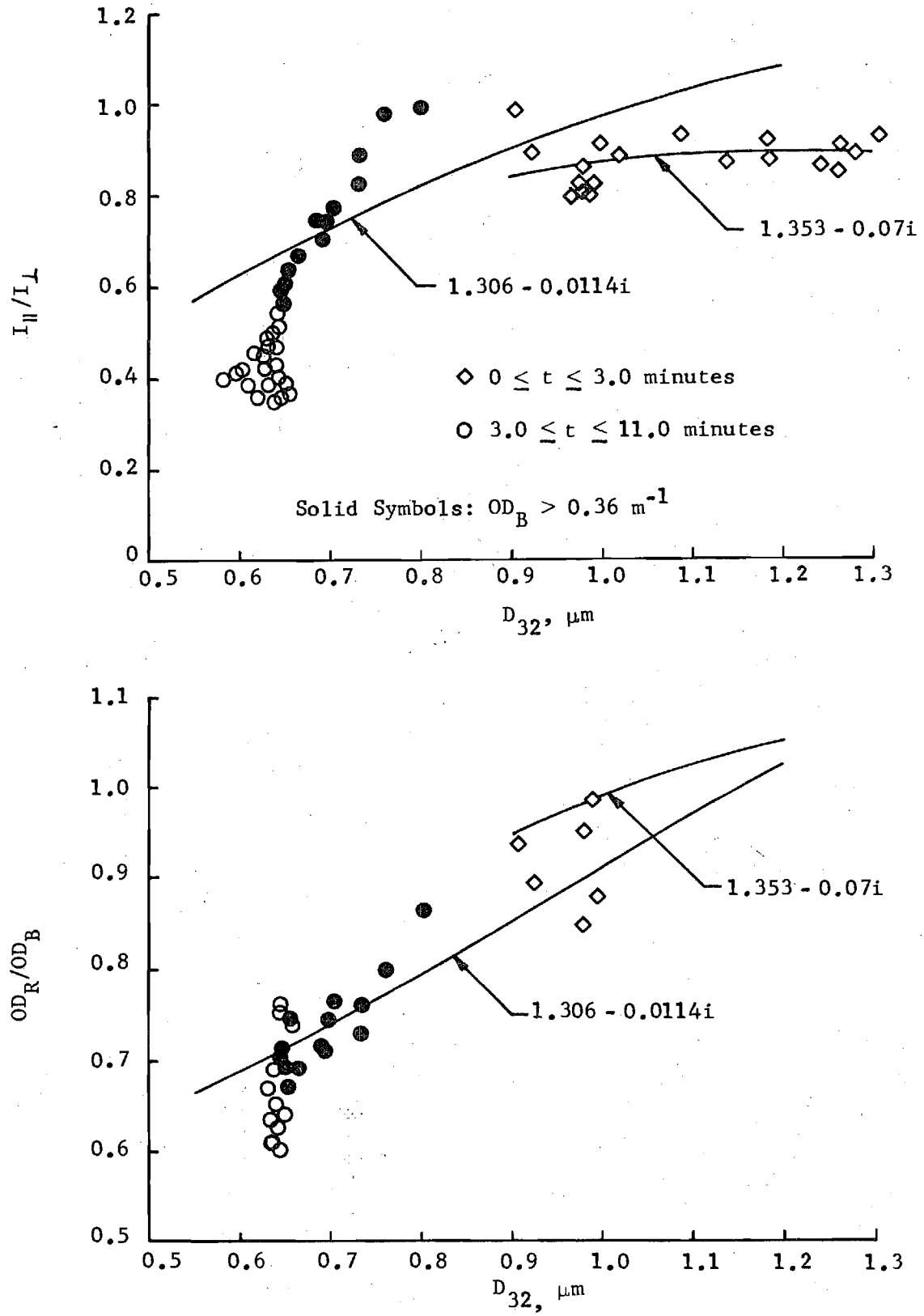

Figure 29. Optical density ratios and 90° - scattering ratios for nonflaming combustion of intumescent paint exposed to a radiant flux of 5 W/cm^2 in room temperature ventilation air (25°C).

some of the data obtained earlier in the test. The curve corresponding to m_B = 1.353 - 0.07i best fits the data obtained during the early phases of the tests; it indicates that significant variations in complex refractive index and hence chemcial composition of the smoke particles occur during the test. This variation appears to be greatest near peak optical density where the variation of D_{32} is small.

Figure 30 shows the same plots for a test conducted in air heated to 100°C. Here the theoretical curve fits the plotted data near maximum optical density much more closely than in the room temperature tests. For this test the best fit of the $I_{\parallel}/I_{\perp}$ data occurs for n = 1.357 and k = 0, indicating nonabsorbing particles. A very good fit of the OD_R/OD_B data was then obtained by allowing the refractive index to vary with wavelength (m_B = 1.357, n_R = 1.346). However two other replicate tests yielded somewhat different results indicating absorbing particles with a somewhat smaller refractive index (about 1.33) and an absorption index of about 0.03. For these latter tests there is also considerably more deviation of the plotted points from the fitted theoretical curves than in the case illustrated by Fig. 30. The complex refractive index given in Table 8 for the nonflaming tests at 100°C is an average of values obtained from the three replicate tests discussed above.

Values of the complex refractive index for nonflaming tests of the Ocean 9788 intumescent paint conducted at 150°C and 200°C were obtained by a similar curve fitting process, but the data is less reliable due to the reduction in light scattering and absorption signals at the higher temperatures. Average values of the complex refractive index shown in

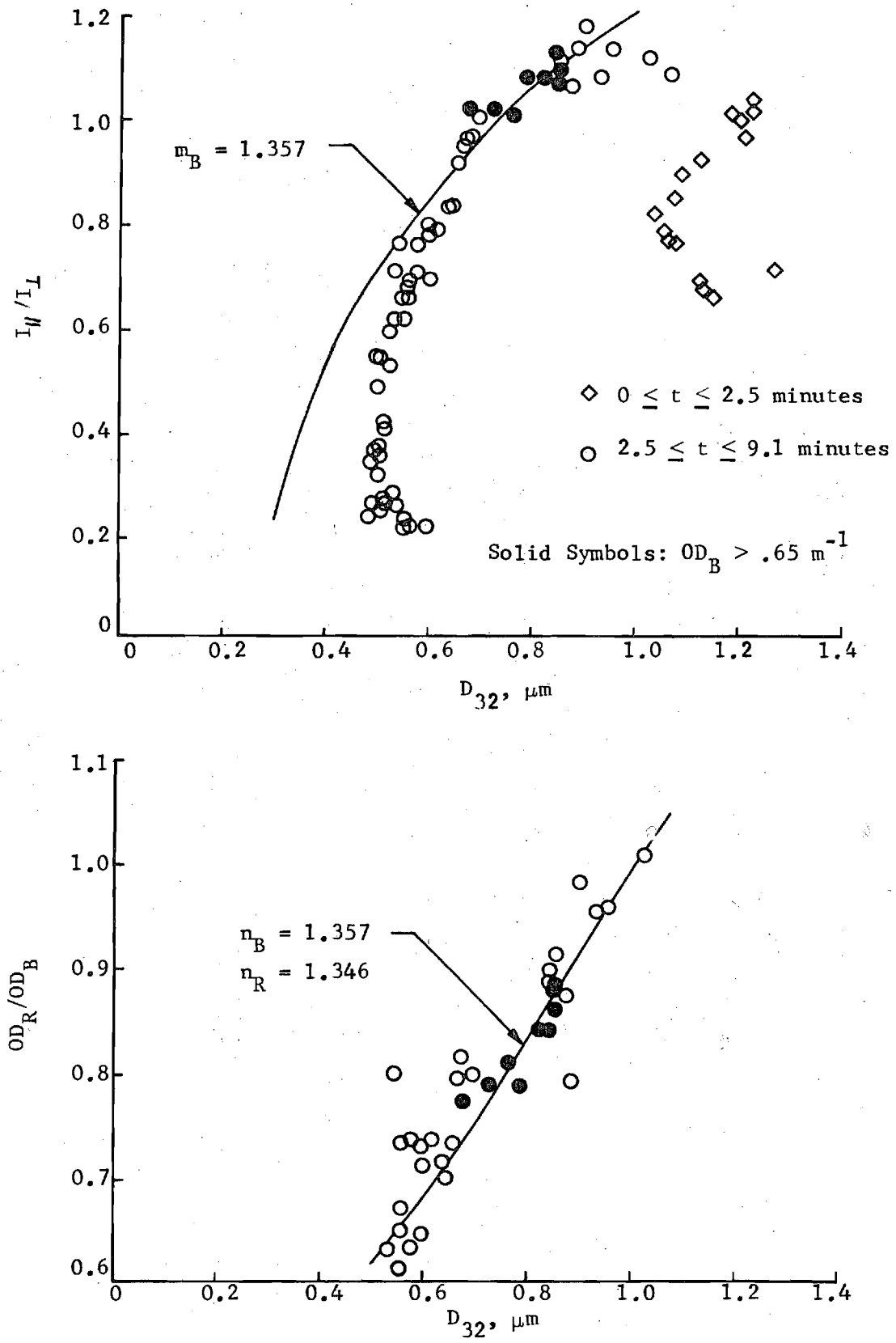

Figure 30. Optical density ratios and 90°-scattering ratios for nonflaming combustion of intumescent paint exposed to a radiant flux of 5 W/cm^2 in ventilation air at 100°C.

Table 8. Smoke Refractive Index, Volume Fraction, and Total Volume for Intumescent Paint.

Mode	Ventilation Air Temperature (^{o}C)	Radiant Flux (W/cm^2)	Refractive Index m_B (NF) or m_S(F)	η_v (F)	Peak Volume Fraction (ppm)	Specific Total Particle Volume (cm^3/g)	$\frac{\Gamma}{\Gamma_{25}}$
NF	25	5.0	1.310-.010i	-	0.23	0.081	1.00
NF	100	5.0	1.341-.022i	-	0.29	0.031	0.33
NF	150	5.0	1.317-0.04i	-	0.16	0.024	0.25
NF	200	5.0	1.32 -0.05i	-	0.06	0.005	0.06
NF*	25	5.0	1.27-0.013i	-	0.20	0.054	-
NF*	100	5.0	1.375-0.17i	-	0.13	0.0095	-
F	100	5.0	1.206-0.15i	0.35	0.18	0.013	-
F	300	5.0	1.155-0.11i	0.26	a	a	-

* Pilot flame on, but nonflaming combustion. At 25°C flaming never occurred, at 100°C samples ignited later in test.

a Insufficient light attenuation for determination of volume fraction and STPV.

Table 8 suggest that for the temperature range 25°C - 200°C the absorption index k of the smoke increases steadily with ventilation air temperature, and that the effect of temperature on the smoke refractive index n is small. This indicates that chemical composition of the smoke produced during nonflaming combustion of the Ocean 9788 intumescent paint is dependent on the ventilation air temperature.

Particulate volume fractions for the nonflaming tests of the Ocean 9788 intumescent paint samples are shown in Fig. 31. These volume fractions were calculated using the constant values of the complex refractive index given in Table 8, which were determined by the curve fitting procedure discussed above. These values of volume fraction are most reliable near the peaks where the values of complex refractive index, mean particle diameter (D_{32}) and optical density used in the calculations are the most accurate. The peak volume fractions, averaged for each set of replicate tests, are also given in Table 8. These peak values, which reach a maximum of about 0.3 ppm at 100°C, are considerably smaller than those obtained for the chlorinated alkyd paint under nonflaming conditions (25°C and 100°C only) when the lower ventilation air flow rate of the intumescent paint tests is taken into account. The shapes of the curves of volume fraction versus time and their dependence on ventilation air temperature are similar to those of the optical density curves given in Fig. 26. This shows that the optical density of the smoke produced by the intumescent paint samples under nonflaming conditions is determined principally by its concentration.

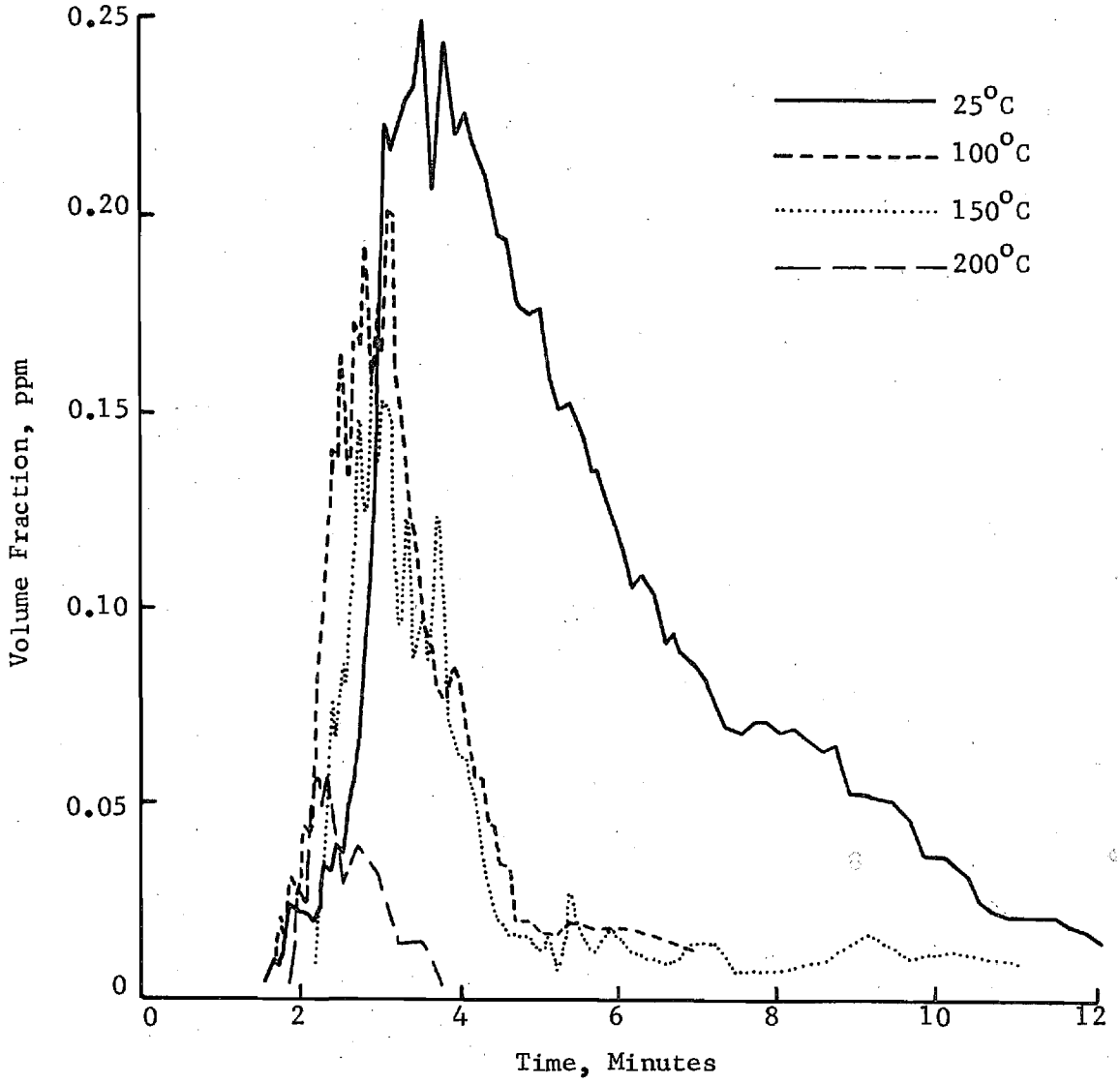

Figure 31. Effect of ventilation air temperature on the particulate volume fraction for nonflaming combustion of intumescent paint exposed to a radiant flux of 5 W/cm^2.

For the case of flaming combustion of the Ocean 9788 intumescent paint, the soot particles produced are nonspherical and highly absorbing, and direct determination of the complex refractive index from the measured values of $I_{\parallel}/I_{\perp}$ and OD_R/OD_B is impossible. As in the case of the chlorinated alkyd paint, the method of downward scaling of the soot particle refractive index to account for the presence of loosely packed, low-density soot agglomerates was used. Data for the best of the flaming tests conducted in air at 100°C are shown in Fig. 32, where values of $I_{\parallel}/I_{\perp}$ are plotted versus D_{32}. This figure shows both data for the initial nonflaming phase, which lasted about five minutes, and the flaming phase, which lasted about two minutes. The flaming data best fitted by an effective refractive index m_s of 1.283 - .21i, while the nonflaming data yielded m_B = 1.407 - .18i. In both cases there is considerable scatter about the theoretical curves.

Averaged values of complex refractive index for both flaming (m_s) and nonflaming (m_B) phases at 100°C and flaming at 300°C are given in Table 8. The corresponding values of η_v, the fraction of the optical mean particle volume that is actually occupied by the particulate material, is also given in Table 8 for the flaming phase of the tests. The η_v values indicate that the soot particulates produced during flaming combustion of the Ocean 9788 intumescent paint are very loose, low density aggregates of smaller primary soot particles similar in density to those produced by flaming combustion of the chlorinated alkyd paint. This data also indicates that the soot agglomerates produced in 100°C air are somewhat denser and more compact than those produced at 300°C.

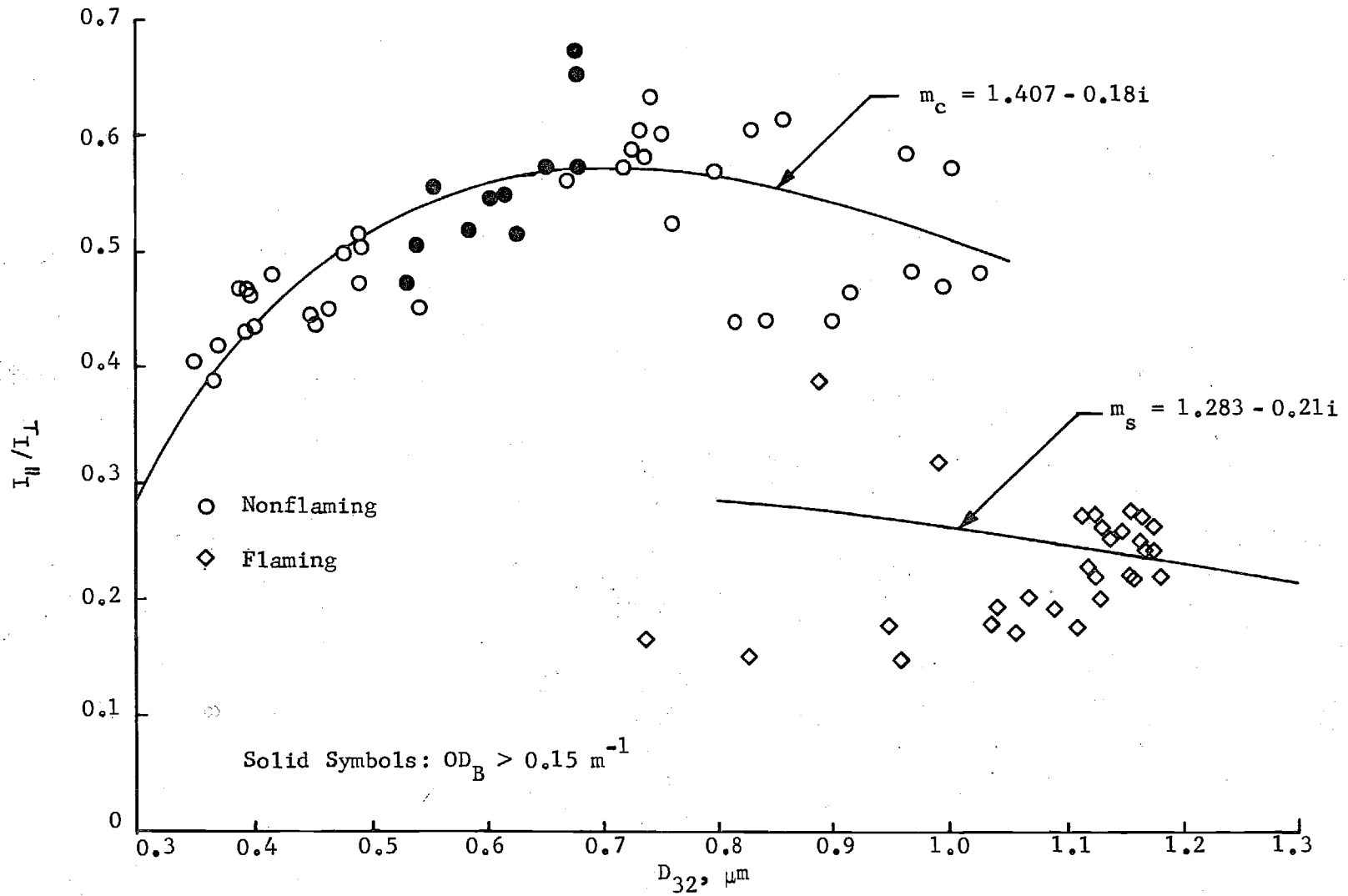

Figure 32. 90°-scattering ratios for combustion of intumescent paint exposed to a radiant flux of 5 W/cm^2 with pilot flame in heated ventilation air at 100°C.

It should also be noted from Table 8 that the complex refractive index of the smoke particles produced during the nonflaming phase of the "flaming" test at 100°C (with pilot flame) was significantly different from that obtained in the purely nonflaming tests (no pilot flame). Since the absorption coefficient (imaginary part) is considerably higher when the pilot flame is lit, this difference may be due to a small quantity of soot generated by the propane flame and mixed with the smoke generated by the paint sample during the nonflaming phase of the test.

Curves showing volume fraction variations during tests of the intumescent paint with the pilot flame lit are presented in Fig. 33. For the test conducted in room temperature air (25°C), flaming ignition did not occur and the resulting volume fraction curve resembles the one shown in Fig. 31 for a room temperature test without the pilot flame (i.e., radiant heating only). For Test B at 100°C the first half of the curve (including the rising part of the sharp peak), which corresponds to nonflaming combustion, is very similar to the 100°C curve (without pilot flame) shown in Fig. 31. The onset of intermittent, localized flaming combustion produces a sudden drop in particulate volume fraction followed by a second lower peak in volume fraction for which the corresponding optical density peak shown in Fig. 28 is much less prominent. For Test C at 100°C the second peak, which corresponds to flaming combustion, is sharper and higher than the first (nonflaming) peak. Again the corresponding optical density peak for flaming combustion (Fig. 28) is much less prominent. These differences in relative peak heights between the corresponding optical density and volume fraction curves for the 100°C tests of the Ocean 9788 intumescent paint are due to

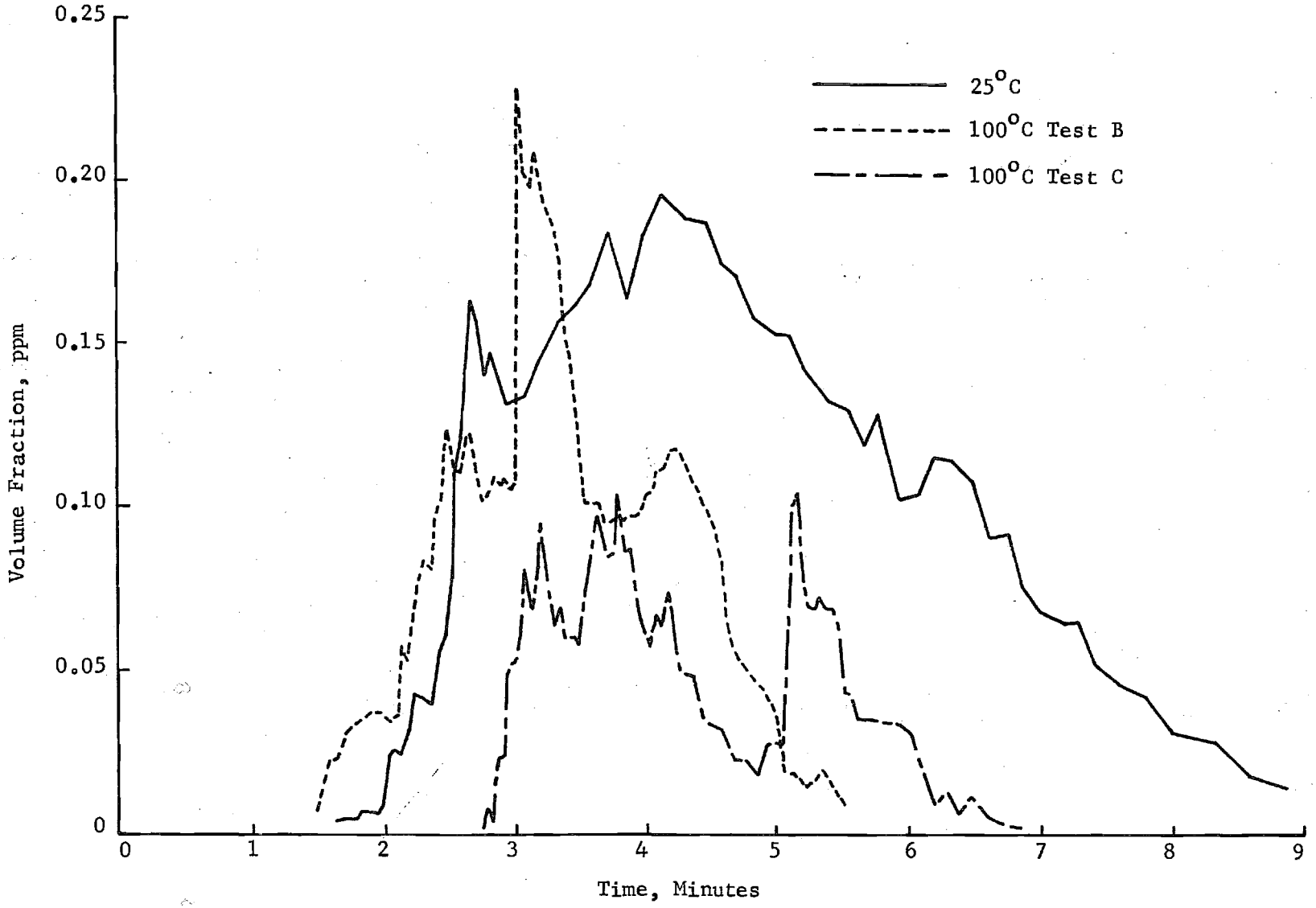

Figure 33. Effect of ventilation air temperature on the particulate volume fraction for combustion of intumescent paint exposed to a radiant flux of 5 W/cm^2 with pilot flame.

the drastic differences in mean particle diameter (Fig. 27) and complex refractive index (Fig. 32) between the smokes produced by flaming and nonflaming combustion of this material. Averaged peak volume fractions for these tests are also given in Table 8.

Values of the specific total particulate volume (STPV) are also given in Table 8. As in the case of the chlorinated alkyd paint, STPV values for nonflaming tests of the Ocean 9788 intumescent paint decrease markedly as the ventilation air temperature is increased. At 200°C the STPV is only about 6% of that obtained at room temperature. For the nonflaming room temperature and 100°C tests, the STPV obtained with the intumescent paint is about twice the STPV yield of the chlorinated alkyd paint (Table 5 and 8). In general the total particulate volume actually produced in the intumescent paint tests was lower than that observed for the chlorinated alkyd paint due to the much smaller sample mass used in the intumescent paint tests. Only at 100°C was it possible to measure the STPV for flaming combustion of the intumescent paint. The value given in Table 8 (.013 cm^3/g) represents only the flaming portion of the test; adding the STPV value for the nonflaming part gives a STPV of about .023 cm^3/g for the total test, which is considerably lower than that obtained in the completely nonflaming tests.

Although no sampling data were available for elevated air temperatures, the effect of ambient temperature on Γ was estimated from the optical data. These relative values of Γ, in which Γ is normalized with respect to the corresponding room temperature value, are presented in Table 8 for nonflaming combustion only. These Γ values follow the same trend with increasing ventilation air temperature as the specific total particulate

volume. Normalized Γ data was not available for flaming combustion of the intumescent paint because the 5 W/cm^2 radiant flux with pilot flame was not sufficient to ignite this material in the room temperature environment.

The total particulate masses produced in the nonflaming tests of the intumescent paint were estimated from the STPV values and the original sample masses assuming a density ρ_p = 1.3 g/cm^3 of the smoke particle material. For the room temperature tests, the optically determined values of the total particulate mass were then compared with the corresponding values estimated by particulate sampling. The sampling data was an average of the particulate masses collected for a test with cascade impactor and absolute filter in series and a test with absolute filter only . This comparison was done for tests conducted without the pilot flame and for tests conducted with the pilot flame. For nonflaming combustion without the pilot flame, the optically determined particulate mass was about 2.4 times as large as the particulate mass estimated by sampling. For nonflaming tests with the pilot flame, this ratio was about 2.0. These discrepancies are similar to those obtained for nonflaming tests of the chlorinated alkyd paint and other previously tested materials. The sources of this discrepancy are probably the same as noted for the chlorinated alkyd paint. Since particulate sampling data is not available for the tests conducted in heated ventilation air and flaming combustion did not occur in the room temperature tests, the comparison of optically determined and sampled particulate masses could not be done for flaming combustion.

Using the same procedure as described for the chlorinated alkyd paint, the values of the specific total particulate volume (STPV) given in Table 8 can be used to estimate the smoke volume concentration and optical density for a known quantity of Ocean 9788 intumescent paint burning in a confined space. Consider a 10 ft x 32 ft surface (29.7 m^2) covered with 3 coats of intumescent paint (approximately 0.63 kg/m^2) burning in a 25,000 ft^3 (708 m^3) space. The weight of the unburned paint in this case is 18.7 kg, which is nearly the same as for the chlorinated alkyd paint example. From Table 8 the worst nonflaming case occurs for a 5.0 W/cm^2 radiant flux in room temperature air, for which the STPV is about 0.081 cm^3/g. This yields a total particulate volume of 1515 cm^3 and a volume fraction of 2.14 ppm. The resulting optical density in blue light (λ = .488 μm) is nearly 5.4 m^{-1}, which indicates very severe attenuation of light, amounting to only 4 millionths of the incident light transmitted over a one meter optical path length. This light obscuration is much greater than that produced by burning an equal mass of the chlorinated alkyd paint under the same conditions. A similar calculation could not be performed for flaming combustion of the intumescent paint due to the localized and intermittent nature of the flaming combustion of this paint in the small scale tests. Large scale tests of this paint applied to PVC-nitrile rubber substrates, however, shows that flaming combustion of this material does occur with the production of large quantities of black smoke.[12]

SUMMARY AND CONCLUSIONS

Smoke physical properties were determined for two paints used aboard ships and submarines: a chlorinated alkyd paint as specified by DOD-E-24607 and an intumescent paint (Ocean 9788). These properties were determined for both smoldering and flaming combustion under a radiant flux of 5 W/cm^2 in both room-temperature and high-temperature atmospheres. The results of these tests are summarized below for each material.

Chlorinated Alkyd Paint

(1) Particle sampling indicates that the size distribution is log-normal for both nonflaming and flaming combustion of the chlorinated alkyd paint in room temperature ventilation air. For nonflaming combustion the smoke particulates consist of pale yellow spherical liquid droplets with a mass median diameter of about 0.9 micron. For flaming combustion, black, sooty particles are produced with a mass median diameter of about 0.6 micron. The size distribution obtained under flaming combustion is considerably broader than that produced under nonflaming combustion.

(2) During smoldering combustion in room temperature air the chlorinated alkyd paint converts about 11% of its total mass loss into smoke particulates. During flaming combustion this material yields slightly less than 4% of its total mass loss as particulates. For both types of combustion about 80% of the original sample mass remains after combustion as carbonaceous char and inorganic pigments.

(3) The in situ optical measurements reveal considerable variation in mean particle diameter (D_{32}) during nonflaming tests of the chlorinated alkyd paint in room temperature ventilation air. The mean particle diameters range between 0.7 and 1.1 microns, with an average of about 0.85 micron during the time of peak optical density. This latter value agrees well with the mass median diameter obtained by sampling. For flaming combustion the mean particle diameter is nearly constant at 1.1 - 1.2 microns, which is nearly twice the value obtained by sampling. This discrepancy is probably due to the nonspherical shape of these particles.

(4) The peak optical density obtained in room temperature tests at a ventilation air flow rate of 425 L/min is about 1.0 per meter for nonflaming combustion, and it is somewhat lower for flaming combustion.

(5) Smoke particles produced during nonflaming combustion of the chlorinated alkyd paint in room temperature air attenuate a light beam primarily by scattering, with very little, if any, absorption. These particles have a refractive index of about 1.34 during the period of maximum light obscuration. On the other hand the smoke particles produced during flaming combustion of this paint are highly absorbing, with a complex refractive index consistent with loosely packed, low density soot agglomerates which occupy slightly more than 25% of the optical mean volume as determined from the forward scattering measurements.

(6) Moderate increases in the temperature of the ventilation air (to about 100°C) for nonflaming tests of the chlorinated alkyd paint reduce the peak optical density, peak particulate volume fraction, and specific total

particulate volume (STPV) to about half of the room temperature values. Similar increases in the ventilation air temperature have little effect on the mean particle diameter at peak optical density, but changes in the chemical composition of the particles result in light absorbing particles with a complex refractive index of approximately 1.42 - 0.1i. Larger increases in ventilation air temperature (above 200°C) result in spontaneous ignition of the material and subsequent flaming combustion.

(7) For flaming combustion of the chlorinated alkyd paint there is a small but definite trend of increasing mean particle diameter as the ventilation air temperature is increased from 25°C to 300°C. Peak values of optical density and volume fraction increase with ambient temperature, but temperature has little effect on the specific total particulate volume or the complex refractive index of the smoke particles. Increased ambient temperature also slightly reduces the percentage of original sample mass remaining as char residue.

Ocean 9788 Intumescent Paint

(1) Due to the fire retardant nature of the intumescent paint, flaming combustion does not occur in room temperature air at the radiant flux of 5 W/cm^2. For tests in heated ventilation air with the pilot flame a brief period of localized, intermittent flaming combustion is usually observed.

(2) Cascade impactor sampling indicates that the particle size distribution is log-normal for nonflaming combustion of the intumescent paint in room temperature ventilation air. The mass median diameters average about

0.6 micron for tests conducted without the pilot flame. Microscopic examination of collected samples reveal that these particles consist of a mixture of white and light tan or beige solid materials.

(3) Sampling data also indicates that between 9% and 11% of the total mass loss appears as particulates during nonflaming combustion of the intumescent paint in room temperature air. Between 55% and 58% of the original sample mass remains after combustion as a thick porous low density carbonaceous char with a coarsely nodular surface texture.

(4) For nonflaming tests of the intumescent paint in room temperature air the mean smoke particle diameter (D_{32}) varies between about 1.2 micron shortly after the beginning of the test to relatively constant values of about 0.7 micron for most of the test. The optical density reaches its peak of about 0.6 per meter (142 L/min ventilation rate) just as D_{32} is leveling off to its nearly constant value. The complex refractive index of the smoke particles varies considerably during the tests, especially near the time of maximum optical density. These particles are mildly absorbing with a complex refractive index of about 1.31 - .01i.

(5) The principal effect of increasing ventilation air temperature for nonflaming combustion of the intumescent paint is a dramatic reduction in peak optical density, peak particulate volume fraction, duration of measurable light obscuration, and specific total particulate volume for temperatures above 100°C. For ventilation temperatures of 300°C and above, light scattering and attenuation by smoke particles is negligible. The effect of environmental temperature on mean particle diameter is not well defined,

with D_{32} ranging between 0.5 and 0.8 micron. Increasing the ventilation air temperature also increases the light absorption index of the smoke particles, which indicates an effect on chemical composition of the particles. Increasing temperature also results in a small decrease in the percentage of initial sample mass remaining as char.

(6) Smoke particles produced during the brief periods of intermittent, localized flaming combustion in the 100°C and 300°C atmospheres appear to consist of loose agglomerates of smaller soot particles. These agglomerates have optical mean diameters ranging between 1.2 and 1.35 microns.

The smoke physical properties of the two paints tested in this program may be compared taking into account the differences in initial sample mass and ventilation air flow rate for these two materials. For nonflaming combustion the smoking tendency Γ of the two paints is about the same. The intumescent paint produces somewhat smaller particles during nonflaming combustion and slightly larger particles during flaming combustion than the chlorinated alkyd paint. For nonflaming combustion the particles produced by the two paints differ greatly in shape, chemical composition, and physical state. For flaming combustion both paints yield loosely packed low density agglomerates of smaller primary soot particles. Most significantly, the specific total particle volume (STPV) produced by the intumescent paint during nonflaming combustion in room temperature air is about twice that produced by the chlorinated alkyd paint under the same conditions. Thus the resulting light obscuration obtained with the intumescent paint is much greater than that produced by burning an equal mass of chlorinated alkyd paint under nonflaming, room temperature conditions. This comparison could

not be made for flaming combustion due to the localized and intermittent nature of the flaming combustion of the intumescent paint.

REFERENCES

1. C. P. Bankston, R. A. Cassanova, E. A. Powell, and B. T. Zinn, "Initial Data on the Physical Properties of Smoke Produced by Burning Materials Under Different Conditions," J. Fire and Flammability 7, 165 (1976).

2. C. P. Bankston, "Determination of the Physical Characteristics of Smoke Particulates Generated by Burning Polymers", Ph.D. Thesis, School of Aerospace Engineering, Georgia Institute of Technology, March 1976.

3. E. A. Powell, C. P. Bankston, R. A. Cassanova, and B. T. Zinn, "The Effect of Environmental Temperature upon the Physical Characteristics of the Smoke Produced by Burning Wood and PVC Samples," Fire and Materials 3, 15 (March 1979).

4. E. A. Powell, R. A. Cassanova, C. P. Bankston, and B. T. Zinn, "Combustion-Generated Smoke Diagnostics by Means of Optical Measurement Techniques," in Experimental Diagnostics in Gas Phase Combustion Systems (Progress in Astronautics and Aeronautics, Vol. 53), edited by Ben T. Zinn, American Institute of Aeronautics and Astronautics, New York, p. 449, 1977.

5. E. A. Powell and B. T. Zinn, "In Situ Measurements of the Complex Refractive Index of Combustion Generated Particulates," in Combustion Diagnostics by Nonintrusive Methods (Progress in Astronautics and

Aeronautics, Vol. 92), edited by T. D. McCay and J. A. Roux, American Institute of Aeronautics and Astronautics, New York, p. 238, 1984.

6. B. T. Zinn, E. A. Powell, R. F. Browner, and M. Pasternak, "The Smoke Hazards Resulting from the Burning of Shipboard Materials Used by the U. S. Navy - Polyphosphazene Insulation," NRL Report on Contract No. N000-80-C-0432, 1984.

7. "Military Specification: Enamel, Interior, Nonflaming (Dry), Chlorinated Alkyd Resin, Semigloss", DOD-E-24607, Amendment 1, 16 December 1981.

8. B. T. Zinn, R. F. Browner, E. A. Powell, M. Pasternak, and R. O. Gardner, "The Smoke Hazards Resulting from the Burning of Shipboard Materials Used by the U. S. Navy," NRL Report 8414, July 1980.

9. I. Glassman, "Phenomenological Models of Soot Processes in Combustion Systems," AFOSR TR-79-1147.

10. R. A. Dobbins, R. J. Santoro, and H. G. Semerjian, "Interpretation of Optical Measurements of Soot in Flames," in Combustion Diagnostics by Nonintrusive Methods (Progress in Astronautics and Aeronautics, Vol. 92), edited by T. D. McCay and J. A. Roux, American Institute of Aeronautics and Astronautics, New York, p. 208, 1984.

11. S. C. Graham, "The Refractive Indices of Isolated and Aggregated Soot Particles," Combustion Science and Technology, Vol. 9, pp. 159-163, 1974.

12. J. I. Alexander, D. J. Bogan, S. L. Brandow, H. W. Carhart, H. G. Eaton, C. R. Kaplan, S. R. Lustig, R. M. Neilon, E. A. Powell, H. J. St. Aubin, R. S. Sheinson, M. B. Simmons, J. S. Stone, T. T. Street, P. A. Tatem, M. R. Wagner, T. M. White and F. W. Williams, "Submarine Hull Insulation Fires - Suppression with Nitrogen Pressurization and Corrosion Rates of Metals," NRL Report 8943, February 21, 1986.